DOCTORAL THESIS

NUMERICAL SIMULATION OF THERMAL DESORPTION SPECTRUM OF HYDROGEN IN HIGH STRENGTH MARTENSITIC AND AUSTENITIC STAINLESS STEELS

September 2013

Ibaraki University

Hitachi, Ibaraki, Japan

Lin Cheng

博士学位論文

高強度マルテンサイト鋼とオーステナイトステンレス鋼における

水素昇温脱離分析のシミュレーション

平成 **25** 年 **9** 月

茨城大学大学院理工学研究科

物質科学専攻

成　林

DOCTORAL THESIS

NUMERICAL SIMULATION OF THERMAL DESORPTION SPECTRUM OF HYDROGEN IN HIGH STRENGTH MARTENSITIC AND AUSTENITIC STAINLESS STEELS

September 2013

Department of Materials Science and Engineering

Ibaraki University, Japan

Lin Cheng

ACKNOWLEDGEMENTS

Long time ago, a name of a famous scholar came into my ear; several years ago, this professor came into my college campus and gave us a report; three years ago, with his generous aid I came to Ibaraki University; and now I am writing my doctoral thesis under his diligent guidance. He expertly introduced me into the new research field of hydrogen embrittlement and also patiently answered my questions in physical metallurgy. He liberally offered me financial support, kindly drove us to his home on the special festivals, and friendly packed me red envelope at my marriage. Here, I express my deepest gratitude to my supervisor Prof. Masato Enomoto. His intelligence and wisdom, his strictness and diligence, and his humor and wit impressed me deeply. He showed me the qualities of the scholar, and the way to carry on research. For the first time in my life I realize that I can make scientific attributions to human being. I am proud of this and sincerely appreciate my supervisor Prof. Masato Enomoto again.

Meanwhile, I would like to gratefully thank Prof. Kaiming Wu (Wuhan University of Science and Technology, China), my master degree supervisor, who introduced me to Prof. Masato Enomoto. I am deeply impressed and greatly benefit from his soaring aspirations, and great broad-minded and far-sighted qualities. Because of him, I truly understand the meaning of that nothing is impossible. Sincere thanks are expressed to Prof. Yasushi Sasajima, Prof. Haruyuki Takahashi, Prof. Hiromichi Onta and Prof. Goroh Itoh for their valuable corrections and discussions on my doctoral thesis.

My warm acknowledgements will go to all members at Enomoto research group for creating a pleasant office atmosphere and for chatting with me on interesting topics regardless of my poor Japanese. Especially thank Dr. R. Wei for discussing the affairs of the home, the state and the world, Dr. Y. Li for increasing my knowledge in

first-principle calculation. Grateful thanks go to all my friends in Japan including the Japanese volunteer teachers for their precious kindness and friendship and gave me a very happy life in Hitachi. Sincere thanks are expressed to all my friends in China and overseas for their concern and greetings, especially during the earthquake.

This research could not have been carried out without the other financial support received from tuition waiver exemption policy as well as the research assistantship supported by Ibaraki University, and the JASSO (Japan Student Services Organization) scholarship.

I am deeply grateful to my mother. She is living in the countryside since she was born but never hesitates to educate me. She works hard for her whole life but never asks me for something. She is not good at verbal expression but I never failed to feel her love. I have been always missing my father. He taught me to study hard and be an upright and promising man. Without him, my life was so miserable and my heart was so empty before. The one who never forgets my birthday in every year is my young sister. I really wish that she lives a peaceful and happy life with her honest and laborious husband, and their adorable children.

I am deeply grateful to my parents-in-law for raising an excellent daughter and betrothing her to me during my doctoral study. A very special appreciation goes to one who will be with me forever, my wife Li Li. She loves me like loving a hero, trusts me like trusting an old friends, and understands me like being a part of me. Her sentimentality and naivete, her tenderness and smartness, and her grace and beauty inspire me, encourage me and make me feel so sweet. Deeply appreciate Li Li for accompanying me in my hard times and tolerating my mood fluctuations due to research from time to time.

Abstract

Thermal desorption analysis (TDA) is widely used to analyze the diffusion and trapping of hydrogen in materials. While thermal desorption spectrum is thought to represent the energy and density of trap sites, the temperature and shape of the peak depend on the size of specimen and the conditions of hydrogen-charge and thermal analysis. Moreover, TDA spectrum is very different between bcc and fcc iron in which the lattice diffusivity of hydrogen differs several orders of magnitude. Accordingly, the influences of charging and testing conditions on the spectrum are studied by numerical simulation based upon McNabb-Foster model. Simulations were conducted in medium carbon martensitic steels and austenitic stainless steels for comparison with experimentally obtained spectra in these steels.

In the McNabb-Foster theory a number of parameters are required to conduct simulation, not only the energy and site density of trap sites, but also the kinetic coefficients (pre-exponential factor) of trapping and detrapping, the values of which are usually not well-established. Hence, before conducting simulations the applicability of the so-called Kissinger equation to TDA spectrum is studied using the McNabb-Foster model. It is shown that a Kissinger-type equation can describe diffusion-controlled desorption after a certain amount of pre-exposure prior to the analysis, albeit the pre-exponential coefficient depends on the specimen size. Moreover, the Choo-Lee plot which is used to determine the detrapping energy from TDA spectra with varying ramp rate can also be applied to diffusion-controlled desorption.

In martensitic steels the peak temperature of TDA spectrum are often considerably lower than those of deformed pure iron. In the literature it is well-known that carbon and hydrogen have a repulsive interaction at close proximity and carbon segregates to dislocations in lath martensite during quenching in low and medium martensitic steels.

Hence, a computer program was developed to incorporate carbon segregation to dislocations into the M-F model; it is treated in the same way as hydrogen trapping, albeit detrapping is assumed not to occur. Introducing a parameter which represents the carbon-hydrogen interaction, experimental TDA spectra could reproduced well in some low and medium carbon martensitic steels.

It is reported that TDA spectra of austenitic stainless steels depend largely on the charging and testing conditions. The dependences of spectrum on the specimen thickness and ramp rates, experimentally reported in Ni alloys and stainless steels, were reproduced fairly well solely from the lattice diffusivity, which implies that the influence of trap sites on the spectrum was often not significant. The initial hydrogen distribution appears to have a large influence on the spectrum; the difference of peak temperature as large as 200°C in SUS304 steel between cathodic charge and hydrogen charge under high-pressure environment could be accounted for from the difference in the penetration of hydrogen in the specimen. Moreover, two peaks can occur when hydrogen is initially confined to the rim of the specimen, because one part of hydrogen diffuses and escapes from the surface in a short time, and the other part diffuses inward and comes back to the surface later.

In this study, McNabb-Foster theory proved to be very useful in analyzing and simulating the hydrogen desorption spectrum in both high strength martensitic and austenitic stainless steels in which the lattice diffusivity of hydrogen differs several orders of magnitude, albeit we need to choose carefully the values of many parameters involved in the simulation. In particular, Kissinger equation and its derivative form Choo-Lee plot proved to be useful in the evaluation of hydrogen detrapping energy if the thermal desorption experiment is performed under proper conditions.

Contents

Chapter 3 Effects of Specimen Shape, Size and Initial Occupancy on Thermal Desorption Spectrum of Hydrogen

Chapter 4 Applicability of the Kissinger Formula in Simulation of Thermal Desorption Spectrum of Hydrogen

Chapter 5 Influence of Carbon Segregation to Trapping Site on the Thermal Desorption Spectrum of Hydrogen in Martensitic Steel

Chapter 6 Simulation of Thermal Desorption Spectrum of Hydrogen in Austenitic Stainless Steel

Chapter 1
Introduction

1.1 Hydrogen solubility in steels

The solubility of hydrogen in iron is proportional to the square root of external hydrogen pressure (fugacity). The hydrogen content (c_S) at the specimen surface in equilibrium with environmental gaseous hydrogen fugacity (f) can be calculated by Sieverts` law [1],

$$c_S = K_S\sqrt{f} \tag{1}$$

$$f = p\exp(\frac{pb}{RT}) \tag{2}$$

$$K_S = K_0\exp(-\frac{\Delta H_S}{RT}) \tag{3}$$

Where K_S is the hydrogen solubility, p is gaseous hydrogen pressure, T is absolute temperature, R is the gas constant and $b=1.584 \times 10^{-5} m^3 mol^{-1}$ is a constant, ΔH_S is the enthalpy of solution of hydrogen and K_0 is the pre-exponential factor. It is shown that by Quick and Johnson [2] that the atom fraction of hydrogen (x_0^H) in equilibrium with hydrogen pressure (P^H) in ferritic iron is,

$$x_0^H = 0.00185\sqrt{P^H}\exp\left(-\frac{3440}{T}\right) \qquad 322K< T >779K \tag{4}$$

It is calculated by first principle method that a hydrogen atom prefers the tetrahedral interstitial site in ferritic iron rather than in the octahedral site [3]. In contrast, an octahedral interstitial site is preferred in austenitic iron [4]. At room temperature, the equilibrium concentration hydrogen in the interstitial site of ferritic iron is about 1.8×10^{-8} under one hydrogen atmosphere pressure, which is too small to cause embrittlement at room temperature. However, much more hydrogen, several weight ppm, can be trapped in defects in steels, such as dislocations, internal boundaries and vacancies, etc.

1.2 Hydrogen diffusion in steels

Hydrogen diffusion in steel satisfies Fick's first and second laws. The Fick's first law reads,

$$J = -D\left(\frac{\partial c}{\partial x}\right)$$

and the Fick's second law reads,

$$\frac{\partial c}{\partial t} = D\frac{\partial^2 c}{\partial^2 x}$$

where D is the hydrogen diffusivity; J is the diffusion flux per unit time of a section in the medium; c is the hydrogen concentration in the lattice and x is diffusion distance.

The hydrogen diffusivity can be expressed as,

$$D^H = D_0 exp\ (-E_D/RT)$$

where D_0 is the pre-exponential term, E_D is the hydrogen diffusion activation energy, R is the gas constant and T is absolute temperature. Hydrogen diffusivity in steel can be determined from permeability experiment or by means of molecular dynamics calculation. In the matrix with hydrogen trap sites, an apparent diffusivity is proposed by Oriani assuming local equilibrium of hydrogen concentrations in trap sites and lattice interstitial sites,

$$D_{app}^H = D^H[1 + \frac{N_T}{N_L} exp\ (\frac{E_b}{RT})]^{-1}$$

where N_T and N_L are the numbers of the trap sites and normal interstitial sites per unit volume, respectively; E_b is the binding energy of the trap sites. At higher temperature, the apparent diffusivity is reduced to hydrogen diffusivity in the pure matrix.

1.3 Hydrogen embrittlement mechanisms

Hydrogen solutes, introduced into metals during processing and exposure to environmental working conditions, are known to markedly lower the ductility, fracture strength and fracture toughness, and thus to accelerate subcritical cracking under sustained and/or cyclic loading [1]. These deteriorating effects of solute hydrogen have been named hydrogen embrittlement and are thought be caused by the following three

main mechanisms, 1) stress-induced hydride formation and cleavage, 2) hydrogen-enhanced localized plasticity and 3) hydrogen enhanced decohesion.

1.3.1 Internal pressure

Besides the three main mechanisms mentioned above, there are other hydrogen-related degradation mechanisms involving hydride formation and internal gaseous species [15] including hydrogen blistering and hydrogen attack. In the former, high hydrogen concentrations result in the formation of internal gaseous hydrogen at internal interfaces, and then lead to high internal pressures and the formation of blistering. Meanwhile, the high pressure developed by molecular hydrogen enhances void growth and crack propagation. In the later, at high temperatures and pressures, internal gaseous hydrogen can react with the carbides in steel to form internal methane gas, which induces an associated loss in strength due to decarburization in return.

1.3.2 Hydride-induced embrittlement

The stress-induced hydride formation and cleavage mechanism is well-established hydrogen embrittlement mechanism with extensive experimental and theoretical support [16] in many metals, such as in niobium [17], titanium [18] and zirconium [19]. It is also supported in thermodynamic calculations [20]. In this case, brittle hydrides form at stress concentrators, such as crack tips, and crack advance takes place by repeated process of the formation and cleavage fracture of hydrides. This phenomenon is characterized by a competition between plasticity, which is responsible for ductile fracture processes, and brittle fracture by stress-induced hydride formation and cleavage. It is a most severe cause of embrittlement at low strain rates and intermediate temperatures at which the mobility of hydrogen is sufficiently high such that hydrides can form and cleave faster than ductile fracture because of the plastic deformation [21]. It was observed in situ in β-Ti [20] that hydrides first nucleated in the stress-field of crack and grew to large sizes not by the growth of individual hydrides but by the nucleation and growth of new hydrides in the stress fields and small hydrides grew together to from the larger hydrides. This auto-catalytic process of hydride nucleation and growth, together with the brittle nature of them, seems to be the main cause of

embrittlement of typical hydride forming elements [16].

1.3.3 Hydrogen enhanced decohesion

The decohesion theory of hydrogen embrittlement was first proposed by Troiano [22]. The dissolved hydrogen lowers the cohesive energy of iron lattice and decreases the force required to separate the crystal along a crystallographic plane due to the filling of the *d* bands of the transition metal by electron from the hydrogen atom. Oriani and Josephic [23, 24] suggested that the atomic bonding at the crack tip is weakened by the presence of hydrogen and the highly elastically stressed region at the crack front lowers sufficiently the chemical potential of dissolved hydrogen, which then attains a concentration that is several orders of magnitude larger than normal. This in turn lowers the maximum cohesive energy between atoms and this weakening effect results in reduction of fracture toughness of steels. Cracks propagate when the local maximum tensile stress normal to the plane of the crack, which is controlled by the externally applied load and the crack-front geometry, is equal to the maximum cohesive energy. It is considered as the dominant mechanism for internal hydrogen assisted cracking and hydrogen environment assisted cracking in high strength alloys that do not form hydrides **[5].**

1.3.4 Hydrogen enhanced localized plasticity

Hydrogen enhanced localized plasticity operates due to shielding the elastic interactions between dislocations and obstacles (or dislocations) or reducing the stacking-fault energy by hydrogen solutes [16]. The former allows dislocations to move at lower stresses and the latter decreases the tendency for cross-slip by increasing the separation distance between partial dislocations. The enhanced dislocation mobility resulted from hydrogen reduced interactions has been supported by experimental evidence [25, 26, 27]. In 310S stainless steel, the presence of hydrogen was observed to reduce the elastic interactions between obstacles and perfect and partial dislocations and thus, enhance the mobility of the dislocations. In high-purity aluminum, the introduction and removal of hydrogen from the system was observed to cause a reversal in the direction of motion of the dislocations piled up against a barrier, which was consistent

with a reduction of the elastic interactions by solute hydrogen. These observations provide direct support for the hydrogen shielding mechanism that has been proposed to account for the observed hydrogen-enhanced mobility of dislocations [26].

However, based on the equations for the equilibrium in a simple dislocation pile-up which takes into account the shielding effects of hydrogen atmospheres, it is argued that hydrogen concentration around the dislocation required for achieving the experimentally observed softening effect is too high [6]. It cannot be achieved in iron even with electrochemical hydrogen charging. Therefore, it is concluded that significant effects of softening observed experimentally in pure iron during electrochemical hydrogen charging in tensile loading cannot be accounted for by the effects of shielding of elastic fields of dislocation pile-ups by hydrogen. It is further pointed out that, perhaps, the enormous effect of hydrogen softening observed in pure iron is related to the processes of the pile-up decomposition, namely, to the fast climb in directions normal to the slip plane [7, 8]. The climb rate is determined by the vacancy concentration and forces normal to the slip plane. Due to strong hydrogen-vacancy interaction in iron, vacancy concentration can be significantly increased when hydrogen is present in solid solution [9, 10, 11], which results in noticeable increase of the climb rate at the heads of dislocation pile-ups. Finally, the experimental softening effect can be caused by the reaction of fast climb in dipole dislocation pile-ups [3] followed by the annihilation of edge dislocations with the opposite Burgers vectors. Then, a mechanism of the formation of spatially ordered structures of plastic flow, which can be considered as a variation of HELP, was proposed.

In situ electrochemical nano-indentations have been performed on different materials to register the onset of plasticity in extremely small volumes, namely perfect crystals in hydrogen-free and charged conditions [12]. It is shown that hydrogen reduces the required stress for the onset of plasticity, i.e. homogeneous dislocation nucleation by reduction in the shear modulus, dislocation line energy and stacking fault energy. The change in the shear modulus can be related to the reduction in crystal cohesion whereas the reduction in dislocation line energy and stacking fault energy is explained by the defactant concept, i.e. reduction in the defect formation energy in the presence of hydrogen. Then, it is concluded that neither hydrogen-enhanced decohesion nor

hydrogen-enhanced plasticity, but the reduction in the cohesion and defect formation energy are responsible for hydrogen embrittlement.

Recently, hydrogen effects [13] in austenitic steels have been studied using the *ab initio* calculations of the electronic structure, conduction electron spin resonance, internal friction and mechanical tests. It is shown that the hydrogen-caused elastic shielding of dislocations is not sufficient for interpretation of hydrogen-enhanced localized plasticity (HELP). Similar effects of hydrogen and nitrogen and the opposite effect of carbon on dislocation mobility are demonstrated, which cannot be explained within the framework of continuum mechanics. Hydrogen in iron and iron-based solid solutions increases the DOS at the Fermi level, i.e., the concentration of conduction electrons, which leads to the decrease in the shear modulus within the hydrogen clouds around the dislocations. For this reason, hydrogen decreases the stress for the start of plastic deformation, enhances mobility of dislocations and decreases the distance between them in the pileups. It is also shown that the elements located on the left of the iron in the periodic table decrease the concentration of conduction electrons in the austenitic steels and improve their plasticity in the hydrogen-charged state. In contrast, the elements located on the right of the iron increase the concentration of conduction electrons and enhance the hydrogen embrittlement.

1.3.5 Hydrogen enhanced strain-induced vacancies

Nagumo et al [29] have proposed that the primary function of hydrogen in degradation is to enhance the strain-induced creation and agglomeration of vacancies, thus promoting easy formation and linking of micro-voids for the fracture process. It is argued that hydrogen concentration is not a decisive factor in hydrogen embrittlement, and that deformation-induced defects, probably vacancy clusters, are related to hydrogen embrittlement susceptibility, which differs depending on the microstructure. The role of hydrogen has been ascribed to the stabilization of vacancy and increases its density. This model replaces hydrogen embrittlement in the context of ductile fracture in general in which vacancies play the primary role. Tensile experimental [28] has provided the evidence that increasing the amount of trap sites for solute hydrogen enhances embrittlement of steels.

Energetics of stability and clusterization calculation of hydrogen-vacancy complexes in α-Fe by means of *ab initio* shows that VH2, one vacancy trapping two hydrogen atoms, is the major complex at ambient condition of hydrogen pressure, which corrects the conventional model implying the VH6 predominance [30]. It is also demonstrated that the presence of hydrogen is found to facilitate formations of line-shaped and tabular vacancy clusters without the improbable accumulation. These anisotropic clusters can be closely associated with the fracture planes observed in experiments on hydrogen embrittlement in Fe-rich structural materials such as steel.

1.4 Hydrogen-trap sites interactions in steels

1.4.1 Dislocations

The interactions between hydrogen atoms and dislocations in metals are considerably important due to their influence on the plastic flow and hydrogen mobility [31]. In regions away from the dislocation core, the energetics of hydrogen are described as an elastic energy caused by the interaction between the stress field of the dislocation and the strain field around the interstitially dissolved hydrogen atom in the frame of continuum mechanics. When hydrogen is in the lattice, the region near screw dislocation core is much more repulsive than in a normal iron lattice. Then, it is considered that hydrogen accumulation could be less favorable near a screw dislocation than an edge dislocation [32]. The distribution of hydrogen around a stress singularity field studied by molecular statics (MS) and molecular dynamics analysis of the hydrogen-trap energy around a {112}<111> edge dislocation in α iron [33] shows that hydrogen atoms exist stably on the edge dislocation core and the exact slip plane, and that high hydrogen concentration is formed along the slip plane near the dislocation core. These results suggest that hydrogen is trapped with the help of shear stress, and therefore screw dislocations are also assumed to interact with hydrogen except at the dislocation core.

A two-step electrochemical permeation technique shows that the binding energy between hydrogen and dislocation core is about 46.2±2.6kJ/mol [34]. Choo and Lee [35] inferred from observed peak temperatures of desorption curves at different heating

rates that it is 19.2 kJ/mol. Zielinski et al [36] concluded that the binding energy was around 27 kJ/mol examined by internal friction measurements. Kumnick et al [37, 38] showed that the binding energies of hydrogen with dislocation core and in the strain field were 59kJ/mol and 20kJ/mol in the deformed iron, respectively. They have concluded for dislocation core that the traps are probably either jogs in dislocations or imperfection debris left behind by moving dislocations. K. Ono and M. Meshi [39] analyzed that the trap site in single crystal iron should be the dislocation with the binding energy of, i.e. 0.47±0.02 eV, i.e., 45.3±1.9kJ/mol. The first principle calculation shows that the binding energy between dislocation core and hydrogen is about $7x10^{20}$J, i.e., 42.14kJ/mol [33].

1.4.2 Vacancy

Vacancy is arguably the simplest defect in metals, consisting of an empty lattice site with modest peripheral relaxation [40]. The attractive interaction between interstitial solute hydrogen and vacancy can be inferred from the open-volume character of the defect. In particular, the surface chemisorptions state of hydrogen is energetically favored over interstitial solution. Moreover, the local open volume associated with the vacancy is relatively large. It is almost sufficient to appear to the hydrogen atom as free surface. As a result, hydrogen is driven to enter the vacancy and show a large binding energy with the vacancy comparable to that for hydrogen in the chemisorbed state [40]. The first principle [41] calculation shows that vacancy provides an isosurface of optimal charge density that induces collective hydrogen binding on its internal surface. The hydrogen atoms are near the tetrahedral interstitial sites neighboring the vacancy. The Fe-H and H-H bonds are formed and their bindings are achieved at the expense of their Fe-Fe neighbors. The interactions mainly involve 3d and 4s atomic orbitals of Fe [42]. The positron annihilation experiment has demonstrated that in the presence of hydrogen, the hydrogen-vacancy binding reduces the effective mobility of the vacancy and thereby delays the vacancy recovery, providing a signature of the hydrogen trapping reaction with vacancy [43]. Because the vacancy formation energy is lowered by the presence of H in comparison with that in the intrinsic metal due to the extra binding energy of hydrogen with vacancy [41, 44], an increases in vacancy densities far exceeding thermal

equilibrium values exists in various metals in the presence of hydrogen [43]. Moreover, extremely high concentration of vacancies is formed in metals heated under high hydrogen pressure atmosphere, called superabundant vacancy formation phenomenon [44, 45, 46].

As hydrogen trap sites, the binding energy of hydrogen to vacancy has been experimentally examined. Two trapping energies in iron were found and they were estimated to be 0.63 eV (assigned to VH1 and VH2) and 0.43 eV (assigned to VH3-VH6) [47]. The first principle calculation also found that vacancies are strong H trap sites with a binding energy of 0.57 eV [48] for one trapped hydrogen, or 0.60 eV for one or two trapped hydrogen atoms and 0.40 eV for three trapped hydrogen [49]. There is a good agreement of the first principle calculation with experiment. Meanwhile, at ambient condition VH2 is the major H-vacancy complex and the amount of VH3 will increase with increasing hydrogen pressure [42, 49, 50]. Under higher hydrogen pressure atmosphere, VH5 and VH6 become the major complexes [51].

1.4.3 Solutes and solutes-defect complex

The interaction of hydrogen with solutes in metals is influenced both by elastic of lattice and electronic differences in hydrogen bonding between the host and impurity atoms [52]. In the case of interstitial solutes, the binding is predominantly due to elastic distortion; for substitutional transition-metal solutes there is a comparable contribution from the electronic effects, with the increasing attraction with the size of the solute and its number of d electrons [53-55]. Some experimental binding energies between the substitutional solutes and hydrogen are summarized in table 1. Recently, W.A. Counts et al [56] performed a series of density functional theory (DFT) calculations to quantify the binding energy of hydrogen to a number of point defects in body-centered cubic iron, e.g. vacancies, interstitial carbon and substitutional solutes. They found that vacancies are the strongest hydrogen trap. Most substitutional solutes (except Si, Cr, Mn, Co, and Mo) trap a hydrogen atom with positive binding energies up to 0.25 eV. The maximum hydrogen binding energy for Si, Cr, Mn, Co and Mo is essentially zero, meaning they do not interact with hydrogen. The hydrogen-substitutional solute binding energies are roughly correlated with the solute atom's electronegativity and size. Finally, the

presence of a solute atom near a vacancy does not affect hydrogen binding to the vacancy provided the solute atom is not significantly larger than an iron atom. Table 2 summarizes the binding energy between hydrogen with substitutional solutes in bcc iron. Later, W.A. Counts et al [57] extended this conclusion to binding between multiple hydrogen atoms and substitutional solute atoms in bcc Fe. They showed that the largest hydrogen-solute defect complex for V, Cr, Co, Ni and Zn contains two hydrogen atoms, while for Sc, Ti, Mn, and Cu the largest defect complex contains four hydrogen atoms.

Table 1 Experimental hydrogen-solute binding energies in metal

	System	Binding energy, eV	Reference
Substitutional	Ti in V	0.15 0.03-0.10	Tanaka and Kimura, 1979 Pine and Cotts, 1983
	Ti in Fe	0.19	Pressouyre and Bernstein, 1978
	Ti in Ni	0.05-0.10	Thomas, 1981
	Fe in Ni	0.07-0.12	Thomas, 1981
	Co in Cu	0.12	Boolchand et al, 1983
	Cr in Nb	0.105	Richter et al, 1983
	Ti in Nb	>0.12	Richter et al, 1983
	V in Nb	0.09	Matsumoto, 1977
Interstitial	C, N in V	0.13	Chang and Wert, 1973
	O in V	0.09	Chang and Wert, 1973
	C in Fe	0.03	Au and Birnbaum, 1978a
	N in Fe	>0.13	Au and Birnbaum, 1978a
	N in Nb	0.12 0.1	Pfeiffer and Birnbaum, 1973 Richter et al, 1976
	O in Nb	0.09	Baker and Birnbaum, 1973
	N in Ta	0.06	Rosan and Wipf, 1976
Solute-vacancy complex	Co in Cu	0.63	Boolchand et al, 1983
	In in Ni	~0.6	Collins and Schuhmann, 1986
	Y in Fe	0.7-0.9	Myers et al, 1989
	Cs in Ni	0.6-0.8	Myers et al, 1989

Table 2 Summaries of the maximum hydrogen binding energies in bcc Fe

System	Binding energy, eV	System	Binding energy, eV
Solute-Vacancy	0.57-0.60	Ti	0.08
Vacancy	0.57	Zn and Nb	0.07
Y-Vacancy	0.49	Cu	0.06
Y	0.25	Al	0.04
Sc	0.20	V and Ni	0.01
Mg	0.15	Co and Mo	0.00
Cd	0.13	Cr and Mn	0.00
C	0.09	Si	0.00

1.4.4 Grain boundary

Grain boundaries in materials are regions of transition between two adjacent crystal lattices. It is well known that solute segregation at grain boundary influences quite significantly the macroscopic properties of polycrystalline materials. Of all defects in bcc metals, grain boundary are of great interest to metallurgist and the interfaces that form them are frequently related to their corresponding free surface [58]. It has been reported that whenever the electron density decreases below certain optimum value at the interstice in metals, the associated defect will act as a trap for hydrogen and vice versa. There are many kinds of open defects in metals and it is widely accepted that the more open they are, the hydrogen atom will become strongly trapped [59]. Based on theoretical considerations, Hirth [60] suggest that the grain boundary should trap hydrogen as strongly as dislocation core. TEM autoradiograph suggests, by the developed silver grains, that the grain boundary and internal interface of ferrite-cementite and ferrite-lath structure can be hydrogen trapping sites [61].

It is also found by the atom superposition and electron delocalization molecular orbital method that hydrogen segregates more to grain boundary than to edge and screw dislocations in iron, grain boundary with binding energy of hydrogen of 0.30eV but mixed dislocation with binding energy of 0.22eV [58]. This is close to the 17.2 KJ/mol obtained by Choo-Lee by heating the specimen with different ramp rates [62]. K. Ono and M. Meshi [63] showed that in polycrystalline iron the main trap site is the grain boundary with the binding energy of 0.51±0.02 eV.

1.4.5 Phase boundary

High strength steel is susceptible to hydrogen embrittlement [64]. To reduce the susceptibility, one of the promising approaches is to introduce hydrogen traps, in particular carbides in steel to trap the hydrogen and prevent it from moving to the tip of a crack, where a local stress concentration occurs. Fine titanium carbide [65] and vanadium carbide [66] and Niobium carbide [67] were reported to have the hydrogen-trapping property and can increase the resistance to hydrogen embrittlement.

The binding energy of hydrogen with incoherent TiC particles in steel is 95kJ/mol

reported by Pressouyre and Bernstein [68] by means of the electrochemical permeation method and 87 kJ/mol reported by Lee and Lee [69] by means of thermal-desorption spectrometry (TDS) analysis. However, another thermal-desorption spectrometry (TDS) analysis showed that incoherent TiC particles in iron do not trap hydrogen at ambient temperature by a cathodic-charging method but trap hydrogen during high-temperature heat treatment in non-protective atmospheres. The binding energy between hydrogen and incoherent TiC is 53kJ/mol [70]. The energy barrier for hydrogen to jump into incoherent TiC was determined to range from 21 to 35kJ/mol, which is too high for hydrogen to be trapped by incoherent TiC at low temperatures [70]. However, it is further reported that the activation energy for hydrogen desorption from the incoherent TiC particle are changed with the particle size. For example, the activation energy in the well-tempered 0.05C-0.22Ti-2.0Ni steel is 85.7kJ/mol; in the 0.42C-0.30Ti steel, a higher activation energy of 116 kJ/mol was obtained for the coarse incoherent TiC; the nano-sized TiC coherent precipitates in the 0.42C-0.30Ti steel were found to have an activation energy ranging from 46 to 59kJ/mol depending on the tempering temperature. [71]. The trapping of hydrogen on the TiC has also been directly observed by using atom probe tomography (APT). It is found that the deuterium atoms were definitely observed on the broad surface of TiC platelets, which indicated that the broad interface between the matrix and TiC was the main hydrogen trapping site [72].

A significant interaction between hydrogen and VC precipitates has been measured by small angle neutron scattering and the homogeneous trapping of hydrogen is within the precipitates rather than at the precipitate/matrix interface [73]. Meanwhile, hydrogen could also be trapped in MnS owing to the slower diffusion and larger trapping energy in MnS [74].

TDS analysis showed that hydrogen evolution rate of pure iron has only one peak, while that of eutectoid steel has two peaks. From TEM and TDS analysis, the lower temperature peak was attributed to hydrogen released from the trapping sites such as point defects, clustered defects and dislocations in ferrite. The higher temperature peak was found to correspond to hydrogen released from the trapping sites such as defects in cementite and/or such as the disordered interface between ferrite and cementite [75]. It is also observed that the permeability and diffusivity of hydrogen in carbon steel

decrease as the ferrite-cementite interfacial area increases. The trap energy of hydrogen at ferrite-cementite interfaces is calculated to be 10.85kJ/mo1 [76]. However, it is also reported that the binding energy between hydrogen and ferrite/cementite interface was estimated to be higher than 84kJ/mol [77].

1.4.6 Retained austenite

In the study by means of electro-chemical permeation of the effects of retained austenite on the hydrogen content and the effective hydrogen diffusivity of an otherwise fully martensitic structure, two steps of hydrogen build-up transient were conducted on the same specimen [78]. It is believed that in the first transient both the reversible and irreversible trap sites are active. However, in the second transient only the reversible trap site is active since the irreversible trap site has been occupied. It is shown that on the first permeation transient high-carbon as-quenched specimens have a lower effective diffusivity than those with an additional subzero treatment due to the presence of retained austenite in the former specimens, which affords more sites for hydrogen trapping and hence lower the hydrogen diffusivity. After hydrogen traps were filled up, the second permeation transients gave similar effective diffusivity for both as-quenched and quenched and subzero-treated specimens. It is further shown that the hydrogen contents of as-quenched specimens were higher than those of the specimens subjected to quenched and subzero treatment due to the existence of retained austenite in as-quenched martensitic matrix. It is also argued that the interfaces between the retained austenite and martensitic plates may be the trap sites for hydrogen [78]. It was also observed that the diffusivity obtained from the permeation curves was smaller and activation energy was larger in steels with retained austenite than those without retained austenite [79]. The charged hydrogen first dissolves in ferrite and then in retained austenite and/or at ferrite/austenite interfaces with prolonged charge [80].

In another work, four samples with different austenite volume fractions were prepared to prove that the retained austenite is an intraphase hydrogen trap site with higher binding energy. The four steels are AISI type 304 stainless steel, super duplex stainless steel, dual-phase steel (12 vol-% retained austenite), high-strength low-alloy (HSLA) steel weld deposit (4 vol-% and 0 vol-% retained austenite), respectively. It is

found that the former three steels show the almost same hydrogen evolution peak at the higher temperature [81]. And when the retained austenite in dual-phase steel was induced to transform into martensite by plastic strain and lower temperature treatment, the higher temperature peaks disappeared. The binding energy of hydrogen to retained austenite was reported to be 90±25kJ/mol by means of the Choo-Lee analysis method [82].

1.5 Thermal Desorption Analysis

Hydrogen trapping effect can be described by the binding energy between hydrogen and the trap site (E_B) or the detrapping activation energy required for hydrogen to escape from the trap site (E_d). Simply, the detrapping energy is the sum of the binding energy, and the hydrogen diffusion activation energy (E_D) in the matrix lattice and the energy difference in the activation energy of atom jump in the vicinity of the trapping site from that in the lattice, as schematically illustrated in Fig.1. The detrapping activation energy can be deduced by electrochemical permeation, gas-permeation, isothermal desorption, internal friction method, the first principle calculation and thermal desorption analysis (TDA), which can in principle distinguish different types of trapping sites unless the binding energies are too close to each other[83, 84]. TDA is performed by heating a hydrogen pre-charged sample at a constant ramp rate and derives a relation between hydrogen desorption rate and the specimen temperature. It is a very sensitive and accurate technique for studying hydrogen diffusion and trapping processes in crystalline and non-crystalline materials [85]. Thermal desorption spectrum (TDS) are usually composed of several desorption peaks, each of which can be associated with a different kinetic process. The main goal of a Thermal desorption spectrum (TDS) experiment is to identify the rate limiting step and to determine the kinetic parameters associated with the process [86]. According to thermal desorption analysis (TDA), the hydrogen trapping states and trapping sites such as dislocations, point defects, solutes and solute-defect composites, grain boundaries and interfaces between different phases can be obtained.

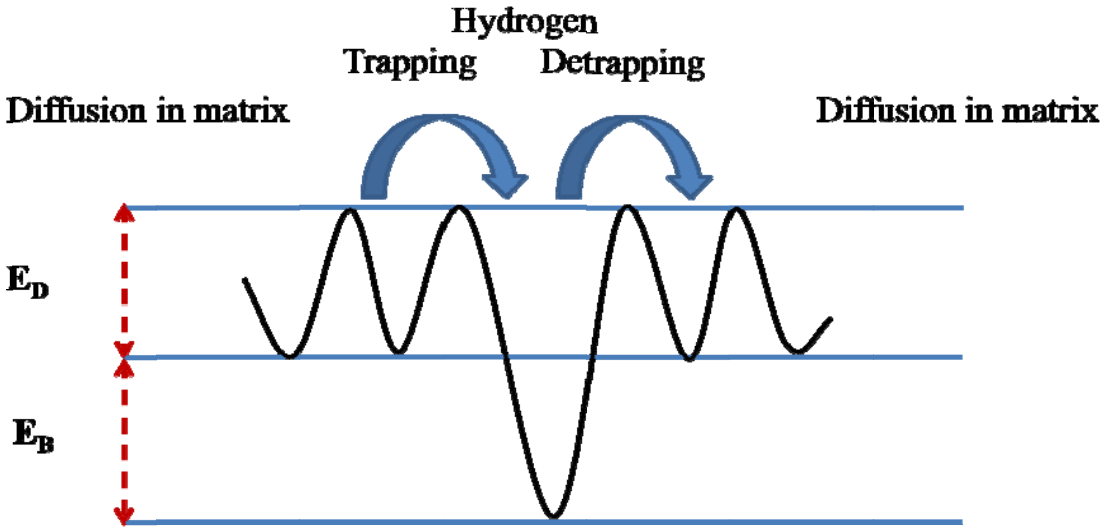

Fig. 1 Schematic illustration of the activation energies for hydrogen diffusion in matrix lattice, trapping by and detrapping from a trap site.

1.6 Main objectives of the present work

As introduced above, to the same trap sites, for example dislocation and grain boundary in ferritic steels, different hydrogen binding energies were obtained in the literatures. To understand the scatter of reported binding energy and effectively analyze the thermal desorption spectrum of hydrogen in ferritic and austenitic steels, the following main objectives are determined in the present research:

(1) To study the effects of specimen shape and size, and initial occupancy on thermal desorption spectrum of hydrogen.

(2) To evaluate the applicability of Kissinger formula as well as its derivative form, Choo-Lee plot, in the analysis of thermal desorption of hydrogen.

(3) To examine the effect of carbon segregation to dislocations on thermal desorption of hydrogen.

(4) To simulate and analyze the thermal desorption spectrum of hydrogen in the austenitic steels with and without pre-strain.

Reference

[1] Sieverts, A.: Z. The solubility of gases in metals. Metallk, 1929; 21: 37-46

[2] Quick, N. R. and Johnson, H. H.: Hydrogen and deuterium in iron, Acta Metall., 1978; 26: 903-907.

[3] W.A. Counts, C. Wolverton and R. Gibala, Acta Mater., 2010; 58: 4730-4741.

[4] J.P. Chateau, D. Delafosse and T. Magnin, Acta Mater., 2002; 50:1507-1522.

[5] Dr.-Ing. Afrooz Barnoush, Hydrogen embrittlement, December 1, 2011.

[6] Yu. Jagodzinski, H. Hänninen, O. Tarasenk and S. Smuk, Scripta mater. 2000; 43: 245-251.

[7] R. W. Cahn, and P. Haasen, Physical Metallurgy, Part II, North Holland, Amsterdam 1983.

[8] D. Delafosse, J.-P. Chatea, A. Chambreuil, and T. Magnin, Mater. Sci. Eng. 1997; A234-236: 889-892.

[9] S. M. Myers, M. I. Baskes, H. K. Birnbaum, J. W. Corbett, G. G. Delo, S. K. Estreicher, E. E. Haller, P. Jena, N. M. Johnson, R. Kirchheim, S. J. Pearton, and M. J. Stavola, Rev. Mod. Phys. 1992; 64: 559-617.

[10] W. A. Oates and H. Wenzl, Scripta Metall. Mater. 1994; 30: 851-854.

[11] P. Maerovic, R. B. McLellan, Acta Mater. 1998; 46: 5593-5597.

[12]Afrooz Barnoush , Horst Vehoff, Acta Mater., 2010; 58: 5274-5285.

[13] V. G. Gavriljuk, B. D. Shanina, V. N. Shyvanyuk and S. M. Teus, J. Appl. Phys., 2010;108: 083723 .

[14] P. J. Ferreira, I. M. Robertson and H. K. Birnbaum, Acta mater. 1998; 46:1749-1757,

[15] P. Novak, R.Yuan, B.P. Somerday, P. Sofronis and R.O. Ritchie, J. Mech. Phys. Solids, 2010; 58: 206-226.

[16]Dr.-Ing. Afrooz Barnoush, Hydrogen embrittlement, December 1, 2011.

[17] S. Gahr and H.K. Birnbaum, Acta Metall., 1978; 26: 1781-1788.

[18] D.S. Shih, I.M. Robertson, and H.K. Birnbaum, Acta Metall., 1988; 36: 111-124.

[19] R. Dutton, K. Nuttal, M.P. Puls, and L.A. Simpson, Metall.Trans. A, 1977; 8: 1553-1562.

[20] T.B. Flannagan, N. B. Mason, and H. K. Birnbaum, Scripta Metall.,1981; 15:

109-112.

[21] P.M. Novak, Dissertation, 2009.

[22] A.R. Troiano, Transactions of the American Society of Metals, 1960; 52: 54-80.

[23] R. A. Oriani and P. H. Josephic, Acta Metall., 1974; 22: 1065-1074.

[24] R. A. Oriani, Acta Metall., 1970;18: 147-157.

[25] P.J. Ferreira, I. M. Robertson and H. K. Birnbaum, Acta Mater., 1998; 46:1749-1757.

[26] E. Sirois and H. K. Birnbaum, Acta Metall. Mater, 1992; 40: 1377-1385.

[27] I. M Robertson, Engineering Fracture Mechanics, 2001; 68: 671-692.

[28] M. Nagumo, M. Nakamura and K. Takai, Metall. Mater. Trans. A, 2001; 32: 339-347.

[29] M. Nagumo, ISIJ Int., 2001; 41: 590-598.

[30] Y. Tateyama and T. Ohno, Phys. Rev. B 2003; **67**: 174105.

[31]S.M Myers et al, Review of modern physics, 1992; 64: 559-617.

[32] A. Juan, B. Irigoyen, S. Gesari, Appl. Surf. Sci., 2001; 172: 8-17.

[33] Shinya Taketomi, Ryosuke Matsumoto, Noriyuki Miyazaki, Acta Mater., 2008; 56: 3761-3769.

[34]Y. Ogino, M. Nagahama and T. Yamada, Transactions of the Japan Institute of Metals, 1988; 29: 540-552.

[35] W.Y. Choo and J.Y. Lee, Metall. Trans. A, 1982; 13A: 135-140.

[36]A. Zielinski, E. Lunarska, M. Smialowski, Acta Metall., 1997; 25:551-556.

[37]A.J. Kumnick and H.H. Johnson, Acta Metall., 1980; 28: 33-39.

[38]R. Gibala, A.J. Kumnick, Nace-5, Nace, Houston, TX, 1997: 244-268.

[39] K. Ono and M. Meshi, Acta Metall. Mater, 1992; 40: 1357-1364.

[40] S.M Myers et al, Review of modern physics, 1992; 64: 559-617.

[41] Yue-Lin Liu, Ying Zhang, Hong-Bo Zhou, and Guang-Hong Lu, Phys. Rev. B, 2009; **79**: 172103.

[42] S. Simonetti, C. Pistonesi, A. Juan, G. Brizuela, J. Phys. Chem. Solids, 2005; 66: 1240-1246.

[43] K. Sakaki, T. Kawase, M. Hirato, M. Mizuno, H. Araki, Y. Shirai and M. Nagumo, Scripta Mater., 2006; 55: 1031-1034.

[44] Masanao Iwamoto and Yuh Fukai, Mater. Trans., JIM, 1999; 40: 606- 661.

[45] Y. Fukai, K. Mori, H. Shinomiya, J. Alloys Compd., 2003; 348: 105-109.

[46] Yuh Fukai, J Alloys Compd.,1995; 231: 35-40.

[47] Besenbacher F, Myers SM, Nordlander P, Nørskov JK. J. Appl. Phys. 1987; 61: 1788-1794.

[48] W.A. Counts, C. Wolverton, R. Gibala, Acta Mater., 2010; 58: 4730-4741.

[49] Yoshitaka Tateyama and Takahisa Ohno, Phys. Rev. B, 2003; **67**: 174105-1: 9.

[50] W. T. Geng, A. J. Freeman, G. B. Olson, Y. Tateyama, and T. Ohno, 11th International Conference on Fracture 2005, ICF11. 2005; 5: 3305-3310.

[51] Y. Fukai, N. Okuma, Jpn. J. Appl. Phys., Part 2, 1993; 32: 1256-1259.

[52] S.M Myers et al, Review of modern physics, 1992; 64: 559-617.

[53] A.I. Shirley and C.K. Hall, Scr. Metall. 1983; 17: 1003-1008.

[54] A.I. Shirley and C.K. Hall, Acta. Metall. 1984; 32: 49-56.

[55] A.I. Shirley, C.K. Hall and N.J. Prince, Acta. Metall. 1983; 31: 1093-1098.

[56] W.A. Counts, C. Wolverton and R. Gibala, Acta Mater., 2010; 58: 4730-4741.

[57] W.A. Counts, C. Wolverton and R. Gibala, Acta Mater., 2011; 59: 5812-5820.

[58] S.B. Gesari, M.E. Prosato and A. Juan, 2002; 187: 207-217.

[59] J.K. Norkov, F. Besenbacher, J. Less, Commen Met., 1987; 130: 475-490.

[60] J.P. Hirth, Metall, Trans. A, 1980; 11: 861-890.

[61] G. Katano, K. Ueyama and M. Mori, J. Mater. Sci., 2001; 36: 2277-2286.

[62] W.Y. Choo and J.Y. Lee, Metall. Trans. A, 1982; 13A:135-140.

[63] K. Ono and M. Meshi, Acta Metall. Mater, 1992; 40:1357-1364.

[64] J.P. Hirth: Metall. Trans. A, 1980; 11A: 861-90.

[65] G.M. Pressouyre and I.M. Bernstein: Acta Metall., 1979; 27: 89-100.

[66]S. Yamasaki and T. Takahashi: Tetsu-to-Hagane, 1997; 83: 454-59.

[67] M. Ohnuma, J.I Suzuki, F.G. Wei and K. Tsuzaki, Scripta Materialia, 2008; 58: 142-145.

[68] G.M. Pressouyre and I.M. Bernstein: Metall. Trans. A, 1978; 9A: 1571-80.

[69] H.G. Lee and J.Y. Lee: Acta Metall., 1984; 32: 131-36.

[70] F.G Wei and K. Tsuzaki, Metall. Mater. Tran. A, 2004 ; 35A: 3155-3163.

[71] F.G Wei, T. Hara and K. Tsuzaki, Metall. Mater. Tran. A, 2004; 35B: 587-597.

[72] J. Takahashi, K. Kawakami, Y. Kobayashi and T. Tarui, Scripta Mater., 2010; 63: 261-264.

[73] B. Malard, B. Remy, C. Scott, A. Deschamps, J. Chene, T. Dieudonne, M.H. Mathon, Mate. Sci. Eng.A, 2012; 536: 110-116.

[74] T. Otsuka and T. Tanabe, J. Alloys Compd., 2007; 446−447: 655-659.

[75] K. Takai, G. Yamauchi, M. Nakamura and M. Nagumo, J. Japan Inst. Metals, 1998; 62: 267-275.

[76]G. W. Hong and J.Y. Lee, J. Mat. Sci., 1983; 18: 271-277.

[77] J.P. Hirth: Metall. Trans. A, 1980; 11A: 861-890.

[78] S.L.I. Chan, H.L. Lee and J.R. Yang, Metal. Trans. A, 1991; 22A: 2579-2586.

[79] H. Tsubakino and H. Harada, Tetsu to Hagane, Vol, 1997;83, No.9: 587-592.

[80]H. Tsubakino, H. Harada and J. Yin, ISIJ Int., 1999; 39: 298-300.

[81]Y. D. Park, I.S. Maroef, A. Landau and D.L. Olson, Welding Research, 2002: 27-35.

[82] D. Pérez Escobar, T. Depover, L. Duprez, K.Verbeken and M. Verhaege, Acta Mate., Issues 6-7, 2012; 60: 2593-2605.

[83] F.G. Wei, T. Hara and K. Tsuzaki, Metall. Mater. Trans. B, 2004; 35B: 587-597.

[84]M. Enomoto, D. Hirakami and T. Tarui, ISIJ Int. 2006; 46: 1381-1387.

[85]E. Tal-Gutelmacher, D. Eliezer and E. Abramov, Mater. Sci. Eng., A, 2007, 445-446: 625-631.

[86] F. J. Castro and G. Meyer, J. Alloys Compd., 2002; 330-332: 59-63.

Chapter 2

Methods of Thermal Desorption Analysis

Four methods have been utilized to analyze the thermal desorption spectrum (TDS) to obtain the activation energy of hydrogen detrapping from the trap sites.

2.1 Choo-Lee plot

This method is based on the reaction kinetics represented by the formula [1],

$$\frac{dX}{dt} = A(1-X)exp(-\frac{E_d}{RT}) \quad (1)$$

where X is the fraction of the exhausted reactant of interest, here hydrogen; A is a constant; R is the gas constant and T is the absolute temperature. At a constant heating rate ($\emptyset$), the peak temperature of the maximum hydrogen evolution rate and the activation energy of the hydrogen detrapping from the trap site can be depicted from the equation as,

$$\frac{d(ln\emptyset/T_p^2)}{d(1/T_p)} = -\frac{E_d}{R} \quad (2)$$

Given different ramp rates, the Arrhenius plot of $ln\emptyset/T_p^2$ against $1/T_p$ will yield the activation energy of detrapping. This method was firstly applied by Choo-Lee to analyze the activation energy of hydrogen detrapping from grain boundary, dislocation and microvoid in deformed pure iron [2]. They are 17.2kJ/mol, 26.8kJ/mol and 35.2kJ/mol, respectively. The detrapping energy of hydrogen from coherent (V, X)C precipitate in a 0.4C-1.0Cr-0.7Mo-0.35V steel is about 29.2kJ/mol [12]. The activation energy for hydrogen desorption from incoherent TiC particles is 86.9kJ/mol [13]. The interfaces between ferrite and Fe_3C and/or interface dislocations located between Fe_3C lamellae in cold-drawing pearlite show the hydrogen binding energy of 65.0kJ/mol [14]. For undeformed TRIP steel, the activation energy for hydrogen trap sites, such as dislocation, grain boundary and retained austenite, are 33±5kJ/mol, 28±5kJ/mol and 90±25kJ/mol, respectively [15].

2.2 Oriani's local equilibrium model

This model is based on the diffusion equation with Oriani's local equilibrium

hypothesis between the hydrogen concentrations in the trap sites and in the matrix interstitial sites [6]. Local equilibrium between the two atomic populations means each one occupying a fraction θ_i, of the available sites, can be described by the equilibrium constants, $K=a_x/a_L$, where a_x and a_L are the activities of the hydrogen upon the trapping sites and upon the normal lattice interstitial sites, respectively. Each of the activities can be expressed in terms of fractional occupancies as $a_i=\theta_i/(1-\theta_i)$. Since the occupancy in the lattice site is far small than unity so that local equilibrium concentration of hydrogen is described as,

$$K = \frac{1}{\theta_L}\left(\frac{\theta_x}{1-\theta_x}\right) = exp\ (\frac{E_b}{RT}) \tag{3}$$

where E_b is the binding energy of hydrogen to the trap sites. Based on this, the effective diffusivity D_{eff} is designed to describe the hydrogen diffusion in the specimen,

$$D_{eff} = D_0/(1 + \frac{N_x}{N_L}K) \tag{4}$$

where D_0 is the normal hydrogen diffusivity in the matrix lattice, N_x and N_L are the trap sites and the lattice interstitial sites densities, respectively. Then, desorption of hydrogen from the specimen can be calculated by solving the diffusion equation with the effective diffusivity to fit the experimental data. An approximate desorption rate for the plate specimen was derived by Ono and Meshii [7] as,

$$\frac{\partial c_L}{\partial t} = -\left(\frac{\pi}{2d}\right)^2 D_{eff}(c - c_0) \tag{5}$$

where d is the half thickness of the plate; and c_0 is the equilibrium concentration of hydrogen in the lattice under the hydrogen atmosphere. By means of this method, they found that the binding energy of hydrogen with grain boundaries in polycrystalline iron and dislocations in single crystal iron are 0.51±0.02eV and 0.47±0.02eV, respectively.

However, the validity of the local equilibrium hypothesis in modeling hydrogen thermal desorption spectrum has been recently questioned [11]. It is concluded that the local equilibrium hypothesis does not hold generally in the thermal desorption process, in particular, for a thin specimen.

2.3 Kissinger formula

This method actually is one application of Eq.1. Different from Choo-Lee method only one set of experimental data are needed in this case. *dX/dt* is plotted against *T* with an appropriate choice of the activation energy E_d and the constant *A* at a given heating rate to fit the experimental data. The value of *X* is defined by c/c_{Total}, where *c* is the content of the hydrogen released and c_{Total} is the total amount of hydrogen trapped by one kind of traps in the specimen before desorption. A set of E_d and *A* values are obtained to fitting the experimental data, as well as the total hydrogen amount [8, 9]. This method has been applied by Wei *et al* [8] to steels with Ti additions. Desorption activation energy for incoherent TiC particles in the well-tempered 0.05C-0.22Ti-2.0Ni steel is 85.7kJ.mol. In the same steel, the activation energy for the grain boundary and dislocation is 21.9kJ/mol. In the 0.42C-0.30Ti steel, the activation energy is 116kJ/mol when tempering temperature is equal and larger than 650^{o}C and decrease to 68kJ/mol when the tempering temperature decreasing to 500^{o}C. In this steel, the averaged activation energy for grain boundary and dislocation is about 32kJ/mol. The activation energy for coherent TiC particles does not change significantly with tempering temperature. It increases from 46 kJ/mol at 500°C to 59 kJ/mol at 550°C and gradually decreases to 54kJ/mol at 700°C. This method was also applied to study the hydrogen trapping capacity in a tempered Fe-0.2C marteniste [10]. The average activation energy for hydrogen desorption from dislocations is 33.9kJ/mol.

2.4 McNabb and Foster model

The McNabb-Foster theory is expressed as follows [3-5],

$$\frac{\partial c}{\partial t} + N_t \frac{\partial \theta_t}{\partial t} = D\nabla^2 c \tag{6}$$

$$\frac{\partial \theta_t}{\partial t} = kc(1-\theta_t) - p\theta_t \tag{7}$$

$$k = k_0 \exp(-\frac{E_D}{RT}) \tag{8}$$

$$p = p_0 \exp(-\frac{E_d}{RT}) = p_0 \exp(-\frac{E_B + E_D}{RT}) \tag{9}$$

$$D = D_0 \exp(-\frac{E_D}{RT}) \tag{10}$$

where c is the hydrogen concentration in the lattice, N_t is the density of trap sites, θ_t is the occupancy fraction at the trap site, D is the diffusivity of hydrogen in normal lattice. k and p represent the probability of hydrogen jumping from the lattice to trap sites and the probability of hydrogen releasing from trap sites, respectively. E_B is the binding energy of the trap site, E_D is the activation energy of lattice diffusion, E_d is the activation energy of detrapping and D_0 the pre-exponential factor. Measured TDA spectra are fitted by this model with reasonable parameters including the activation energy of hydrogen detrapping, determined by trial and error. Recently, by means of this model, Enomoto *et al* [16, 17] simulated the thermal desorption spectra of SCM435 steel and 0.8%C steel, and of high strength martensitic steels.

2.5 Numerical solution of McNabb and Foster model

For a cylindrical specimen with radius r_0, the Laplacian in Eq.1 can be written as,

$$\Delta = \frac{\partial^2 c}{\partial r^2} + \frac{1}{r}\frac{\partial c}{\partial r} \tag{11}$$

The dimensionless time is define by,

$$\tau = \frac{\int_0^t D dt}{r_0^2} \tag{12}$$

is used throughout the calculation, also the radial coordinate r_0 is normalized as $\rho = r/r_0$. Then, Eqs.1 and 2 are reduced to,

$$\frac{\partial c}{\partial \tau} + \frac{\partial c^t}{\partial \tau} = \frac{\partial^2 c}{\partial \rho^2} + \frac{1}{\rho}\frac{\partial c}{\partial \rho} \tag{13}$$

$$\frac{\partial c^t}{\partial \tau} = N_t k' c(1-\theta_t) - N_t p' \theta_t \tag{14}$$

$$k' = \frac{r_0^2}{D} k \tag{15}$$

$$p' = \frac{r_0^2}{D} p \tag{16}$$

Since Eq.14 is nonlinear with respect to the hydrogen concentration, Eqs.13 and 14 are solved by the finite difference method which combines the forward and backward differences called DuFort-Frankel method [18]. In this method the 2nd derivative of the

concentration with respect to the spatial coordinate is calculated from the equation,

$$\frac{\partial^2 c}{\partial \rho^2} \approx \frac{c(\rho+\Delta\rho,\tau)+c(\rho-\Delta\rho,\tau)-c(\rho,\tau+\Delta\tau)-c(\rho,\tau-\Delta\tau)}{\Delta\rho^2} \quad (17)$$

the 1st derivatives of concentrations of hydrogen in lattice site and trap site with respect to the spatial coordinate and deduced dimensionless time become,

$$\frac{\partial c}{\partial \rho} = \frac{c(\rho+\Delta\rho,\tau)-c(\rho-\Delta\rho,\tau)}{2\Delta\rho} \quad (18)$$

$$\frac{\partial c}{\partial \tau} = \frac{c(\tau+\Delta\tau,\rho)-c(\tau-\Delta\tau,\rho)}{2\Delta\tau} \quad (19)$$

$$\frac{\partial c^t}{\partial \tau} = \frac{c^t(\tau+\Delta\tau,\rho)-c^t(\tau-\Delta\tau,\rho)}{2\Delta\tau} \quad (20)$$

This procedure makes the solution stable in principle for all $\lambda=\Delta\tau/\Delta\rho^2$ values and thus, can take a larger time interval to reduce the computation time [16]. Then, the discretized equations for hydrogen concentrations in the matrix and trapping sites are written in terms of dimensionless variables as,

$$\begin{aligned}(1+2\lambda+\frac{\alpha k'\Delta\tau}{1+k'\Delta\tau c_{i,j}+p'\Delta\tau})c_{i,j+1} &= \frac{2(k'c_{i,j}+p')\Delta\tau}{1+k'\Delta\tau c_{i,j}+p'\Delta\tau}c^t_{i,j+1}\\ &+(1-2\lambda-\frac{\alpha k'\Delta\tau}{1+k'\Delta\tau c_{i,j}+p'\Delta\tau})c_{i,j-1}\\ &+(2+\frac{1}{i})\lambda c_{i+1,j}+(2-\frac{1}{i})\lambda c_{i-1,j}\end{aligned} \quad (21)$$

$$c^t{}_{i,j+1} = \frac{\alpha k'\Delta\tau}{1+k'\Delta\tau c_{i,j}+p'\Delta\tau}(c_{i,j+1}+c_{i-1,j})+\frac{1-k'\Delta\tau c_{i,j}-p'\Delta\tau}{1+k'\Delta\tau c_{i,j}+p'\Delta\tau}c^t_{i,j-1} \quad (22)$$

where i is the grid number of the radial coordinate and j is the reduced dimensionless time step. The amount of hydrogen desorbed from the specimen surface per unite time is calculated as,

$$E = 2\pi r_0 lJ = -2\pi lD(\frac{\partial c}{\partial \rho})_{\rho_0} \approx -2\pi lD\frac{c_{i_0-1,j}-c_s}{\left(1+\frac{1}{2i_0}\right)\Delta\rho} \quad (23)$$

where i is the grid number at the surface, l is the length of the specimen and c_s is the hydrogen concentration at the surface, which is assumed to be zero in the calculation.

When m kinds of trap sites exist in the specimen, the discretized equations for

hydrogen concentrations in the matrix and trapping sites are written in terms of dimensionless variables as,

$$(1+2\lambda+\sum_m \frac{\alpha_m k'_m \Delta\tau}{1+k'_m \Delta\tau c_{i,j}+p'_m \Delta\tau})c_{i,j+1} = \sum_m \frac{2(k'_m c_{i,j}+p'_m)\Delta\tau}{1+k'_m \Delta\tau c_{i,j}+p'_m \Delta\tau} c^m_{i,j+1}$$
$$+(1-2\lambda-\sum_m \frac{\alpha_m k'_m \Delta\tau}{1+k'_m \Delta\tau c_{i,j}+p'_m \Delta\tau})c_{i,j-1} \quad (24)$$
$$+(2+\frac{1}{i})\lambda c_{i+1,j}+(2-\frac{1}{i})\lambda c_{i-1,j}$$

$$c^m{}_{i,j+1} = \frac{\alpha_m k'_m \Delta\tau}{1+k'_m \Delta\tau c_{i,j}+p'_m \Delta\tau}(c_{i,j+1}+c_{i-1,j})+\frac{1-k'_m \Delta\tau c_{i,j}-p'_m \Delta\tau}{1+k'_m \Delta\tau c_{i,j}+p'_m \Delta\tau} c^m_{i,j-1} \quad (25)$$

Reference

[1] H.E. Kissinger, Analysis Chemistry, 1957; 29(11): 1702-1706.

[2] W.Y. Choo and J.Y. Lee, Metall. Trans. A, 1982; 13A:135-140.

[3] A. McNabb --and P.K. Foster: Trans. TMS-AIME, 1963; 227: 618-27.

[4] K.L. Wilson and M.I. Baskes: J. Nucl. Mater., 1978; 76-77:291-97.

[5] A. Turnbull, R.B. Hutchings, and D.H. Ferriss: Mater. Sci. Eng. A, 1997; A238: 317-28.

[6] R.A. Oriani, Acta Metall., 1970; 18: 147-57.

[7] K. Ono and M. Meshii, Acta Metall., 1992; 40:1357-64.

[8] F.G. Wei, T. Hara and K. Tsuzaki, Metal. Mater. Tran. B, 2004; 35B: 587-597.

[9] F.G. Wei, M. Enomoto and K. Tsuzaki, Computational Materials Science, 2012; 51: 322-330.

[10] F.G. Wei and K. Tsuzaki, Scripta Mater., 2005; 52: 467-472.

[11] K.I. Ebihara, H. Kaburaki, T. Suzudo and K. Takai, ISIJ Int., 2009; 49: 1907-1913.

[12] T. Tsuchida, T. Hara, and K. Tsuzaki: Tetsu-to-Hagane, 2002; 88: 771-78.

[13] H.G. Lee and J.Y. Lee: Acta Metall., 1984; 32: 131-36.

[14] K. Takai and R. Watanuki: Iron Steel Inst. Jpn. Int., 2003; 43: 520-26.

[15]D. Pérez Escobar, T.Depover, L.Duprez, K.Verbeken and M.Verhaege, Acta Mater., 2012; 60: 2593-2605.

[16] M. Enomoto, D. Hirakami and T. Tarui, ISIJ Int., 2006; 46:1381-1387.

[17]M. Enomoto, D.Hirakami and T. Tarui, Metall. Mater. Trans., 2012; 43: 572-581.

[18] G. E. Forsythe and W. R. Wasow: Finite-Difference Methods for Partial Differential Equations, John Wiley & Sons, New York, 1960:124.

Chapter 3

Effects of Specimen Shape, Size and Initial Occupancy on the Thermal Desorption Spectrum of Hydrogen

3.1Introduction

Thermal desorption analysis (TDA) is widely used to analyze where hydrogen atoms reside, e.g. the trapping of hydrogen, in materials. While the temperature and shape of thermal desorption peak is related to represent the energy and density of trap sites, they depend on the size and shape of specimen and the condition of hydrogen-charge and thermal analysis, e.g. ramp rate. In this Chapter, the thermal desorption spectrum (TDS) of hydrogen in the plate, rectangular, cylindrical and spherical specimens are simulated varying specimen size, ramp rate and initial hydrogen occupancy (the ratio of the amount of the hydrogen to the trap density) by McNabb-Foster equations introduced as follows,

$$\frac{\partial c}{\partial t} + N_t \frac{\partial \theta_t}{\partial t} = D \nabla^2 c \tag{1}$$

$$\frac{\partial \theta_t}{\partial t} = kc(1-\theta_t) - p\theta_t \tag{2}$$

$$k = k_0 \exp\left(-\frac{E_D}{RT}\right) \tag{3}$$

$$p = p_0 \exp\left(-\frac{E_d}{RT}\right) = p_0 \exp\left(-\frac{E_B + E_D}{RT}\right) \tag{4}$$

The Laplacian can be written as,

$$\left(\frac{\partial^2 c}{\partial x^2}\right) \quad \text{for a plate;} \tag{5}$$

$$\left(\frac{\partial^2 c}{\partial r^2} + \frac{2}{r}\frac{\partial c}{\partial r}\right) \quad \text{for a sphere;} \tag{6}$$

$$\left(\frac{\partial^2 c}{\partial r^2} + \frac{1}{r}\frac{\partial c}{\partial r}\right) \quad \text{for a cylinder;} \tag{7}$$

and

$$\left(\frac{\partial^2 c}{\partial x^2}+\frac{\partial^2 c}{\partial y^2}\right) \text{ for a rectangle, respectively.} \quad (8)$$

3.2 Effect of specimen shape and size

3.2.1 Detrapping-controlled desorption

In this simulation, two binding energies 40kJ/mol 60kJ/mol were utilized. They are both the possible binding energy of hydrogen to dislocation core. For each binding energy p_0 value is assumed be $30s^{-1}$ and $3x10^5s^{-1}$, respectively, to achieve the detrapping-controlled and diffusion-controlled desorption. This will be explained later. Hydrogen diffusivity in the pure iron lattice is chosen to be $5.8x10^{-8}$exp(-4.5kJ/mol) m^2/s [1]. For detrapping-controlled desorption, hydrogen diffusion in the matrix and hydrogen retrapping by the trap sites can be ignored; for diffusion-controlled desorption, equilibrium is held between hydrogen concentrations in the trap sites and matrix lattice sites, the effective diffusivity is used to describe the hydrogen evolution behavior in the matrix with trap sites.

For detrapping-controlled desorption, hydrogen concentration in the matrix lattice during desorption was much smaller than the concentration equilibrium with hydrogen concentration in the trap sites. Equilibrium concentration in the matrix lattice with hydrogen concentration in the trap sites was calculated by the Oriani's local equilibrium model. Fig.1a shows that for the chosen parameters for detrapping-controlled desorption the thermal desorption spectra are almost the same for all specimens of different shape; and meanwhile the ratio of the hydrogen concentration in the matrix to the equilibrium concentration is much smaller than one as shown in Fig.1b. However, when specimen size increases, the hydrogen diffusion time in the lattice is increased and also the hydrogen retrapping probability at the trap sites is increased as a result. Therefore, the hydrogen desorption will deviate from the detrapping-controlled mechanism. As shown in Fig.2b, the ratio of hydrogen in the matrix lattice to the equilibrium concentration became significant in the larger specimen. Meanwhile, the specimen in different shape showed different thermal desorption spectrum with the different peak temperature and shape as shown in Fig.2a.

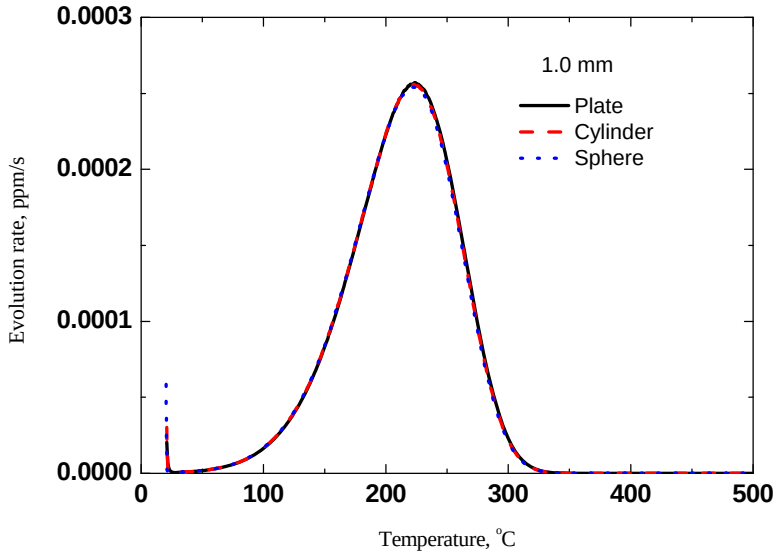

(a)

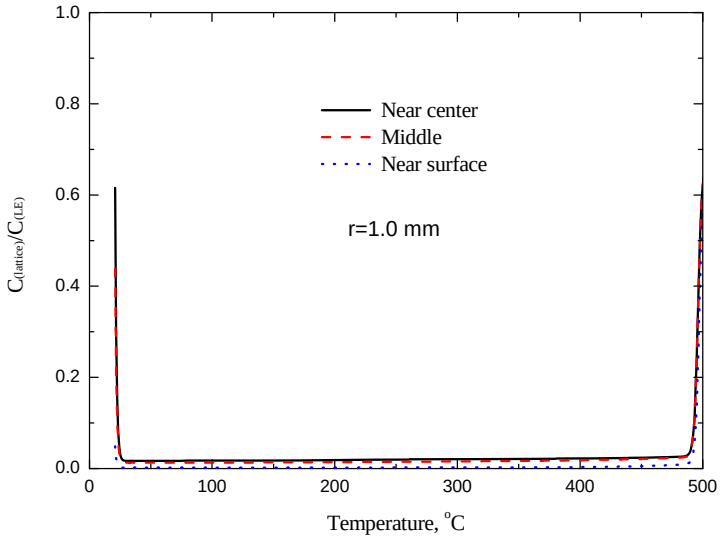

(b)

Fig.1 a) Thermal desorption spectra of plate with half-thickness of 1.0mm, cylinder and sphere with the same radius of 1.0mm; b) state of local equilibrium during thermal desorption for plate specimen with size of 1.0 mm. The matrix is ferrite with the trap sites of binding energy 40kJ/mol to hydrogen; the total hydrogen amount is 1.0ppm for all the specimens; the initial occupancy in the trap site is 0.1166; the ramp rate is 100^{o}C/hr and the p_0 value is $30s^{-1}$.

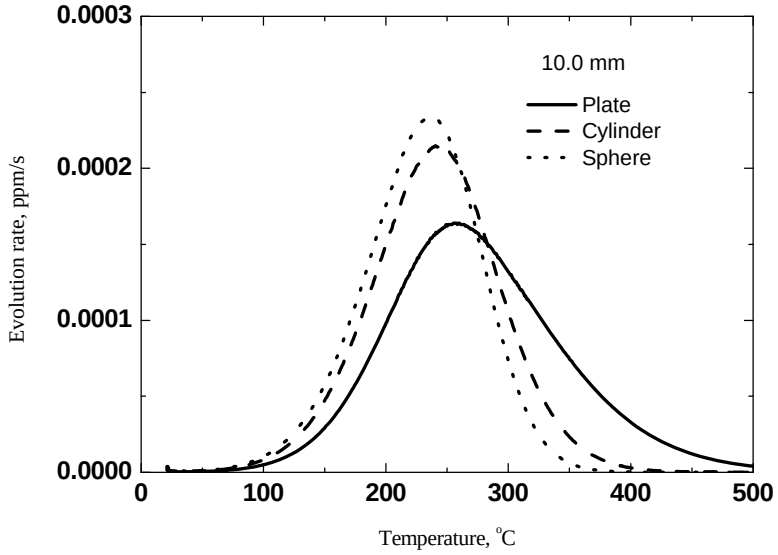

(a)

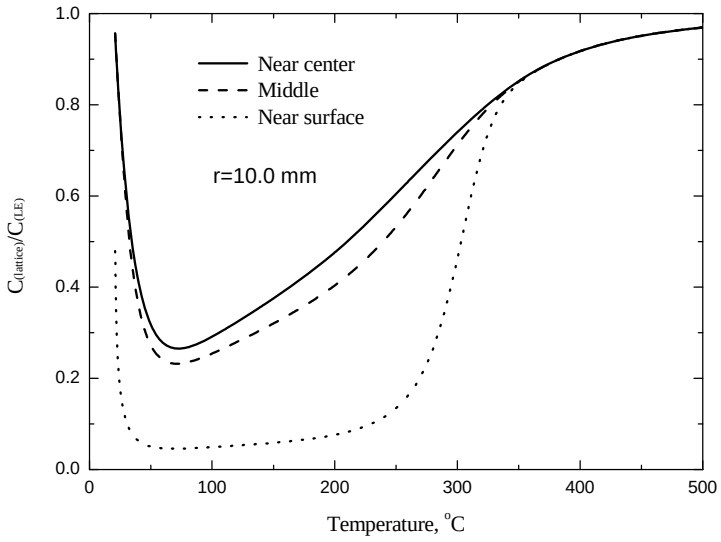

(b)

Fig.2 a) Thermal desorption spectra of plate with half-thickness of 10.0mm, cylinder and sphere with the same radius of 1.0mm; b) state of local equilibrium during thermal desorption for plate specimen with size of 10.0 mm. The matrix is ferrite with the trap sites of binding energy 40kJ/mol to hydrogen; the total hydrogen amount is 1.0ppm for all the specimens; the initial occupancy in the trap site is 0.1166; the ramp rate is 100^{o}C/hr and the p_0 value is $30s^{-1}$.

3.2.2 Diffusion-controlled desorption

For diffusion-controlled desorption, hydrogen desorption away from specimen is controlled by hydrogen diffusion in matrix lattice. Fig.3a shows TDS of a plate specimen with half-thickness of 1.0 mm, and cylindrical and spherical specimens with radii of 1.mm. Fig.3b shows that the ratio of hydrogen concentration in matrix lattice to hydrogen equilibrium concentration with hydrogen concentration in trap sites was almost 1 for all specimens, which means local equilibrium of hydrogen concentrations in trap sites and matrix lattice was held throughout hydrogen desorption.

Fig.4a shows TDS of a plate specimen with half-thickness of 10.0 mm, and cylindrical and spherical specimens with radii of 10.mm. Fig.4b shows that the ratio of hydrogen concentration in matrix lattice to hydrogen equilibrium concentration with hydrogen concentration in trap sites was also almost 1 for all specimens, which means local equilibrium of hydrogen concentrations in trap sites and matrix lattice was held throughout hydrogen desorption.

Different from detrapping-controlled desorption, hydrogen desorption spectrum of smaller specimen in different shape was different from each other. TDS peak temperature increased in the order of sphere, cylinder and plates. The larger specimens showed the same phenomena. This is because hydrogen spatial distributions are different among plate, cylindrical and spherical specimens.

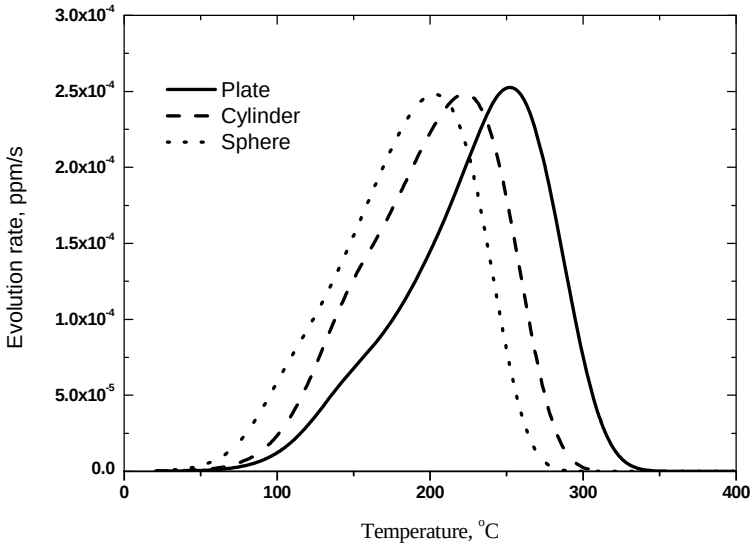

(a)

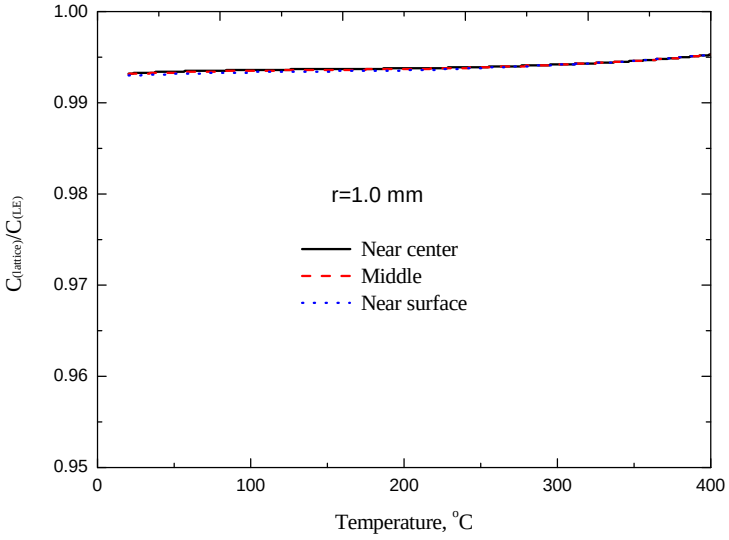

(b)

Fig.3 a) Thermal desorption spectra of plate with half-thickness of 1.0mm, cylinder and sphere with the same radius of 1.0mm; b) state of local equilibrium during thermal desorption for plate specimen with size of 1.0 mm. The matrix is ferrite with the trap sites of binding energy 60kJ/mol to hydrogen; the total hydrogen amount is 1.0ppm for all the specimens; the initial occupancy in the trap site is 0.1166; the ramp rate is 100°C/hr and the p_0 value is $3x10^5 s^{-1}$.

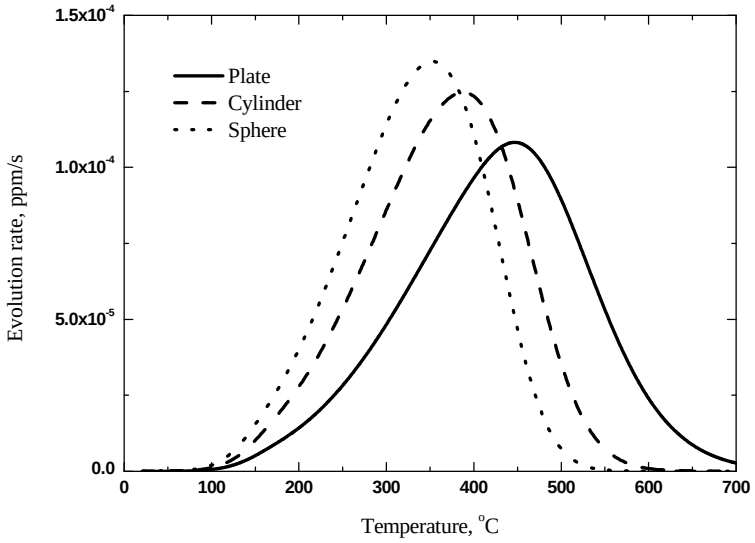

(a)

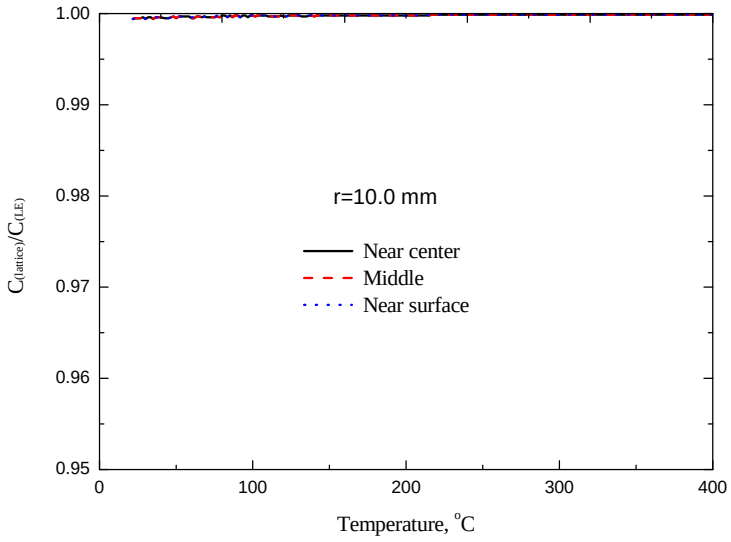

(b)

Fig.4 a) Thermal desorption spectra of plate with half-thickness of 10.0mm, cylinder and sphere with the same radius of 1.0mm; b) state of local equilibrium during thermal desorption for plate specimen with size of 10.0 mm. The matrix is ferrite with the trap sites of binding energy 60kJ/mol to hydrogen; the total hydrogen amount is 1.0ppm for all the specimens; the initial occupancy in the trap site is 0.1166; the ramp rate is 100°C/hr and the p_0 value is $3x10^5 s^{-1}$.

3.2.3 Rectangular specimen

Fig. 5a shows the schematic of the rectangular rod of varying aspect ratio and the cylindrical specimen. They have the same area of sections. It is found that in the detrapping-controlled desorption, TDS of the rectangular rods and the cylindrical specimen are almost the same. However, the peak temperature decreased with the increasing aspect ratio in diffusion-controlled desorption parameters. In other words, the peak temperature moves to the left with increasing ratio.

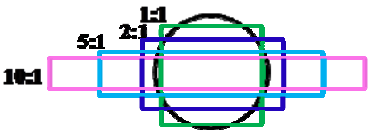

(a)

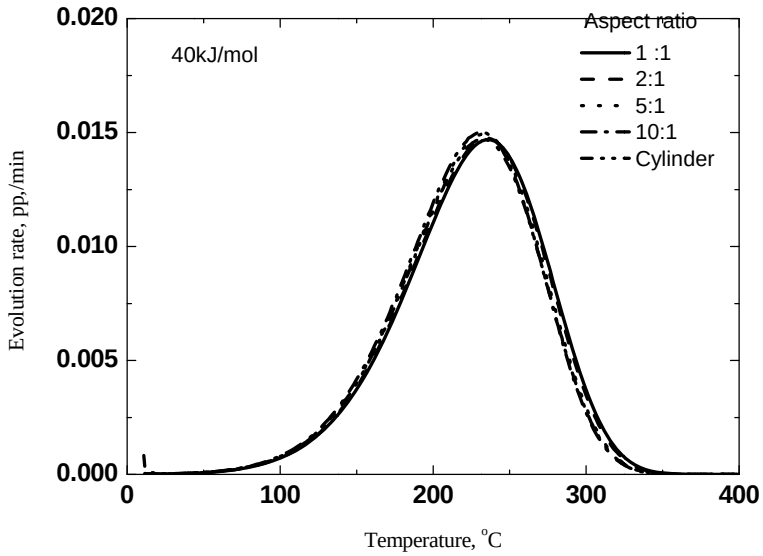

(b)

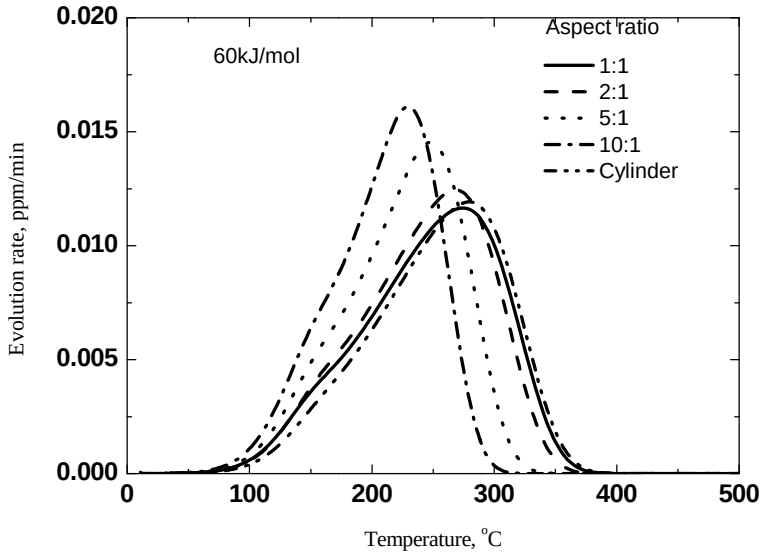

(c)

Fig.5 a) Schematic of the rectangular rod of varying aspect ratio and the cylindrical specimen with the same area, thermal desorption spectra of these specimens b) in the detrapping-controlled desorption c) diffusion-controlled desorption. Total hydrogen amount is 1.0ppm; initial occupancy in the trap site is 0.1166; the ramp rate is 100°C/hr.

3.3 The effect of initial occupancy

3.3.1 Constant amount of hydrogen with varying trap site density

Firstly, the density of trap sites is varied keeping the amount of hydrogen constant. For detrapping-controlled desorption, specimens with different initial occupancies showed almost the same TDS, see Fig.6a. However, the further increase in the trap site density decreased initial occupancy to a very small lever, e.g., 0.012 and 0.0012. Then, TDS peak temperature shifted to higher temperature because the possibility of hydrogen retrapping at the trap sites increased.

In the case of diffusion-controlled desorption, the peak temperature of TDS increased with deceasing initial occupancy, i.e. increasing trap site density, see Fig.6b. This can be seen from the equation of effective diffusivity,

$$D_{app}^{H} = D^{H}[1 + \frac{N_T}{N_L} exp\,(\frac{E_b}{RT})]^{-1}$$

which indicates that the effective diffusivity decreases with increasing trap sites density. Hence, TDS will be shifted to the higher temperature when the trap sites density increases.

3.3.2 Constant trap site density with varying hydrogen amount

For detrapping-controlled desorption, peak temperatures of the specimens are the same but evolution rate increases with hydrogen amount as shown in Fig.7a. However, for diffusion-controlled desorption, peak temperature increases with decreasing initial occupancy due to the higher retrapping possibility at the trap sites, which delays the hydrogen desorption from the specimen , see Fig.7b.

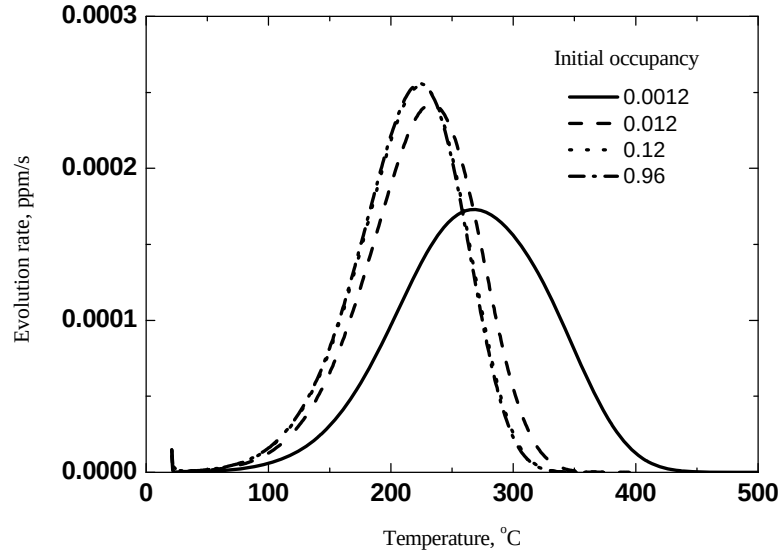

(a)

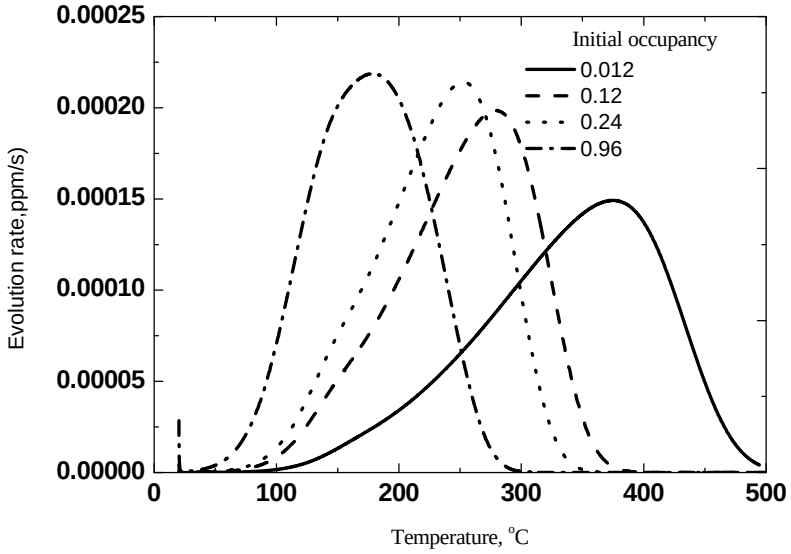

(b)

Fig.6 The influence of the initial occupancy at a fixed initial hydrogen content on the thermal desorption spectra of cylindrical specimen, a) for detrapping controlled desorption and b) for diffusion controlled desorption. The hydrogen content is 1.0ppm; the radius of cylinder is 2.5mm and the ramp rate is 100^{o}C/hr. The trap site density is changed to obtain the same hydrogen content but different initial occupancy.

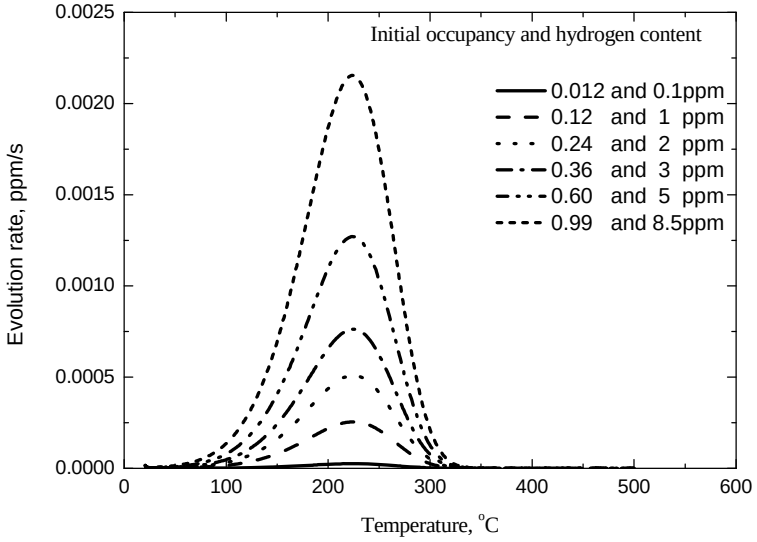

(a)

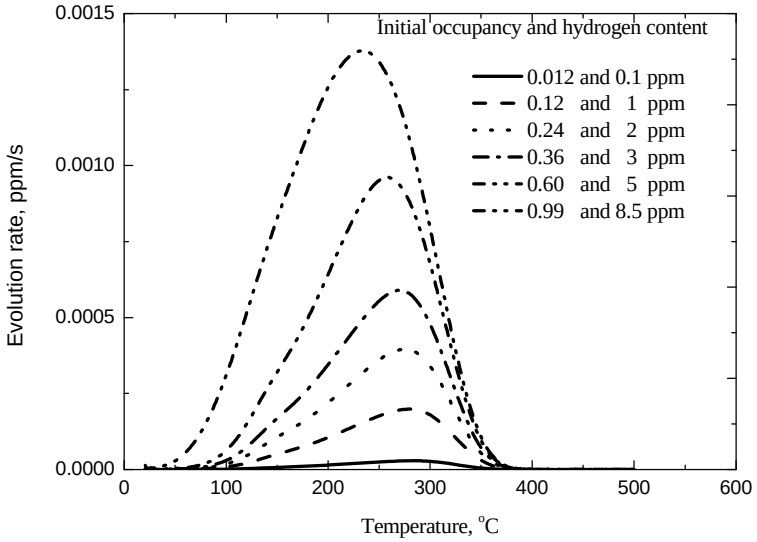

(b)

Fig.7 The influence of the initial occupancy at a fixed trap site density on the thermal desorption spectra of cylindrical specimen, a) for detrapping controlled desorption and b) for diffusion controlled desorption. The radius of cylinder is 2.5mm and the ramp rate is 100^{o}C/hr. The hydrogen content is changed with occupancy.

3.4 The effect of initial distribution

Practically, it is interesting to see the influence of initial distribution of hydrogen on TDS because experimental condition and external condition, under which hydrogen is absorbed into material during service, varies widely. Fig.8a shows three initial hydrogen distributions in the trap sites in the cylindrical specimens, uniform distribution, distributions only in the center and only in the rim of the specimen. In order to achieve the same hydrogen content in all specimens, the hydrogen concentrations are varied from each other in the cylindrical specimen. It is found that in Fig.8b for detrapping-controlled desorption, the spectra are almost the same. However, for diffusion-controlled desorption, the peak shape is considerably different from each other. The peak temperature is lowest in the specimen in which hydrogen was distributed in the rim initially.

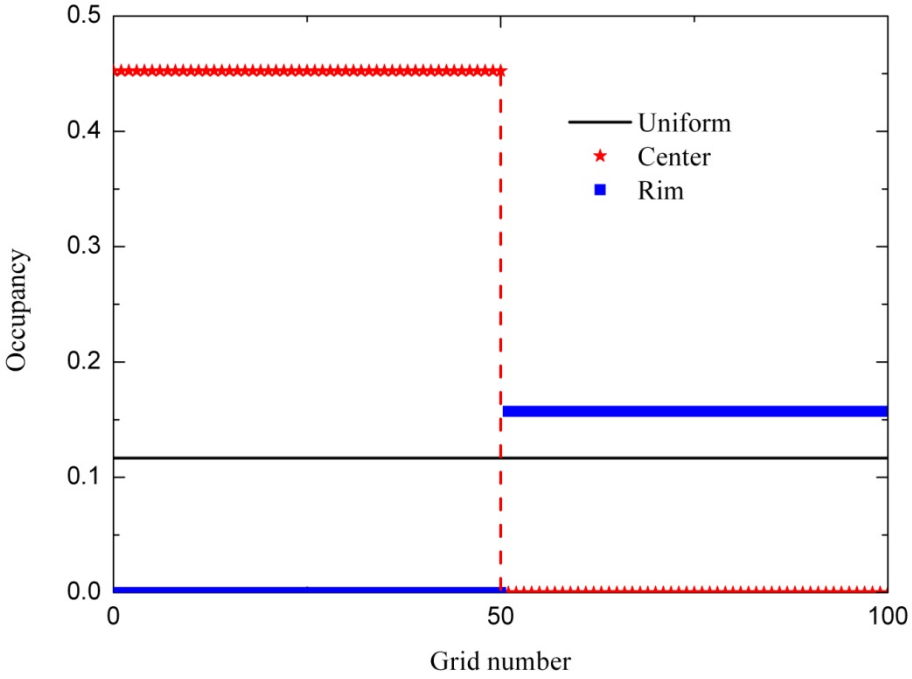
0.5
0.4
0.3
0.2
0.1
0.0
Occupancy
0
50
100
Grid number
Uniform
Center
Rim

(a)

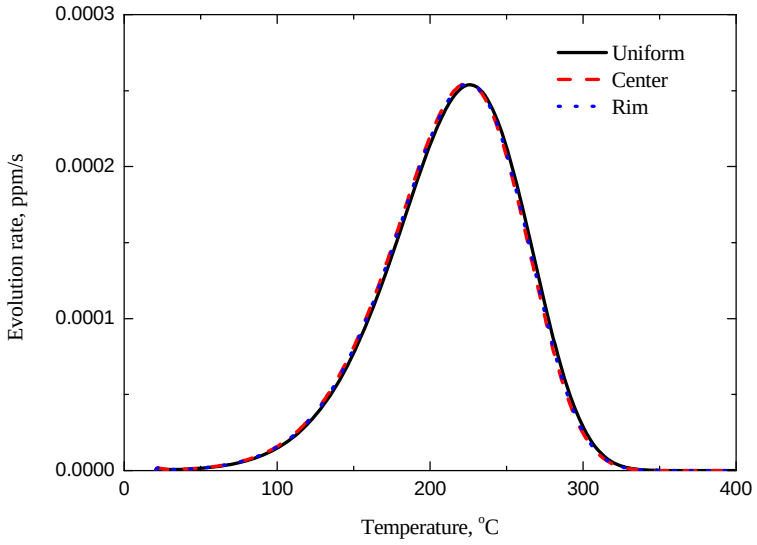
0.0003
0.0002
0.0001
0.0000
Evolution rate, ppm/s
0
100
200
300
400
Temperature, °C
Uniform
Center
Rim

(b)

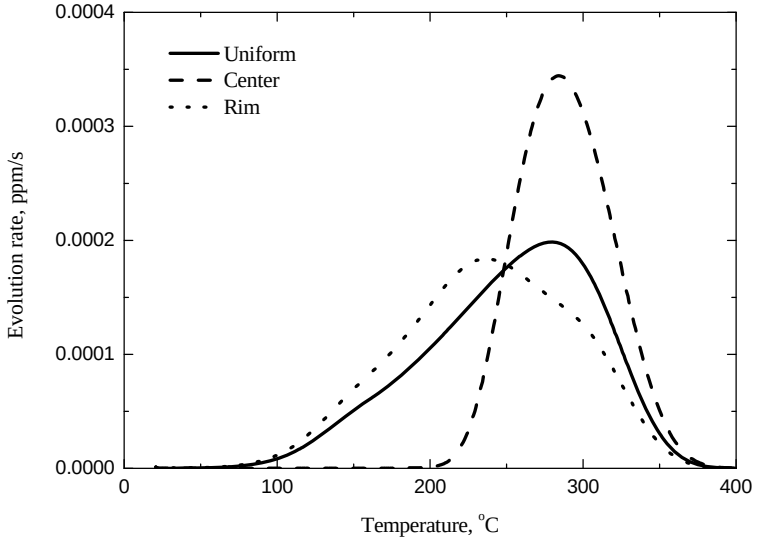

(c)

Fig.8 The influence of the initial distribution at a fixed hydrogen content on the thermal desorption spectra of cylindrical specimen, a) three different initial hydrogen distributions, thermal desorption spectra b) for detrapping controlled desorption and c) for diffusion controlled desorption. The hydrogen content is 1.0ppm; the radius of cylinder is 2.5mm and the ramp rate is 100°C/hr.

3.5 Summary

In detrapping-controlled desorption, specimen shape and size have no effects on TDS. However, when hydrogen diffusion time in the matrix cannot be ignored as specimen size increases, hydrogen desorption will deviate from detrapping-controlled desorption. For diffusion-controlled desorption, peak temperature of TDS increases with specimen size. Meanwhile, with the same radius or half-thickness, peak temperature increases in the order of sphere, cylinder and plate.

In detrapping-controlled desorption, initial occupancy and trap site density have no effects on TDS. However, when trap site density remarkably increases hydrogen re-trapping at the trap site will induce the TDS to shift to the higher temperature. For diffusion controlled desorption, at constant initial hydrogen content, peak temperature increases with trap sites density. And at constant trap site density, peak temperature increases with decreasing initial occupancy.

In detrapping-controlled desorption, initial hydrogen distribution in the trap site have no effects on TDS. The peak temperature is lowest in the specimen in which hydrogen is distributed in the rim initially.

Reference

[1] H. Hagi, Mater. Trans. JIM., 1994; 35: 112.

[2] A.D. Le Claire, Numerical Data and Functional Relationships in Science and Technology, Landolt-Börnstein, New Series, Vol, ed, H. Mehrer, 1990: 528.

[3] S.M. Lee and J.Y. Lee, Metall. Trans. A, 1983; 13A :135.

[4] H. Mizuno et al, CAMP-ISIJ Hydrogen Symposium, 2012:13.

[5]K.H. Lo, C.H. Shek and J.K.L. Lai, Mater. Sci. Eng., R, 2009; 65: 39.

[6]H. Mizuno et al, CAMP-ISIJ Hydrogen Symposium, 2012:13.

[7] Y. Sakamoto and H. Katayama, J. Japan Inst. Metals, 1982;46:805.

[8] G.J. Thomas, in: I.M. Bernstein, A.W. Thompson (Eds.), AIME, Warrendale,, PA, 1981:7.

[9] L. Cheng, T. Nagano and M. Enomoto, CAMP-ISIJ Hydrogen Symposium, 2012:19.

Chapter 4
Applicability of the Kissinger Formula in Simulation of Thermal Desorption Spectrum of Hydrogen

4.1 Introduction

Delayed fracture of steel is caused by hydrogen that is introduced in the material during high temperature process or from environment during service [1]. Hydrogen absorbed into the material is accumulated in various kinds of lattice defects such as vacancies, dislocations, grain boundaries, precipitate interfaces and microvoids etc. Among these lattice defects some may cause embrittlement when hydrogen accumulates while others may possess a beneficial effect to act a reservoir to alleviate hydrogen accumulation at detrimental traps. The most important factor governing the hydrogen distribution in lattice containing defects is the trapping property of these defects. One of the techniques to deduce the trapping property of defects is thermal desorption spectrometry analysis (TDA). The desorption rate of hydrogen diffusing through lattice containing defects is controlled by the trapping and detrapping energies, the amount of defects, and so on. Generally, desorption rate of hydrogen from a given specimen can be predicted by diffusion equation incorporating the trapping effect of these lattice defects. Diffusion equations based on the McNabb-Foster (M-F) model [2] which are expressed in Eqs. (1) and (2) for a single type trap,

$$\frac{\partial c}{\partial t} + N_t \frac{\partial \theta_t}{\partial t} = D_L \nabla^2 c \tag{1}$$

$$\frac{\partial \theta_t}{\partial t} = kc(1-\theta_t) - p\theta_t \tag{2}$$

are widely accepted where c is the hydrogen concentration in the lattice, N_t is the density of trap sites, θ_t is the occupancy fraction at the trap site, D_L is the diffusivity of hydrogen in normal lattice. k and p represent the probability of hydrogen jumping from the lattice to trap sites and the probability of releasing hydrogen from trap sites, respectively. They are written as,

$$k = k_0 \exp\left(-\frac{E_D}{RT}\right) \tag{3}$$

and,

$$p = p_0 \exp\left(-\frac{E_d}{RT}\right) = p_0 \exp\left(-\frac{E_B + E_D}{RT}\right) \quad (4)$$

where E_B is the binding energy of hydrogen to the trap site, E_D is the activation energy of lattice diffusion, and E_d(=E_B+E_D) is the activation energy of detrapping.

Although the M-F model provides a general method to predict the desorption rate or simulate the thermal desorption spectrum, it is not easy in practice to solve the diffusion equations since complicated numerical calculation is needed. Instead, the model is used at a limited condition of small specimen where diffusion process and/or re-trapping event during desorption can be ignored and then Eq. (2) is reduced to,

$$\frac{dX}{dt} = A(1 - X)\exp\left(-\frac{E_d}{RT}\right) \quad (5)$$

where X is the fraction of hydrogen released from the trap site, A is a constant, R is the gas constant and T is temperature. This equation is known as Kissinger formula originally intended for the description of surface reaction of gas molecules on the solid surface [3, 4]. From this equation, the peak temperature T_p at which hydrogen evolution rate passes through a maximum satisfies the equation,

$$\frac{E_d \phi}{RT_p^2} = A\exp\left(-\frac{E_d}{RT_p}\right) \quad (6)$$

where ϕ is ramp rate. Hence, the detrapping energy can be determined from the slope of $\ln(\phi/T_p^2)$ vs $1/T_p$ plot, which is known as Choo-Lee plot [5] and is widely used for the evaluation of trap energy.

In another extreme case in which the Oriani's local equilibrium between traps and lattice is assumed, the McNabb-Foster equation, eq. (1), can be simplified to an ordinary diffusion equation with an effective diffusivity replacing the diffusivity on the right hand side [6]. As far as desorption activation energy is concerned, in the frame of diffusion-controlled desorption, Lee and Lee [7] derived another equation similar to eq. (6) and claimed that the desorption activation energy can be determined from the slope of $\ln(\phi/T_p)$ vs $1/T_p$ plot, noticing that $\ln(\phi/T_p^2)$ in the Choo-Lee plot is substituted by $\ln(\phi/T_p)$. Obviously, the Lee-Lee and the Choo-Lee plots contradict with each other. It is necessary to resolve which is correct in analysis of trap energy. Before discussion of the difference between the two plots we like to point out that the Choo-Lee plot and the

Kissinger-type formula are based on a detrapping-controlled desorption and thus there remains a question about whether or not the Choo-Lee plot and the Kissinger-type formula are also applicable in a diffusion-controlled desorption.

In contrast to the Kissinger formula, the general M-F equation does not require a condition on the character of desorption of either detrapping- or diffusion-control. Desorption rate can be determined by numerically solving Eqs. (1) and (2) under appropriate boundary conditions and trapping parameter assumption. However, difficulty in solution of the M-F equation which is usually only possible by numerical calculation restricts its extensive application. Additional assumptions like detrapping-controlled desorption or local equilibrium are usually made for practical application as mentioned above. In practice, it is desirable to use a simple model instead of the general but too complicated M-F model to analyze a thermal desorption spectrum. Such an attempt has been made recently by the present authors [8]. Extension of the simple Kissinger-type formula to diffusion-controlled desorption has a great merit that it is easy to determine trapping parameters experimentally and numerically irrespective of detrapping- or diffusion-controlled character with an accuracy as high as that using the M-F model. Analysis of linkage of the formula with diffusion and comparison of numerical result on a cylinder specimen with that using the M-F showed an excellent agreement on simulation of the thermal desorption spectra for typical detrapping- and diffusion-controlled desorptions provided that chosen parameter values satisfy each condition. Only a qualitative consideration was given to the limit of applicability of the formula in the authors' previous paper.

The present work continues to verify the validity of the Kissinger-type formula in simulation of thermal desorption spectrum on the types of specimens of plate and sphere besides cylinder. After a description of the relation between the Kissinger-type formula and diffusion-controlled desorption, an emphasis is put on the limit of the validity of the formula on a semi-quantitative manner when it substitutes the M-F model to describe a thermal desorption spectrum. Another purpose is to examine whether the Choo-Lee equation or the Lee-Lee equation is applicable in the case of diffusion-controlled desorption.

4.2 Derivation of Kissinger-type formula for diffusion-controlled anisothermal hydrogen desorption

According to Oriani [6], as long as local equilibrium of hydrogen is maintained between the lattice and the trap sites, the effective diffusivity of hydrogen is given by the equation,

$$D_{eff} = \frac{D_L}{1 + \frac{N_t}{N_L}\exp\left(\frac{E_d}{RT}\right)} \tag{7}$$

where N_L is the number of lattice sites. At higher temperatures due to usually very small Nt/N_L values it is approximately equal to D_L. In contrast, at lower temperatures the 2nd term in the denominator becomes predominant and D_{eff} is given by the equation,

$$D_{eff} \sim \frac{D_0 N_L}{N_t}\exp\left(-\frac{E_d}{RT}\right) \tag{8}$$

where D_0 is the pre-exponential factor of lattice diffusivity. It is often orders of magnitude smaller than the lattice diffusivity at low temperatures

In an anisothermal process, in which the diffusivity is time-dependent, it is a common practice to define dimensionless time defined by,

$$\tau = \frac{\int_0^t D_{eff}\,dt}{a^2} \tag{9}$$

where a is the size of specimen, i.e. half-thickness for plate (denoted d) or radius for cylinder and sphere (denoted r_0), and t is time [9]. The diffusion equation is then written as,

$$\frac{\partial c}{\partial \tau} = \nabla^2 c \tag{10}$$

where the Laplacian is written in terms of dimensionless distance, $\xi = x/d$ for plate specimen and $\rho = r/r_0$ for cylindrical and spherical specimens. Thermal desorption analysis is usually performed in vacuum (Q-mass) or an atmosphere without hydrogen (gas chromatography). Thus, the hydrogen concentration at the specimen surface can be set to zero as the following,

$$c = 0 \qquad at \quad \xi = 1 \quad or \quad \rho = 1 \qquad for \quad all \quad \tau \tag{11}$$

Since the diffusivity in equation (10) is apparently a constant (=1), the solution for

isothermal diffusion can be utilized. Equation for plate, cylinder and sphere are recapitulated as,

$$c(\xi,t)=\frac{4}{\pi}\sum_{n=0}^{\infty}\frac{(-1)^n}{2n+1}\cos\left[\frac{(2n+1)\pi\xi}{2}\right]\exp\left[-(2n+1)^2\left(\frac{\pi}{2}\right)^2\tau\right]$$

$$\frac{c(\rho,t)}{c_0}=\frac{2}{r_0}\sum_{n=1}^{\infty}\frac{J_0(\alpha_n r_0\rho)}{\alpha_n J_1(\alpha_n r_0)}\exp(-\alpha_n{}^2 r_0\tau) \tag{12}$$

$$c(\rho,t)=-\frac{2}{\pi\rho}\sum_{n=1}^{\infty}\frac{(-1)^n}{n}\sin(n\pi\rho)\exp\left[-n^2\pi^2\tau\right]$$

where c_0 is the initial concentration which is assumed to be uniform within the specimen, J_0 and J_1 are, respectively, the Bessel function of the first kind of order zero and the first order, and the α_n's are roots of $J_0(\alpha_n r_0)=0$. After a sufficiently long time, at which the 2nd and higher order terms are no longer significant, the remaining hydrogen content in the specimen is expressed by the equation,

$$\frac{\bar{c}}{c_0}=B\exp(-C\tau) \tag{13}$$

where $B=4/\alpha_1{}^2 r_0{}^2$ and $C=\alpha_1{}^2 r_0{}^2$. Coefficients for plate and spherical specimens are shown in Table 1. Replacing the left-hand side (c/c_0) of Eq. (13) by (1-X) where X donotes the fraction of hydrogen evolved from the specimen, differentiation with respect to τ yields,

$$\frac{dX}{d\tau}=C(1-X) \tag{14}$$

Hence,

$$\frac{dX}{dt}=\frac{dX}{d\tau}\frac{d\tau}{dt}=\frac{CD_{eff}}{a^2}(1-X)\equiv A(1-X)\exp\left(-\frac{E_d}{RT}\right) \tag{15}$$

where $A=CD_0N_L/N_t a^2$. This indicates that as long as the temperature is not too high and the effective diffusivity is expressed by Eq.(8) the evolution rate follows the Kissinger-type equation during thermal desorption analysis. This equation can also be derived from the equation of hydrogen evolution rate by Ono and Meshii which takes into account the time dependent diffusivity (eq. (7) in ref. [10]), by replacing eq. (8) for D_{eff} [11,12]. One may argue that the original Kissinger formula was proposed for desorption of gas molecules from the solid surface and does not deal with diffusion. However, the above derivation indeed indicates that the Kissinger-type formula can

represent the desorption rate of hydrogen during thermal analysis which involves detrapping and lattice diffusion, albeit with coefficient A dependent on specimen size and trap site density. This is practically important because one can evaluate the trap parameters in principle by a single TDA spectrum provided that the requirements of the first order approximation of hydrogen distribution, eq. (13), and the existence of effective diffusivity, eq. (8), are satisfied.

Table 1

Coefficients of Kissinger-type equation for diffusion-controlled desorption and the pre-exposure time or pre-release hydrogen content needed for a Kissinger-type desorption.

Specimen	B	C*	Pre-exposure time τ_{pre}	Hydrogen content f_{pre}
Plate	$8/\pi^2$	$\pi^2/4$	0.122	0.60
Cylinder	$6.83/\pi^2$	$\pi^2/1.71$	0.119	0.35
Sphere	$6/\pi^2$	π^2	0.109	0.21

* Coefficient A in eq. (15) is $A=CD_0N_L/N_t a^2$.

4.3 Procedure of fitting with Kissinger formula

TDS peaks were produced by finite difference simulation by M-F model, eqs. (1) and (2). The finite difference formulae of these equations with dimensionless variables for cylindrical specimens have been presented elsewhere [13]. The corresponding formulae for plate and sphere are readily obtained by modification of the first derivative term with respect to the radial coordinate. The initial hydrogen content was 1 ppm and the hydrogen concentration was assumed to be in equilibrium between the lattice and the trap sites at the start of simulation. The trap site density was assumed to be N_t= $4x10^{24}$ m^{-3} throughout the paper which is equivalent to ten trap sites per atom length of dislocations of 10^{14} m^{-2} and accommodates ca. 10 ppm hydrogen if all sites were occupied. The lattice diffusivity of hydrogen proposed by Hagi [14] (D_0=$5.8x10^{-8}$ m^2/s and E_D = 4.5 kJ/mol) was employed in the calculation.

The curves simulated by M-F model were compared with those produced by Kissinger-type formula with the same detrapping energy and theoretically derived A value. It is equal to p_0 in the detrapping-controlled condition, and is defined in Table 1 for different specimen geometry in the diffusion-controlled condition. The calculation was initiated at a sufficiently low temperature which ensured that the fraction of released hydrogen and evolution rate are both zero. Then, the temperature was raised successively by $\phi\Delta t$, where Δt is the real time step. The fraction of released hydrogen at the (i+1)-th time step X_{i+1} was calculated from the equation,

$$X_{i+1} = X_i + \frac{dX_i}{dt}\Delta t = X_i + A(1 - X_i)\exp\left(-\frac{E_d}{RT_i}\right)\cdot\Delta t \qquad (16)$$

where T_i=i$\phi\Delta t$ is the temperature at the i-th time step.

4.4 Fitting with Kissinger formula in detrapping-controlled condition

Although fitting with Kissinger formula in detrapping-controlled desorption looks trivial, Figs. 1a and 1b illustrate the spectra of plate, cylindrical and spherical specimens at the ramp rate of 100°C/hr calculated by both the M-F model and the Kissinger formula. A relatively lower binding energy E_B= 40 kJ/mol and a low p_0 value of 30 s^{-1} (k_0 was calculated from the relationship k_0~p_0/N_L) are adopted because close values are

often used to simulate experimental TDS peaks of martensitic steels. The primary trap sites in these steels are considered to be dislocations, lath boundaries, martensite packet and prior austenite grain boundaries [13, 15]. As expected, the simulated spectra fit very well at a small specimen size (a=10^{-3} m) while a significant amount of deviation, increasing in the order of sphere, cylinder and plate, is observed at a large specimen (a=5x10^{-3} m). Detrapping-controlled desorption has to meet two requirements. One is that re-trapping occurs less frequently. Thus, the ratio of trapping (k term in the r.h.s. of eq.(2)) to detrapping frequencies (p term) was calculated. This ratio is identical to c/c_{LE}, where $c_{LE} = N_L\theta_{LE}$ is the hydrogen concentration in the lattice at equilibrium with trap sites. Indeed, Fig. 2 shows that for specimen of a=5x10^{-3} m this ratio is considerably smaller than unity throughout TDA except at very high temperatures with these E_B and p_0 values.

The other requirement is that the diffusion time be less than the interval of detrapping events, namely,

$$\frac{a^2}{D_L} << p^{-1} \tag{17}$$

hold during temperature ramp. Since re-trapping does not occur due to the 1st requirement, the lattice diffusivity is relevant. As shown in Fig. 3, this condition is not satisfied in this specimen at ϕ=100°C/hr or higher. As shown in Fig. 4, the Choo-Lee plot deviates significantly from the straight line expected from pure detrapping-controlled condition ($E_d=E_B+E_D$=44.5 kJ/mol, solid line), which decreased the overall slope as low as 40.4±0.6 kJ/mol. In contrast, the peak temperatures of a= 10^{-3} m specimen which all satisfy eq. (17) do exhibit a slope of 44.1±0.6 kJ/mol.

For trap of a larger binding energy eq. (17) is apparently satisfied. However, the ratio of re-trapping to detrapping frequencies does not decrease, but tends to increase because p decreases faster and thereby, eq. (17) which involves only D_L no longer is applicable. As a result the slope of Choo-Lee plot begins to deviate at a lower ramp rate. Hence, not only the diffusion time but also c/c_{LE} ratio have to be small in order to correctly deduce the detrap energy in the detrapping-controlled desorption. Small specimen size and slow ramp rate are favorable to make both of them small.

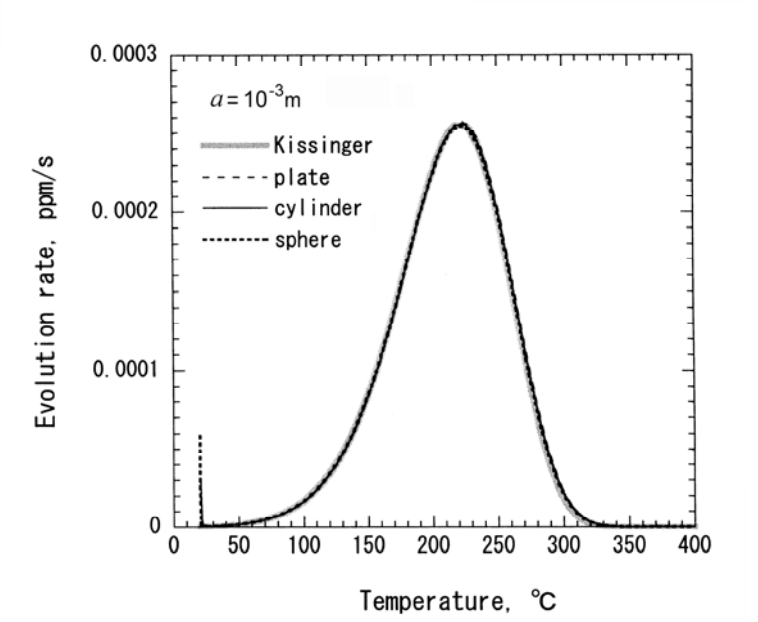

(a)

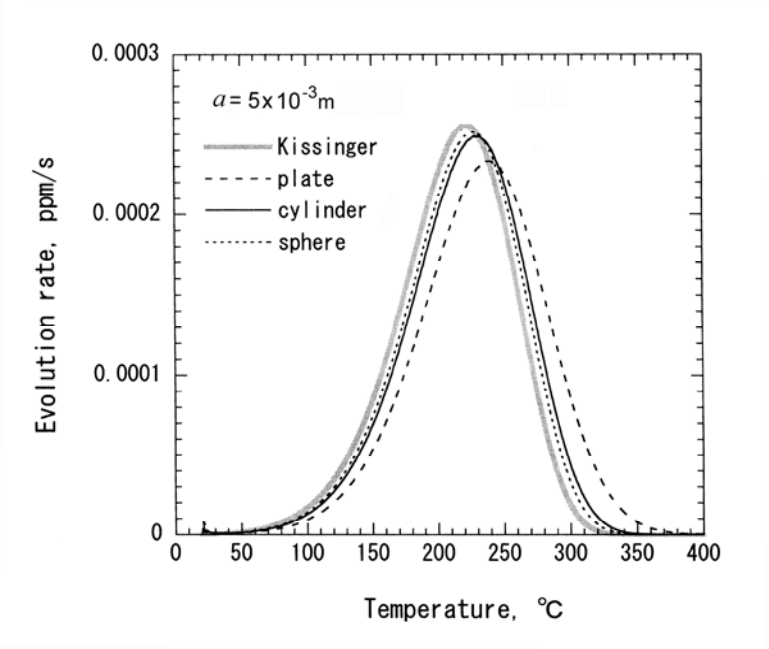

(b)

Figure 1 Comparison of TDA spectra of plate, cylinder and spherical specimens simulated by M-F model with E_B=40 kJ/mol and p_0=30 s^{-1}, with those calculated by Kissinger formula with E_d=44.5 kJ/mol and A=30 s^{-1} (gray curve). The ramp rate is ϕ=100°C/hr. The specimen size is a) a=10^{-3} m, and b) a=5x10^{-3} m.

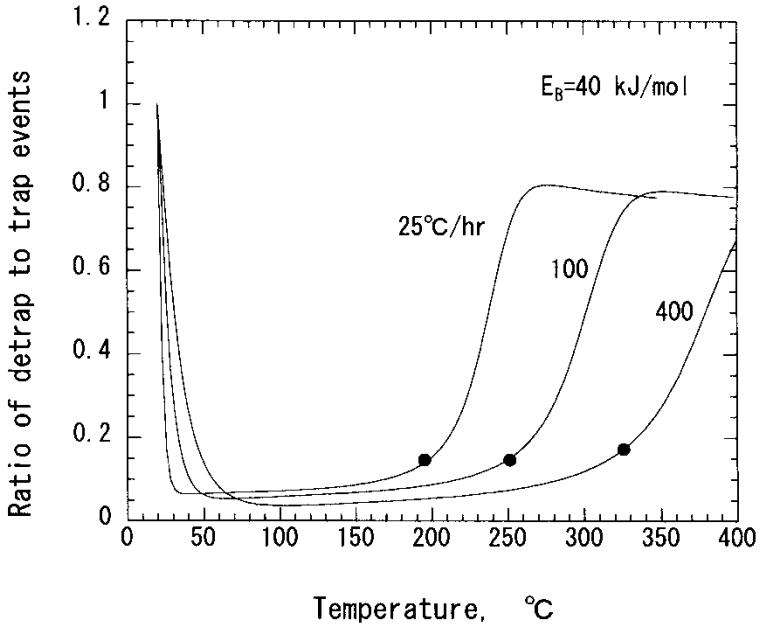

Figure 2 Variation of the ratio of trap to detrap frequencies (or c/c_{LE} ratio) with temperature in a cylindrical specimen of a=5x10^{-3} m with trap energy of E_B=40 kJ/mol. Solid circles indicate a peak temperature at the ramp rate.

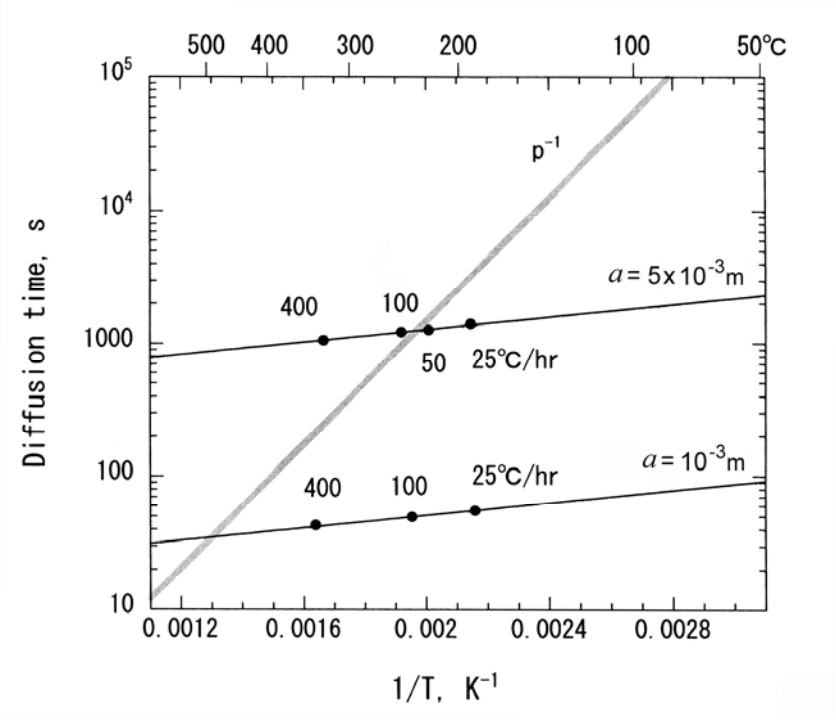

Figure 3 Comparison of diffusion time eq.(17) with the interval of detrapping p^{-1} (gray line) in cylindrical specimens of a=10^{-3} and $5x10^{-3}$ m. Solid circles indicate a peak temperature.

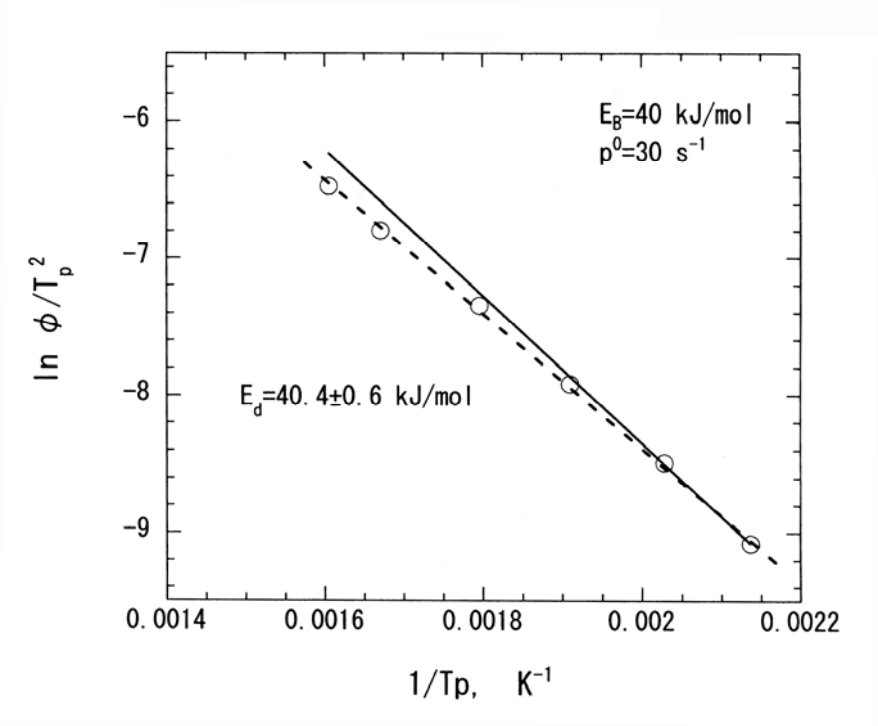

Figure 4 Choo-Lee plot of peak temperature of a=5x10^{-3} m with trap energy of 40 kJ/mol at ramp rates varying from 25 to 600°C/hr. The solid line has a slope corresponding to the detrap energy (E_d=44.5 kJ/mol).

4.5 Fitting with Kissinger-type formula in diffusion-controlled condition

In the diffusion-controlled condition a TDA spectrum can fit with Kissinger-type formula only when the concentration profile is approximated by the 1st term of series expansion, Eq. (13). Such a concentration profile is obtained by exposure prior to TDA [7]. Accordingly, the dimensionless time τ_{pre} at which the 2nd and higher terms become less than 1% of the 1st term in the series expansion of the equation of remaining hydrogen, and the fraction of hydrogen f_{pre} at τ_{pre} were calculated. Results are shown in Table 1. If pre-exposure is conducted to the fraction f_{pre}, the spectrum will fit with Kissinger-type equation no matter how the temperature is varied thereafter.

In order to see fitting with Kissinger-type equation simulations are conducted with E_B=60 kJ/mol. At this binding energy local equilibrium is achieved with p_0 greater than ~10^5 s^{-1}, as seen from the ratio of trapping to detrapping frequencies close to unity during TDA. These parameters could be applied to trapping at the interfaces of alloy carbides in high strength martensitic steels [11, 16, 17]. Figures 5a through 5c show simulated spectra of plate, cylindrical and spherical specimens pre-exposed at 100°C until the remaining hydrogen decreased to ~0.2 (< f_{pre}) with p_0=3x10^5 s^{-1}. At a small specimen size the spectra fit very well with those simulated from Kissinger-type formula incorporating coefficient A in Table 1, whilst the peak height becomes smaller at a large specimen than those calculated from the Kissinger-type equation. In a previous study [8] this was noted as a reduction in coefficient A in fitting the spectra.

Figure 6 shows the Arrhenius plot of D_{eff} at E_B= 60 kJ/mol. It is expected from its derivation that the limit of applicability of Kissinger-type equation in diffusion-controlled desorption is the limit of the low temperature form of D_{eff} (arrowed). Indeed, the peak height begins to deviate below this temperature in specimens of a= 10^{-2} m, see Fig. 5a etc. However, the peak temperature agrees quite well with those of Kissinger equation even if the peak temperature is close to the limit temperature. Thus, in this condition one can evaluate the detrapping energy from the Choo-Lee plot without much concern about the limit of applicability. This is also a case with trap of a smaller binding energy because both the peak temperature and the limit of low temperature form of D_{eff} decrease.

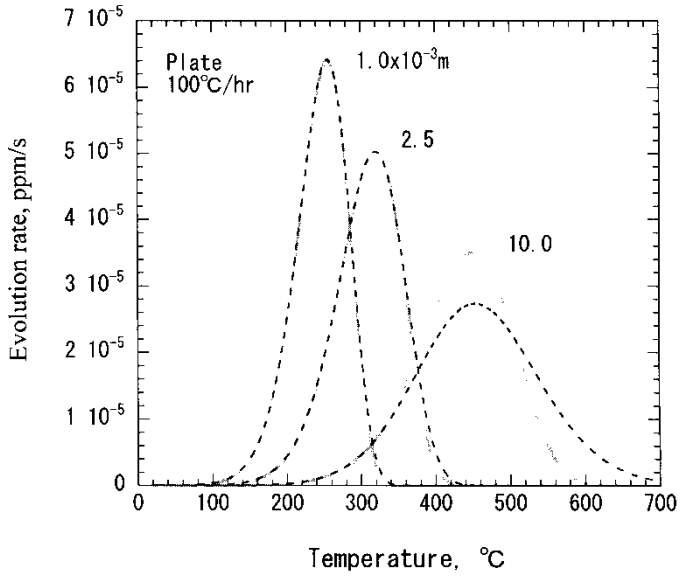
Plate
100℃/hr
1.0x10⁻³m
2.5
10.0
Evolution rate, ppm/s
Temperature, ℃

(a)

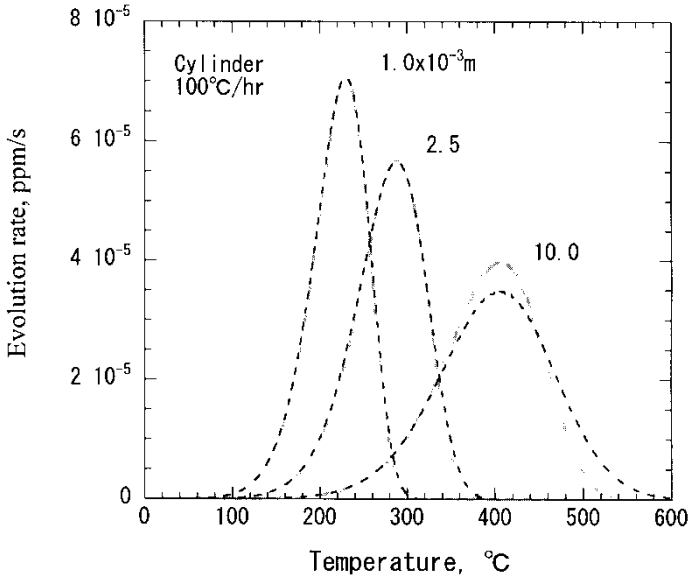
Cylinder
100℃/hr
1.0x10⁻³m
2.5
10.0
Evolution rate, ppm/s
Temperature, ℃

(b)

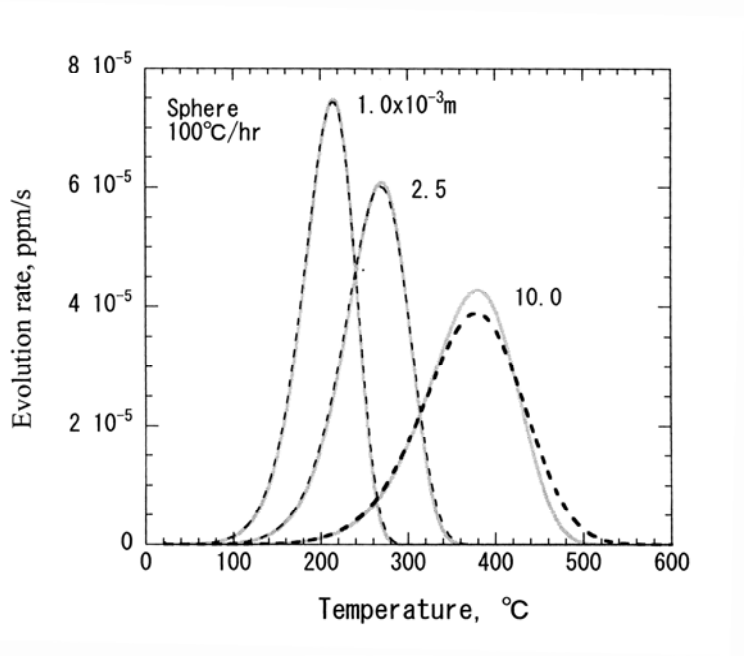

(c)

Figure 5 Comparison of TDA spectra of pre-exposed specimens of varying size simulated by M-F model with E_B=60 kJ/mol and p_0=3x10^5 s^{-1} (dashed curves) with those calculated by Kissinger-type formula with E_d = 64.5 k/mol and corresponding A defined by eq. (15) (gray curves). The ramp rate is ϕ=100°C/hr. a) Plate, b) cylinder and c) sphere.

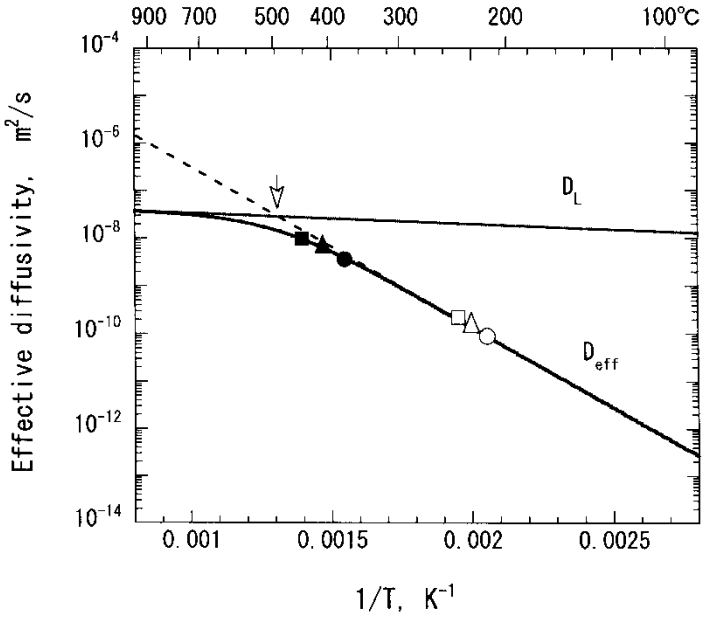

Figure 6 Arrhenius plot of lattice diffusivity and effective diffusivity proposed by Oriani [6] with E_B= 60 kJ/mol and N_t=4x10^{24} m^{-3}. Solid and open symbols are the peak temperatures of plate (square), cylinder (triangle) and spherical (circle) specimens of a=10^{-2} and 10^{-3} m, respectively. The arrow indicates a kind of the limit of low temperature form of effective diffusivity, eq.(8).

4.6 Choo-Lee plot in diffusion-controlled condition

Since TDA spectra can fit with Kissinger-type formula in diffusion-controlled desorption a Choo-Lee plot was performed for peaks simulated at a=10^{-3} m with E_B =60 kJ/mol and p_0=$3x10^5$ s^{-1} with pre-exposure to the hydrogen content of 0.2. As shown in Fig. 7a, $\ln(\phi/T_p^2)$ vs $(1/T_p)$ plot fits a straight line very well and moreover, the slope yielded E_d=64.8±0.4, E_d=64.6±0.1 and E_d=64.4±0.02 kJ/mol for spherical, cylindrical and plate specimens, respectively. Thus, the Choo-Lee plot does reproduce the detrapping energy (E_d=64.5 kJ/mol) and thus, is very useful for the evaluation of detrapping energy in the diffusion-controlled condition.

Lee and Lee [7] proposed a different dependence of peak temperature on ramp rate in the diffusion-controlled condition, which is expressed as,

$$\frac{\partial \ln(\phi / T_p)}{\partial (1/T_p)} = -\frac{E_d}{R} \tag{18}$$

As seen in Fig. 7b, this plot again fits a straight line very well. However, the slope yields E_d=68.9±0.5, E_d=68.8±0.08 and E_d=68.9±0.05 kJ/mol for spherical, cylindrical and plate specimens, considerably greater than the expected E_d value. As described in Appendix, the derivation of eq. (18) by Lee and Lee [7] seems to have a problem; they differentiated the diffusivity in the equation which is applicable only to isothermal diffusion. To the best of the authors' knowledge the plot proposed by Lee and Lee has not been applied to experimental TDA spectra.

4.7 Summary

The validity and limit of Kissinger-type formula to thermal desorption analysis of hydrogen was assessed semi-quantitatively. It has been verified analytically and numerically that as long as desorption occurs from traps of a single binding energy, the peak can fit with Kissinger-type formula in not only detrapping-controlled, but also diffusion-controlled conditions in which local equilibrium of hydrogen concentration is achieved between the lattice and the trap sites.

In the detrapping-controlled condition one can evaluate the activation energy of detrapping and the pre-exponential factor of detrapping coefficient from one TDA

spectrum if the specimen size is sufficiently small and the ramp rate is not too fast. The limit of applicability is that the ratio of trapping to detrapping frequencies is sufficiently small and the peak temperature has to be lower than the temperature at which the diffusion time is substantially less than the time interval of detrapping.

In the diffusion-controlled condition one can evaluate not only the activation energy of detrapping, but also the density of traps from coefficient A which depends on specimen size. Pre-exposure for a sufficiently long time is necessary prior to temperature ramping, the duration of which depends on specimen shape. The limit of applicability in this condition is that the peak temperature is lower than the temperature at which the effective diffusivity begins to deviate from the low temperature form.

It was also shown that the Choo-Lee plot is useful in the diffusion-controlled condition because the peak temperature of desorption agrees with Kissinger-type formula even if the effective diffusivity deviates substantially from its low temperature form. A plot proposed by Lee and Lee [7] for diffusion-controlled condition may not yield the correct activation energy of detrapping.

In summary, the Kissinger formula, including its derivative forms like the Choo-Lee plot, provides a simple and reliable technique for hydrogen thermal desorption analysis with an accuracy as high as that analyzed on the base of the McNabb-Foster model if the thermal desorption experiment is performed under proper conditions.

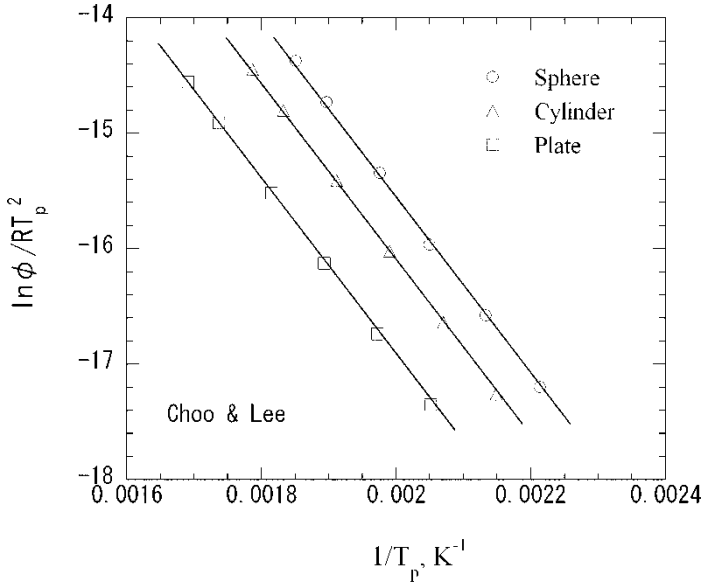

(a)

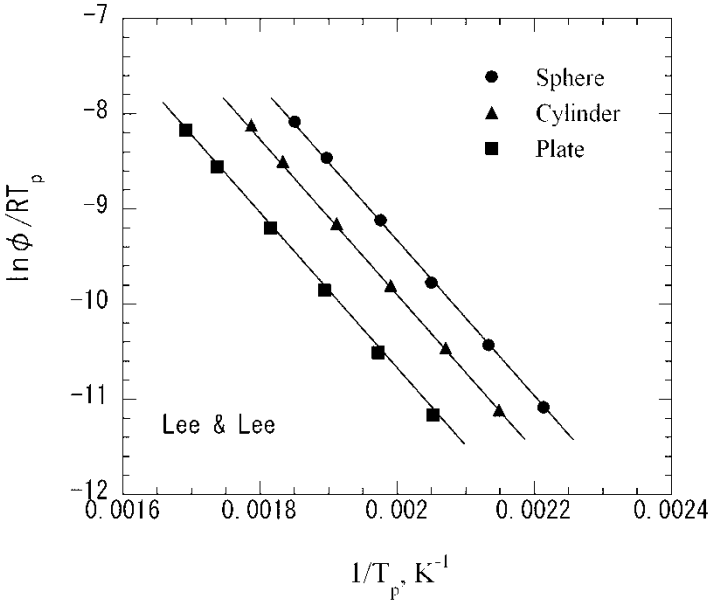

(b)

Figure 7 a) Choo-Lee plot of peak temperatures for specimens of plate, cylinder and sphere (a=10^{-3} m) simulated by M-F model at ramp rates varying from 25 to 600°C/hr. b) Plot of peak temperatures proposed by Lee and Lee [7] for the same specimens as a).

References

[1] M. Nagumo, Mater. Sci. Tech. 20(2004), 940

[2] A. McNabb and P.K. Foster, Trans. Metall. Soc. AIME 227 (1963), 618

[3] P.A. Redhead, Vacuum 12(1963), 203

[4] H.E. Kissinger, Anal. Chem. 29 (1957), 1702.

[5] W.Y. Choo and J.Y. Lee, Metall. Trans.A, 13A (1982), 135.

[6] R.A. Oriani, Acta Metall. 18 (1970), 147

[7] J.Y. Lee and J.L. Lee, Phil.Mag. A 56(1987), 293

[8] F.G. Wei, M. Enomoto and K. Tsuzaki, Comput.Mater.Sci. 51 (2012), 322.

[9] J. Crank, The Mathematics of Diffusion, 2nd ed. Clarendon Press, Oxford, (1972), 104.

[10] K.Ono and M.Meshii, Acta Metall.Mater., 40(1992), 1357

[11] F.G. Wei, T. Hara and K. Tsuzaki, Metall.Mater.Trans.B, 35B(2004), 587

[12] M. Nagumo, “Fundamentals of Hydrogen Embrittlement”, Uchida Rokakuho, Tokyo, (2008), 57

[13] M. Enomoto, D. Hirakami and T. Tarui, ISIJ Int. 46 (2006), 1381.

[14] H. Hagi, Mater. Trans. JIM. 35 (1994), 112.

[15] G.M. Pressouyre and I.M. Berstein, Metall.Trans.A, 9A(1978), 1571

[16] F.G. Wei and K. Tsuzaki, Metall.Mater.Trans.B, 37A(2006), 331

[17] I. Maroef, D.L. Olson, M. Eberhart and G.R. Edwards, Int.Mater.Rev., 47(2002), 191

Appendix

Re equation proposed by Lee and Lee for dependence of TDA peak temperature on ramp rate under diffusion-controlled condition

Lee and Lee [7] proposed that the apparent activation energy for bulk diffusion of hydrogen is obtained by plotting $\ln(\phi/T_p)$ against $1/T_p$ (ϕ is ramp rate and T_p is the peak temperature) when the alloy contains reversible traps which are equilibrated with hydrogen in the lattice. In their derivation the amount of hydrogen which remains in the cylindrical specimen in time t is given by the equation,

$$c_t' = c_\infty - c_t = c_\infty \sum_n \frac{4}{r_0^{\,2}\alpha_n^2} \exp\left(-D_{eff}\alpha_n^2 t\right) \tag{A1}$$

where c_t and c_∞ are the amount of hydrogen which left the cylinder and the initial amount in the specimen, respectively, see eq.(23) in ref.[7] (r_0 is *a*, D_{eff} is D_A, and T_P is T_C in their equation). This equation is applicable to a case of isothermal diffusion in which diffusivity is constant. In case that the diffusion coefficient is time-dependent as in TDA it is convenient to use a variable defined by,

$$\tau' = \int_0^t D_{eff}(t)dt\,. \tag{A2}$$

With τ' eq. (A1) is written as,

$$c_t' = c_\infty \sum_n \frac{4}{r_0^{\,2}\alpha_n^2} \exp\left(-\alpha_n^2 \tau'\right) \tag{A3}$$

The desorption rate can be calculated by differentiating eq.(A1) or eq.(A3) with respect to t as,

$$-\frac{dc_t'}{dt} = c_\infty \frac{4}{r_0^{\,2}} D_{eff} \exp\left(-D_{eff}\alpha_0^2 t\right) = \frac{4c_\infty D_0 N_L}{r_0^{\,2} N_t} \exp\left\{-\left(\frac{E_d}{RT} + D_{eff}\alpha_0^2 t\right)\right\} \tag{A4}$$

or,

$$-\frac{dc_t'}{dt} = \frac{4c_\infty D_0 N_L}{r_0^{\,2} N_t} \exp\left\{-\left(\frac{E_d}{RT} + \alpha_0^2 \tau'\right)\right\} \tag{A4'}$$

where D_0N_L/N_t is the pre-exponential factor of effective diffusivity, see eq.(8) and only

the n=0 term is retained following Lee and Lee [7]. One should use eq.(A4)' to obtain the peak of desorption rate as,

$$-\frac{E_d}{RT_p^2}\phi + D_{eff}\alpha_0^2 = 0 \qquad \text{(A5)}$$

In the Lee and Lee's paper an additional term E_d/RT_p remains in the l.h.s., see eq. (25) in ref. [7]. This term seems to arise from differentiation of D_{eff} in the exponent of eq.(A4), which should vanish because D_{eff} is regarded as a constant in eq. (A1). From eq. (A5) we obtain,

$$\frac{E_d}{RT_p^2}\phi = \alpha_0^2 D_0 \frac{N_L}{N_t}\exp\left(-\frac{E_d}{RT_p}\right) \qquad \text{(A6)}$$

Taking the logarithm of both sides of eq. (A6), the activation energy of detrapping is equal to the slope of $\ln(\phi/T_p^2)$ vs $1/T_p$ plot identical to the case of detrapping-controlled condition proposed by Choo and Lee [5]. This indicates that E_d is obtained by plotting $\ln(\phi/T_p^2)$ against $1/T_p$ even in the diffusion-controlled condition.

Chapter 5

Influence of Carbon Segregation to Trapping Site on the Thermal Desorption Spectrum of Hydrogen in Martensitic Steel

5.1. Introduction

Hydrogen embrittlement in high carbon martensitic steel, i.e. PC (prestressed concrete) and high strength bolts etc, have attracted considerable attention for many years. It is believed that a very small amount of hydrogen of the order of 1 ppm accumulates at various kinds of defects in steel such as dislocations, lath boundaries, martensite packet boundaries and prior austenite boundaries and serves as a preferential site for the formation of microcracks during service. A considerable amount of evidence is available to indicate the influence of carbon on hydrogen trapping [1-4]. Hagi and Hayashi [2] earlier noticed that the potency of dislocation for hydrogen trapping was weakened considerably by segregation of carbon to dislocations in iron. TDS peak temperatures of hydrogen are considerably different between deformed pure iron [5-7] and quenched martensitic steels [8-10]. Moreover, recently conducted electronic theory calculations showed that carbon and hydrogen have a strong repulsive interaction in not only the normal lattice [3] but also dislocation core [4].

Under this circumstance a computer program was developed to simulate competitive carbon segregation and hydrogen trapping by means of McNabb-Foster theory [11]. The carbon segregation is treated as trapping of carbon and a total of four equations, i.e. diffusion equations and differential equations for the site occupancies of hydrogen and carbon, were solved by finite difference method. The developed program allows one to simulate competitive segregation of carbon and trapping of hydrogen in all heat treatments including quenching, room temperature exposure and temperature ramping of thermal desorption analysis. In this report, thermal desorption analysis (TDA) spectra of hydrogen previously simulated assuming a single trap energy of hydrogen, are re-analyzed assuming a trap energy which is dependent on the carbon occupancy fraction at the trap site. Results are compared with some experimental TDA spectra reported in low and medium carbon martensitic steels.

5.2. Simulation method

5.2.1 Basic formulation

To start with, the McNabb-Foster equations are written in cylindrical coordinates as,

$$\frac{\partial c_i}{\partial t} + \alpha_i \frac{\partial \theta_i}{\partial t} = D_i \left(\frac{\partial^2 c_i}{\partial r^2} + \frac{1}{r} \frac{\partial c_i}{\partial r} \right) \tag{1}$$

$$\frac{\partial \theta_i}{\partial t} = k_i c (1 - \theta_i) - p_i \theta_i \tag{2}$$

where c_i is the concentration of i atom (i=1 and 2 for hydrogen and carbon, respectively), θI is the fractional occupancy at the trap site, D_i is the diffusivity in the lattice, α_i is the density of trap sites, r is the radial coordinate, t is time, k_i and p_i are the kinetic coefficients of trapping and detrapping given by,

$$k_i = k_i^0 \exp\left(-\frac{E_i^D}{RT} \right) \tag{3}$$

and,

$$p_i = p_i^0 \exp\left(-\frac{E_i^D + E_i^B}{RT} \right) \tag{4}$$

respectively. E_i^D is the activation energy of diffusion and E_i^B is the binding energy of i atom to the trap site and RT has its usual meaning. In order to simulate anisothermal diffusion it is convenient to write Eqs. (1) and (2) in terms of dimensionless variables as,

$$\frac{\partial c_1}{\partial \tau} + \alpha_i \frac{\partial \theta_1}{\partial \tau} = \frac{\partial^2 c_1}{\partial \rho^2} + \frac{1}{\rho} \frac{\partial c_1}{\partial \rho} \tag{5}$$

$$\frac{\partial c_2}{\partial \tau} + \alpha_2 \frac{\partial \theta_2}{\partial \tau} = \beta \left(\frac{\partial^2 c_2}{\partial \rho^2} + \frac{1}{\rho} \frac{\partial c_2}{\partial \rho} \right) \tag{6}$$

$$\frac{\partial \theta_1}{\partial \tau} = k_1' c_1 (1 - \theta_1) - p_1' \theta_1 \tag{7}$$

and,

$$\frac{\partial \theta_2}{\partial \tau} = k_2' c_2 (1 - \theta_2) - p_2' \theta_2 \tag{8}$$

where the dimensionless variables are defined by,

$$\tau = \frac{\int_0^t D_1 dt}{r_0^{\,2}} \quad , \quad \rho = \frac{r}{r_0}, \quad \beta = \frac{D_2}{D_1}, \quad k_i' = \frac{r_0^2}{D_1} k_i$$

and,

$$p_i' = \frac{r_0^2}{D_1} p_i .$$

The equations for hydrogen and carbon are not independent because the binding energy of hydrogen is assumed to depend on the fractional occupancy of carbon at the trap site. Counts et al [3] and Simonetti et al [4] reported that the two interstitial atoms have a strong repulsive interaction in close proximity in the iron lattice and dislocation core region, respectively. Here, this is taken into account phenomenologically assuming that the hydrogen trap energy is dependent on the carbon occupancy fraction as,

$$E_1^B = E_{1,0}^B \left(1 - A\theta_2\right) \qquad (9)$$

where A is a coefficient and $E_{1,0}^{B}$ is the binding energy in the absence of carbon. We also assume in this report that the binding energy of carbon E_2^{B} is independent on the fractional occupancy of hydrogen because the accumulation of carbon is favored in the dislocation core region [4] when they are in close proximity.

Eqs.(5) through (8) were solved by an explicit finite difference method as described elsewhere [9]. The boundary condition of hydrogen is,

$$\frac{\partial c_1}{\partial \rho} = 0 \qquad \text{at } \rho=1 \ (r=r_0) \qquad (10)$$

during quenching and,

$$c_1 = 0 \qquad \text{at } \rho=1 \qquad (11)$$

during TDA. On the other hand, the boundary condition of carbon is,

$$\frac{\partial c_2}{\partial \rho} = 0 \qquad \text{at } \rho=1 \qquad (12)$$

for all the time.

5.2.2 Parameter values for hydrogen and carbon

Table 1 shows the parameter values used in the simulation. The binding energy of hydrogen to edge dislocation was taken from the result of molecular statics calculations

using EAM potential [12], which is very similar to that evaluated from elastic theory by Wolfer and Baskes [13]. The binding energy of carbon to dislocation calculated recently [14] also is similar to that reported earlier using elasticity theory [15].

The size of dislocation core is usually a few times the Burgers vector b. The number of octahedral sites for carbon within the distance of 2b in a set of atom planes, iron-atom plane and adjacent iron-free plane, perpendicular to the [112] dislocation line is 9~12 [16]. Since all three sets of octahedral sites, i.e. O_x, O_y and O_z sites, possibly are not available due to stresses of dislocation, 3~4 atom sites could be available for carbon per iron atom plane. These sites can be filled with carbon in a steel containing more than 0.1mass% carbon [16]. Indeed, Maruyama and Takahshi [17] observed in 3D atom probe that on the average 1.3 carbon atoms were trapped per Fe atom plane within 0.5 nm (~2b) distance from dislocations in a pre-strained very low carbon steel (0.0043% carbon). Moreover, Wilde et al [18] reported that 20 carbon atoms segregated within several nanometers from dislocations in ~0.2C martensite, which probably include carbon atoms trapped in the strain field of dislocations. The dislocation density of low and medium carbon martensite is reported to be ~10^{15} m^{-2} [19]. If the number of tetrahedral interstitial sites is the same as in the normal lattice, it is 18~24 within the core region. However, since hydrogen distribution depends on the local stress state we simply assume that the number of sites available for hydrogen is two times the number of sites for carbon. Thus, if the steel contains ~3 ppm and all hydrogen are trapped, the initial occupancy fraction is ~0.05 in the core region at the dislocation density of 5x10^{15} m^{-2}.

The detrapping coefficient of hydrogen from dislocation p_1^0 was evaluated from TDS peaks of hydrogen from deformed iron. The reported peak temperatures scatter widely presumably because the specimen shape and size, ramp rate and the amount of charged hydrogen are not the same. As shown in Table 2, Takai et al [6] reported the peak temperature of ~500K for hydrogen desorption from cold rolled polycrystal iron using rod specimen of 5 mmϕ at the ramp rate of 200°C/hr while Choo and Lee [5] reported the peak temperature around 200°C (473K) with cylindrical specimen of 8 mmϕ at a ramp rate of ~150°C/hr. Hydrogen was charged electrically at room temperature by these authors. Whilst these authors evaluated the binding energy of

hydrogen from their own data, the binding energy reported by Taketomi et al [12] (Table 1) is employed to evaluate p_1^0 using the simulation conditions as close as possible to those of experiment. Fig. 2 shows the TDA spectra calculated at three p_1^0 values assuming that the initial hydrogen content was 3ppm. With the E^B values presently employed the peak temperature does not vary with assumed p_1^0 if it is greater than 10^4 s^{-1}. This indicates that local equilibrium of hydrogen (LE) is achieved at these p_1^0 values. As seen in the figure, the calculated peak temperature is close to that of Takai et al [6] at $p_1^0=10^2$ s^{-1} where the hydrogen concentration in the lattice presumably deviates from LE to a small extent. This p_1^0 value reproduced the peak temperature of Choo and Lee quite well because the ramp rate is smaller. Only the peak temperature was fitted in these simulations because the initial amount of hydrogen in the specimen was not reported.

Table 1 Parameters of carbon and hydrogen used in the simulation

	hydrogen	carbon
Diffusivity	D_0=5.8x10^{-8} m^2/s E^D=4.5 kJ/mol [26]	D_0=1.36x10^{-6} m^2/s E^D= 84.1 kJ/mol [21]
Binding energy	$E_{1,0}^B$ = 42.14 kJ/mol [12]	E_2^B 63.6 kJ/mol [14]
Detrapping parameter	1.0x10^2 s^{-1}	—
Trapping parameter	p_1^0/N_V	1x10^{-17} ~5x10^{-16} m^3/s
Number of occupancy sites per atom plane	6	3

Table 2 Peak temperatures and conditions of TDA in deformed pure iron reported in the literature

	Specimen size and shape	Hydrogen charge	Ramp rate	Peak temperature
Takai et al. [6]	0~83% C.R. rod, 5 mmϕ	r.t. up to 48 hr	200°C/hr	500K(230°C)
Choo and Lee [5]	0~83% C.W. cylinder, 8 mmϕ	0.1 MPa hydrogen at 400°C	156°C/hr	~473K(200°C)

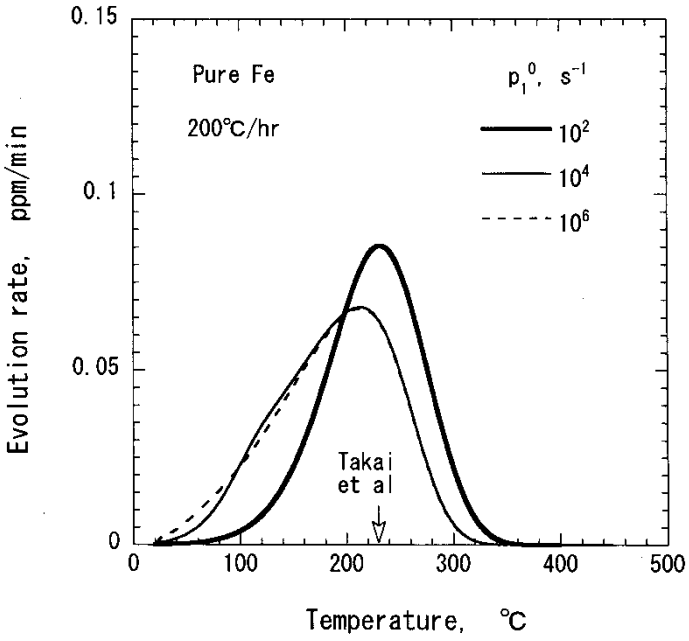

Fig. 2 Evaluation of detrapping parameter of hydrogen p_1^0 from experimental TDA spectrum of deformed pure iron [6] assuming E_1^B =42.14 kJ/mol.

5.2.3 Trapping coefficient of carbon to dislocation

The trapping parameter of carbon k_2^0 is determined from the Cottrell-Bilby equation for strain aging [20]. In this theory the fraction of carbon segregated to dislocation is expressed as,

$$W = 2\gamma\rho\left(\frac{AD_C t}{kT}\right)^{2/3} \tag{7}$$

where $\gamma=(\pi/2)^{1/3}$ is a coefficient, ρ is the dislocation density, t is time and kT has its usual meaning. The coefficient A is given by,

$$A = \frac{1+\nu}{3\pi(1-\nu)}\mu b\Delta v\,, \tag{8}$$

where μ is the shear modulus, ν is the Poisson ratio, b is the Burgers vector and Δv is the change of volume of the lattice per carbon atom. The value of A is calculated to be ~1.9 $x10^{-29}$ $N{\cdot}m^2$ from the newly reported strain due to carbon in the bcc Fe lattice [21]. The variation of W with time was calculated in an Fe-0.05mass%C alloy, in which all carbon atoms can be accommodated near the dislocation core at the dislocation density of $\rho=5x10^{15}$ m^{-2}. It is seen in Fig. 1 that the fraction of segregated carbon calculated with $k_2^0=5x10^{-16}$ m^3/s agrees well with that of Cottrell-Bilby theory at early stages. Speich [22] calculated the diffusion distance of carbon during quenching and speculated that complete segregation of carbon to dislocation occurs in Fe-C martensite with carbon concentration less than 0.57mass%. Assuming the same dislocation density, we obtain complete segregation with k_2^0 one order of magnitude smaller.

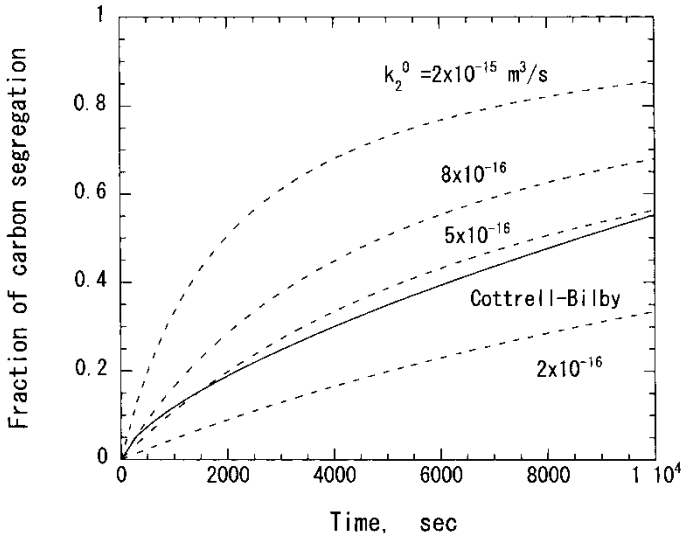

Fig. 1 Comparison of trapping parameter of carbon to dislocation k_2^0 with segregation kinetics calculated from Cottrell-Bilby theory.

5.3. Results and discussion

5.3.1 Carbon segregation during quenching

In the evaluation of carbon segregation Speich [22] took the average of M_s and M_f as the effective transformation temperature. Here, the temperature of 50% transformation was calculated from the Koistinen-Marburger equation [23],

$$f = 1 - \exp\left[-\alpha\left(M_s - T\right)\right] \quad (9)$$

with M_s calculated from the equation by Andrews [24]. In fact, the former temperature was 67°C lower than the M_s irrespective of carbon content as long as the coefficient is taken to be α=-0.011 [23]. As shown in Fig. 3a, assuming the higher k_2^0(=5x10^{-16} m^3/s) carbon segregation is completed almost instantly at M_{50} in steels containing carbon up to 0.6%. It is also the case at the lower k_2^0(=1x10^{-17} m^3/s) except in steel containing 0.6%C (Fig. 3b).

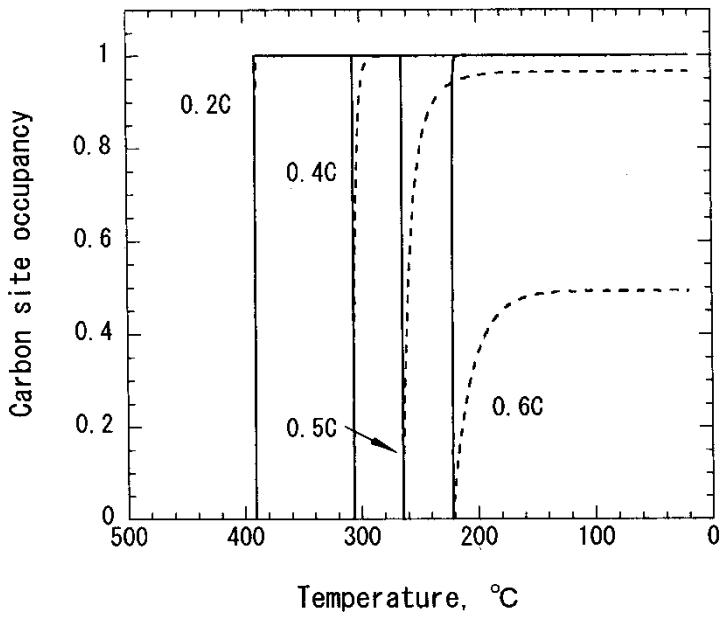

Fig. 3 Variation of carbon occupancy fraction with temperature (or time) during quenching at $k_2^0=5x10^{-16}$ (solid line) and $1x10^{-17}$ m^3/s (dashed line) in steels of various carbon content.

5.3.2 TDA spectrum of specimens charged with hydrogen at room temperature

Table 3 shows the peak temperatures of TDA spectra reported in Fe-0.2C, 0.33C and 0.58C martensitic steels together with some details of alloy specimens and TDA conditions. It is seen that the peak temperatures in these steels are 50~100°C lower than those of deformed pure iron.

Following the experimental procedure, the steels were quenched at a cooling rate of 1000°C/s and charged with hydrogen at room temperature. Fig. 4a shows that the best fit with experiment of TDA spectra of the 0.33C steel simulated at the identical conditions to the experiment, e.g. ramp rate and specimen radius and the amount of charged hydrogen, is achieved at A=0.27. Since carbon is likely to be fully segregated in this steel, the simulated spectra do not depend significantly on the assumed k_2^0 value. A similar comparison is made in the Fe-0.2C steel, in which the observed spectrum was adjusted by Kissinger formula [25]. While the peak temperature is somewhat high because of the larger specimen radius, the spectrum fits quite well with experiment at A=0.23, see Fig. 4b. Whilst these A values yield E_1^B values (=30.7~32.3 kJ/mol) somewhat greater than that previously assumed (E_1^B=27 kJ/mol), this cam be interpreted phenomenologically that hydrogen is expelled from the dislocation core region and is trapped presumably in the outer region of lower trap energy.

If steel was quenched very rapidly, little carbon would segregate to dislocations even in medium carbon steel. Indeed, the carbon occupancy fraction θ_2 is equal to 0.16 in 0.33C steel immediately after quenching to room temperature at a rate of 10^4°C/s. Simulations results at two quenching rates, 10^3 and 10^4°C/s and are shown in Figs. 5a and 5b. It is seen that the spectra start to rise slowly in steel quenched at the faster rate because hydrogen is trapped with a larger binding energy in the absence of carbon. The spectra with full carbon occupancy prior to temperature ramp (Fig. 5a) are closer to experiment (Fig. 5c) in terms of peak height and evolution rate at low temperatures, e.g. around 50°C, while those of low carbon occupancy prior to temperature ramp (Fig. 5b) are closer to experiment in that with increasing ramp rate the peak starts to rise at a progressively higher temperature. This is probably because carbon segregation to dislocation is delayed at higher ramp rates although carbon is likely to fully segregate by the time at which the temperature reaches the peak.

The Choo-Lee plot of the peak temperature is shown in Fig. 6. The peak temperatures somewhat differ at slow ramp rates, which raised the detrap energy from E_d=34.2±0.14 to 38.2±1.6 kJ/mol. This is probably because carbon segregation is yet to be completed at the peak temperature. The simulated spectra at the quenching rate of 10^3°C/s fit better with experiment (E_d=30.3±2.7 kJ/mol).

Table 3 Peak temperatures and conditions of TDA in martensitic steels reported in the literature

Steel	Specimen size and shape shape	Hydrogen charge	Peak area	Ramp rate	Peak temperature	M_s/M_{50}, °C (cal.)*3
0.2C [8]	cylinder, 10 mmϕ, 40 mmL	1 A/m^2, 48 hr, r.t.	~1 ppmH*^{2}	100°C/hr	130°C	454/391
0.33C* [9], [10]	cylinder, 5 mmϕ, 100mmL	0.2 mA/cm^2 for 18 hr, r.t.	~1 ppmH	25~400°C/hr	~100°C	322/259
		950°C, 1 hr, 1 atmH	3ppmH	100°C/hr	95~100°C	
0.58C* [10]	cylinder, 5 mmϕ, 100mmL	950°C, 1 hr, 1 atmH	2.5ppmH	100°C/hr	100~110°C	256/193

* These are high strength steels which contain alloying elements such as Si, Mn, Cr and Mo.

*^{2} The peak area was calculated from the peak simulated by Kissinger formula.

*^{3} Calculated from the equation in refs. [21] and [23].

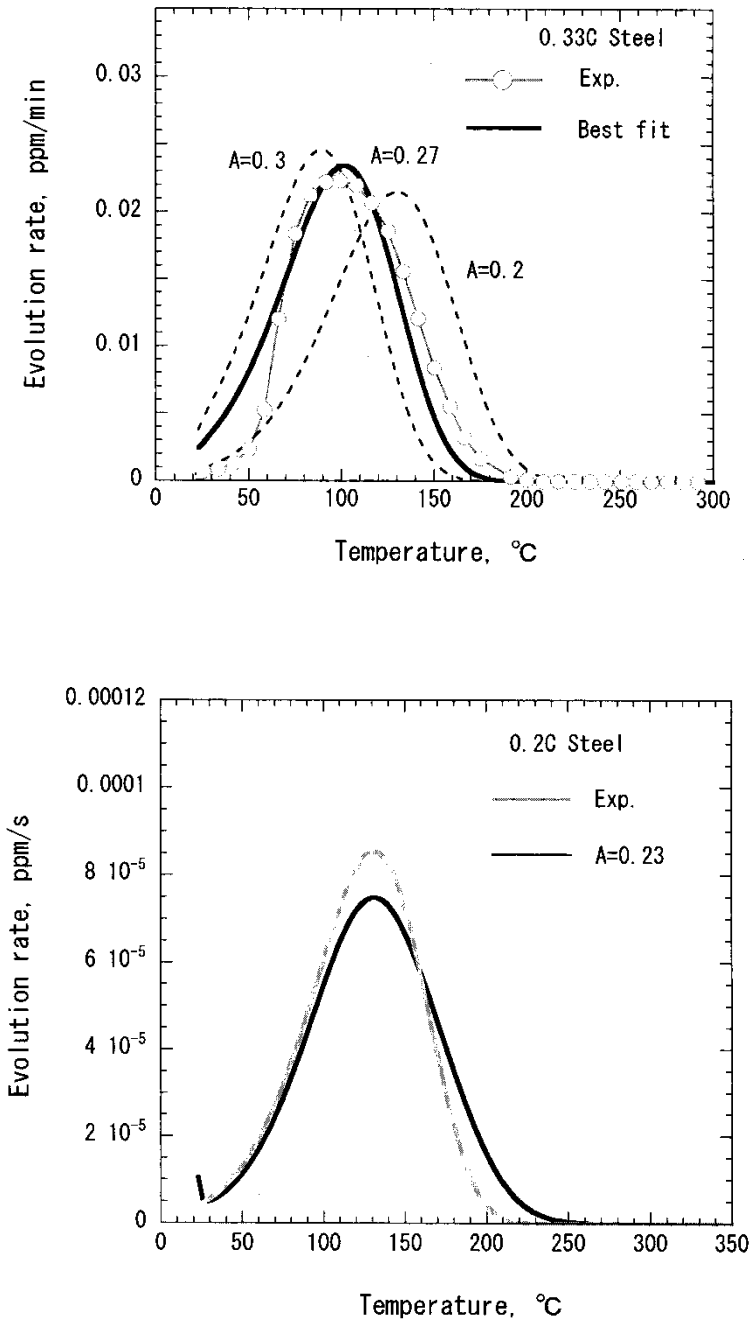

Fig. 4 Comparison of calculated TDA spectra with experiment. The peak areas (hydrogen contents) of calculated peaks are identical to that of experiment. a) 0.33C steel and b) 0.2C steel (see Table 3).

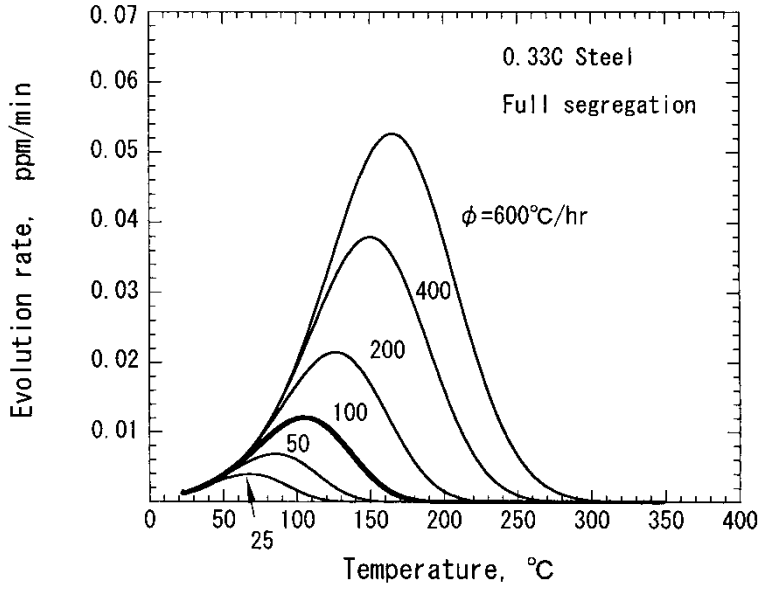
0.33C Steel
Full segregation
φ=600℃/hr
400
200
100
50
25
Evolution rate, ppm/min
Temperature, ℃
0.07
0.06
0.05
0.04
0.03
0.02
0.01
0
50
100
150
200
250
300
350
400

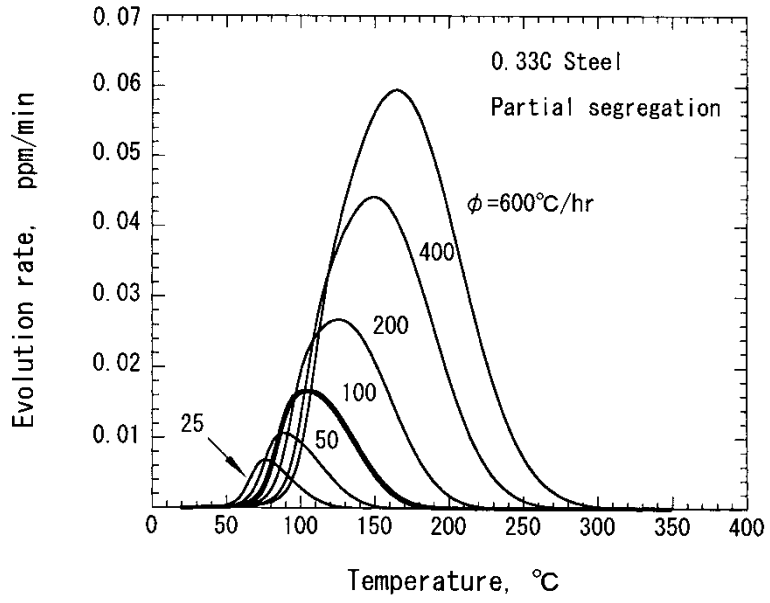
0.33C Steel
Partial segregation
φ=600℃/hr
400
200
100
50
25
Evolution rate, ppm/min
Temperature, ℃
0.07
0.06
0.05
0.04
0.03
0.02
0.01
0
50
100
150
200
250
300
350
400

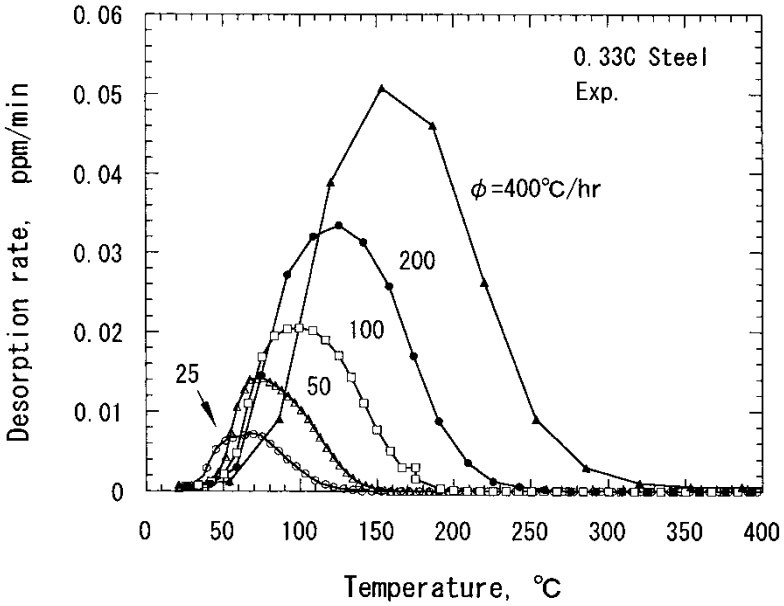

Fig. 5 TDA spectra of 0.33C steel simulated at various ramp rates. a) High k_2^0 and slower cooling rate (10^3°C/s) which ensures full carbon occupancy, b) low k_2^0 and faster cooling rate (10^4°C/s) which causes a partial carbon occupancy prior to temperature ramp, and c) experimental TDA spectra [9].

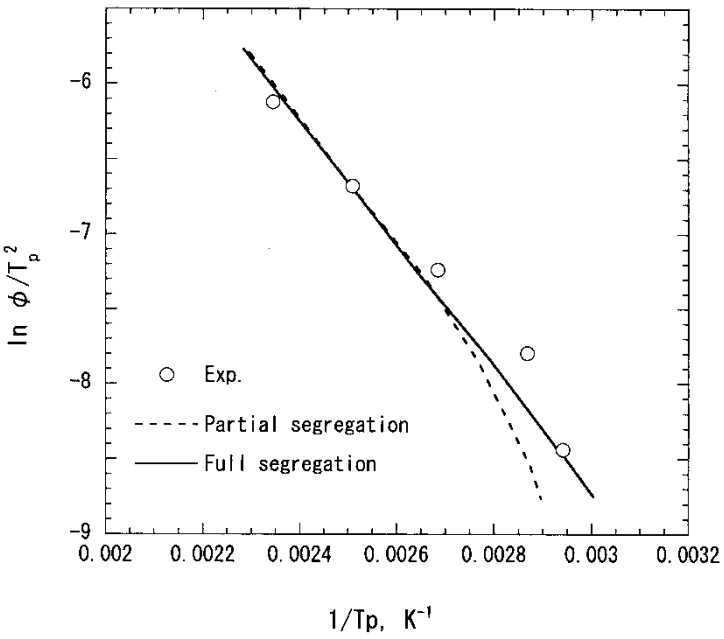

Fig. 6 Choo-Lee plot of calculated peak temperatures in Figs. 5a) and 5b) for comparison with the plot of experimental peak temperatures in Fig. 5c).

5.3.3 TDA spectrum of specimens charged with hydrogen at high temperature

Fig. 7 shows the calculated variation with time of fractional occupancies of carbon and hydrogen during quenching and subsequent holding at room temperature in the 0.58C steel. During room temperature holding the boundary conditions of eq. (10) for hydrogen and eq.(12) for carbon were applied, which implies that the specimen surface was Cd-plated to prevent hydrogen desorption prior to temperature ramp. At the larger k_2^0 carbon fully segregated to dislocation while carbon segregation occurred to a small extent at the smaller k_2^0 (* this is because the 0.58C steel contains alloying elements so that the M_s temperature is considerably lower than that of an Fe-0.58C alloy). Compared to carbon, hydrogen trapping proceeded slowly due to the much lower concentration in the lattice and reached a stationary value at the end of holding, namely, equilibrium was achieved between the lattice and the trap site. The difference of these θ_1 values happened to be minute although the concentration in the lattice differed by two orders of magnitude, i.e. $\theta_L=10^{-7}$ and 10^{-9} for the larger and smaller k_2^0, respectively. Similar features of site occupancies of carbon and hydrogen were observed in the 0.58C steel. These steels were then subjected to TDA at a ramp rate of 100°C/hr and results are shown in Figs. 8a and 8b, in which slightly different A values were used, i.e. A=0.29 and 0.27, respectively. In both steels the simulated peaks with the larger k_2^0 fit very well with experiment, which indicate that carbon may have fully segregated in the martensite of these steels.

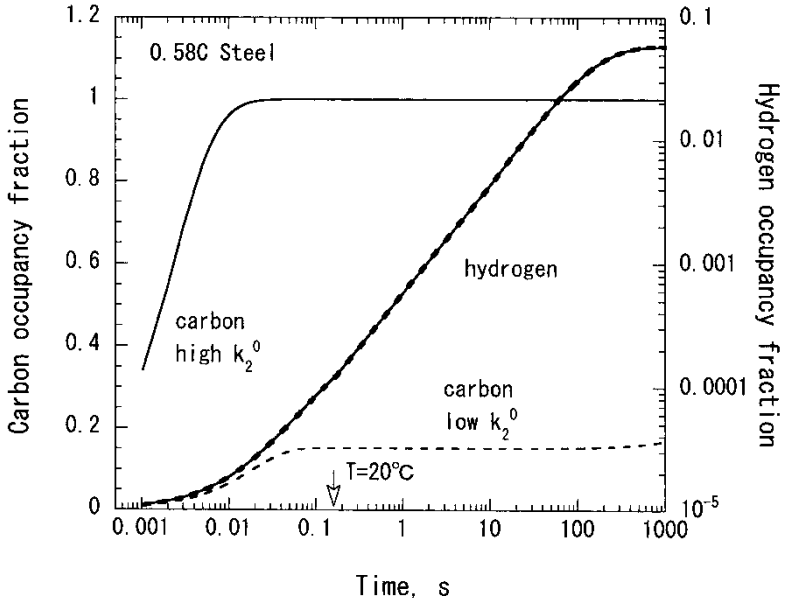

Fig. 7 Variation of hydrogen (θ_1) and carbon (θ_2) occupancy fractions with time during quench and subsequent holding at room temperature in 0.58C steel. The temperature is equal to M_{50}(=193°C) at t= 0 s and was cooled to 20°C at t=0.17 s (arrowed).

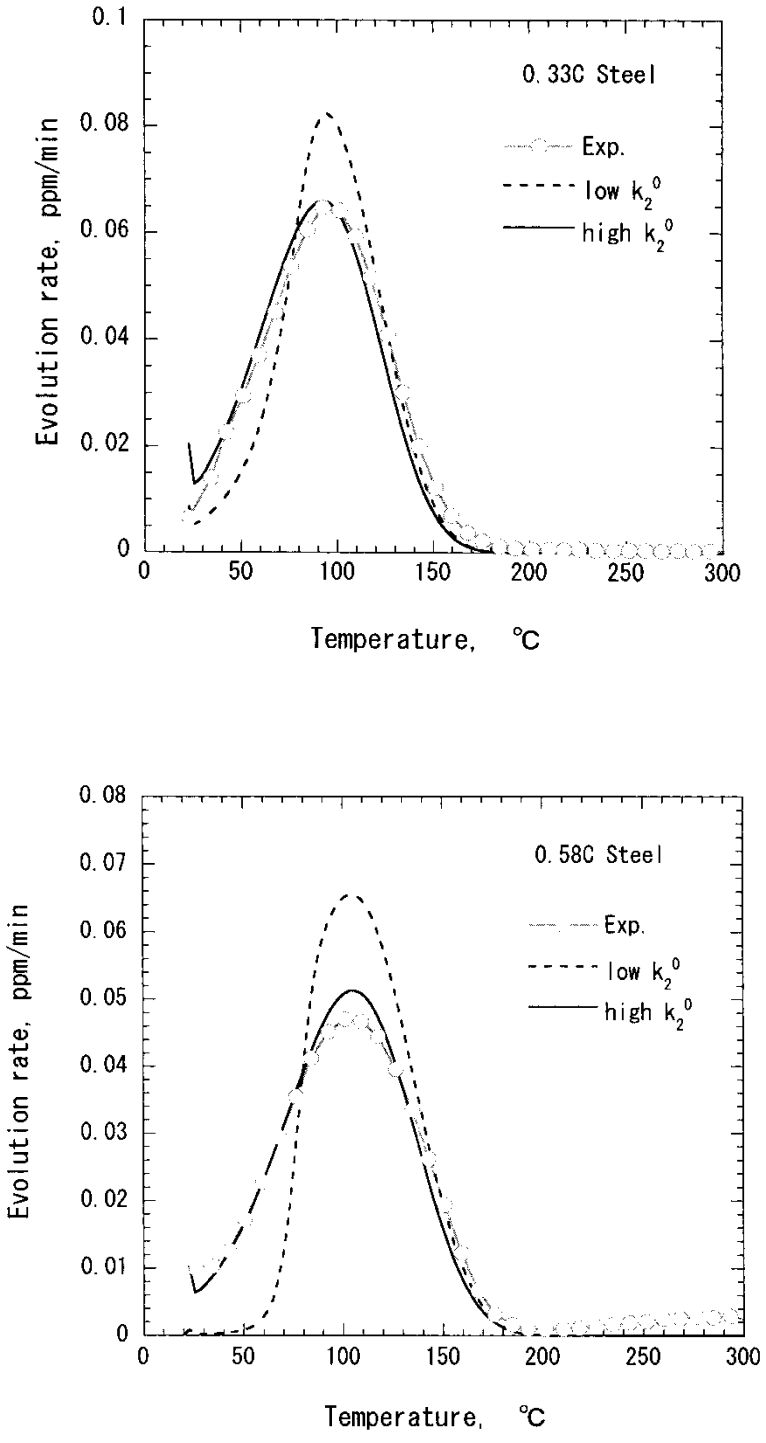

Fig. 8 Comparison of TDA peaks calculated with the high (dashed curve) and low k_2^0 values (solid curve) with experiment. Peak areas are identical to each other. Hydrogen was charged at 950°C. a) 0.33C and b) 0.58C steels.

5.4. Summary

Thermal desorption spectra of hydrogen in low and medium carbon martensitic steels, analyzed previously assuming a single trap energy, were re-examined incorporating carbon segregation to hydrogen trap site by means of McNabb-Foster equations. The carbon segregation was treated as trapping to the defect site. The finite difference equations for diffusion and site occupancies of hydrogen and carbon were solved simultaneously incorporating a phenomenological interaction coefficient between carbon and hydrogen (denoted A) within the trap site. Assuming that the primary trap site is dislocation, the binding energies of hydrogen and carbon to dislocation were taken from the results of electronic theory calculations in the literature. The trapping and detrapping coefficients of hydrogen were evaluated from experimental TDS peaks of deformed pure iron while the trapping coefficient of carbon was evaluated from Cottrell-Bilby theory and earlier experiment in low carbon martensite.

The temperature and shape of TDS peak and moreover, the 50~100°C difference in peak temperature between deformed iron and low and medium carbon martensite could be accounted for assuming a narrow range of interaction coefficient (A=0.23~30) no matter whether hydrogen was charged at room temperature after quenching or at high temperature prior to the formation of martensite. It is likely that carbon segregation occurs faster than hydrogen trapping during quenching due to larger concentration of carbon in the matrix than hydrogen unless the M_s temperature is too low. Whether or not carbon segregates prior to TDA may have a significant influence on the spectrum shape, but does not appear to have an appreciable influence on the peak temperature unless it is too low.

References

[1] J.J. Au and H.K. Birnbaum, Acta Metall., 26(1978) 1105-16

[2] H. Hagi and Y. Hayashi, Trans. Japan Inst. Metals, 28(1987) 375-382.

[3] W.A. Counts, C. Wolverton, R. Gibala, Acta Mater., 58(2010), 4730-4741

[4] S. Simonetti, M.E. Pronsato, G. Brizuela and A. Juan., Appl. Surf. Sci. 217 (2003) 56–67.

[5] W.Y. Choo and J.Y. Lee, Metall.Trans.A, 13A(1983), 135-140

[6] K. Takai, G. Yamauchi, M. Nakamura and M. Nagumo, J. Japan Inst. Metals, 62(1998), 267-275

[7] M. Nagumo, K. Takai, N. Okuda, J. Alloys Comp., 293-295(1999) 310-316

[8] F.-G. Wei and K. Tsuzaki, Scripta Mater. 52 (2005) 467–472

[9] M. Enomoto, D. Hirakami, and T. Tarui, ISIJ International, 46(2006) 1381-1387.

[10] M. Enomoto, D. Hirakami, and T. Tarui, Metall.Mater.Trans.A, 43A(2011) 572-581.

[11] A. McNabb and P.K. Foster, Trans. Metall. Soc. AIME 227 (1963) 618-627.

[12] S. Taketomi, R. Matsumoto, N. Miyazaki. Acta Mater. 56 (2008) 3761–3769.

[13] W.G. Wolfer and M.I. Baskes, Acta Metall 33(1985) 2005-2111.

[14] E. Clouet, S. Garruchet, H. Nguyen, M. Perez and C.S. Becquart. Acta Mater. 56 (2008) 3450-3460.

[15] A. W. Cochardt, G. Schoek and H. Wiedersich, Acta Met., 3(1955) 533-537

[16] D. Kalish and M. Cohen, Mater.Sci.Eng. 6(1970) 156-166.

[17] N. Maruyama and M. Takahashi, Tetsu-to-Hagane, 93(2007), 506-512

[18] J. Wilde, A. Cerezo and G.D.W. Smith, Scrpta Mater., 43(2000), 39-48

[19] S. Morito, J. Nishikawa and T. Maki, ISIJ Int., 43(2003), 1475-1477

[20] A.H. Cottrell and B.A. Bilby, Proc. Phys. Soc. A62(1949) 49-62.

[21]C.S. Becquart, J.M. Raulot, G. Bencteuz, C. Domain, M. Perez, S. Garruchet, and H. Nguyen: Comp. Mater. Sci., 40(2007) 119–129.

[22] G. R. Speich, Trans. AME, 245(1969) 2553-2564

[23]D.P. Koistinen and R.E. Marburger: Acta Metall., 1959, vol. 7, pp. 59–60.

[24] K.W. Andrews: JISI, 1965, vol. 203, pp. 721–27.

[25] F.G. Wei, M. Enomoto, K. Tsuzaki, Comp.Mater.Sci., 51(2012) 322-330

[26] H. Hagi, Mater.Trans., JIM, 35(1994) 112-117

Chapter 6

Simulation of Thermal Desorption Spectrum of Hydrogen in Austenitic Stainless Steel

6.1 Introduction

Austenitic stainless steels are commonly used for components of hydrogen generator, storage and transportation systems. While austenitic stainless steels have higher resistance to hydrogen embrittlement (HE) than ferritic steels, they suffer from brittle fracture in a hydrogen atomosphere of high pressure [1, 2]. It is thus very important to understand the diffusion and trapping of hydrogen in austenitic steels. Thermal desorption analysis (TDA) curves in austenitic stainless steel are expected to be very different from those of ferritic and high carbon martensitic steels because of the large solubility [3] and orders of magnitude slower lattice diffusivity of hydrogen in austenitic steels [4]. As a consequence of this, one would expect that the peaks are broad and tend to occur at a higher temperature.

In the study of thermal desorption of hydrogen in a Ni alloy (Inconel 625) and austenitic steel (SUS316L) Takai et al [5] inferred fundamental features of TDA curves in fcc metals from experimental observation. Yagodzinsky et al [6] analyzed TDA curves of stainless steels (AISI series) taking hydrogen trapping into account by means of McNabb-Foster equation. Moreover, it was reported recently that the peak temperature and shape of TDA spectra varied widely depending on the method of hydrogen charge in SUS316L and SUS304 stainless steels [7]. This is presumably because highly non-uniform distribution of charged hydrogen is readily formed due to large solubility and slow diffusivity in austenitic steel. In this report, we studied the influence of specimen size, ramp rate, trap sites and initial distribution of hydrogen on TDA curves in Ni alloys and stainless steels, deformed or non-deformed, by computer simulation with emphasis on their variable nature with charging and testing conditions.

To do this McNabb-Foster model may be appropriate because the model can cope with various aspects of thermal desorption analysis by varying parameter values related to trapping, specimen size and the hydrogen distribution prior to temperature ramp. Simulation results are compared with available experimental TDA curves, and the features thereof and the applicability of Choo-Lee plot to the spectra of fcc metals are discussed.

6.2 Simulation method

According to McNabb and Foster [8] the diffusion and trapping of hydrogen in metallic materials can be described by the following equations,

$$\frac{\partial c}{\partial t} + N_t \frac{\partial \theta_t}{\partial t} = D\nabla^2 c \tag{1}$$

$$\frac{\partial \theta_t}{\partial t} = kc(1-\theta_t) - p\theta_t \tag{2}$$

where c is the hydrogen concentration in the lattice, N_t is the density of trap sites, θ_t is the occupancy fraction at the trap site, D is the diffusivity of hydrogen in normal lattice,

$$k = k_0 \exp\left(-\frac{E_D}{RT}\right) \tag{3}$$

and,

$$p = p_0 \exp\left(-\frac{E_d}{RT}\right) = p_0 \exp\left(-\frac{E_B + E_D}{RT}\right) \tag{4}$$

are the kinetic coefficients of trapping and detrapping, respectively. Here, E_D is the activation energy of lattice diffusion, E_B is the binding energy of the trap site and E_d ($=E_B+E_D$) is the activation energy of detrapping. Table 1 shows the activation energy and the pre-exponential factor of lattice diffusion in a Ni alloy and SUS304 steel in the literature, together with those of pure Ni and fcc iron [9-12]. These diffusivities are compared with that in bcc iron reported by Hagi [13] in Fig. 1. In order to simulate TDA curves of deformed stainless steels, the hydrogen trap sites are assumed to be dislocations. It is noted that the binding energy of hydrogen with dislocation (=13.5

kJ/mol [14]) is considerably smaller in fcc metals than that in bcc iron (=42 kJ/mol [15]). It is also smaller than the activation enthalpy of lattice diffusion, opposite to the ferritic case. Shintani and Muarata [16] reported that the dislocation density does not exceed 5.0×10^{14} m^{-2} with increasing strain of cold rolling in SUS304 stainless steels. Hence, the dislocation density is assumed to be 5×10^{14} m^{-2} for 40% deformation. Following the discussion made in bcc martensite [17], the number of octahedral sites within the distance of two times the Burgers vector is evaluated to be ca. 5 per atom plane perpendicular to the [112] dislocation line in fcc iron. The p_0 value of hydrogen detrapping (=10^8 s^{-1}) was assumed to be large enough to achieve local equilibrium of hydrogen between the lattice and the trap sites, and k_0 was obtained from the relationship $k_0=p_0/N_V$ where N_V (= 8.68×10^{28} m^{-3}) is the number of available sites of hydrogen in the lattice [18].

These equations can be used to simulate not only desorption, but also diffusion into the specimen during hydrogen charge. One of the key parameters is thus the hydrogen concentration at the specimen surface. According to Sievert's law the hydrogen concentration at the specimen surface is expressed as,

$$c_S = K_S \sqrt{f} \tag{5}$$

where f is the hydrogen fugacity in the environment given by,

$$f = p \exp\left(\frac{pb}{RT}\right) \tag{6}$$

and K_S is the hydrogen solubility given by,

$$K_S = K_0 \exp\left(-\frac{\Delta H_S}{RT}\right) . \tag{7}$$

Here, p is gaseous hydrogen pressure, b(=1.584×10^{-5} $m^3 mol^{-1}$) is a constant applicable to high-pressure gaseous hydrogen, ΔH_S (= 2.34 kJ/mol) is the enthalpy of solution of hydrogen, K_0 (=52.8 $molH_2 m^{-3} MPa^{-1/2}$) is the pre-exponential factor, R is the gas constant and T is absolute temperature [11]. Table 2 shows the conditions of

hydrogen-charge and thermal desorption analysis as well as specimen shape and size employed in the experiment with which simulations are compared.

Table 1 Diffusivities of hydrogen used in simulation.

Alloy		D_0	Q, kJ/mol	reference
bcc iron		$5.8x10^{-8}$	4.5	[13]
pure nickel		$1.07x10^{-6}$	42.37	[9]
Inconel 625		$9.14x10^{-8}$	46.4*	[5]
		$1.75\ x10^{-6}$	52.6	[10]
fcc iron		$6.63X10^{-7}$	44.8	[9]
SUS304		$1.21x10^{-5}$	63.1	[11]
SUS304	non-deformed	$4.41x10^{-7}$	53.51	[12]
	deformed	$4.51x10^{-7}$	49.9	〃

* Calculated from the values of diffusivity reported in ref. [5].

Table 2 Conditions of hydrogen charge and thermal desorption analysis reported in the literature

Alloy	Hydrogen charge	specimen	Ramp rate	reference
Pure Ni	0.1MPa (1 atm) gas environment	Plate, 0.35~0.91 mm	3°C/min	19
Inconel 625	Cathodic charge in H2SO4 aqueous solution with 0.1mass% NH_4SCN at $50A/m^2$ and 90°C	Plate, 0.1~0.8 mm	50~300°C/hr	5
SUS304	140MPa gas environment, 1000 hr, 85°C	Plate, 0.77 mm	100°C/hr	7
	Cathodic charge in 3%NaCl aqueous solution with 3g/ℓ NH_4SCN at $10mA/m^2$			

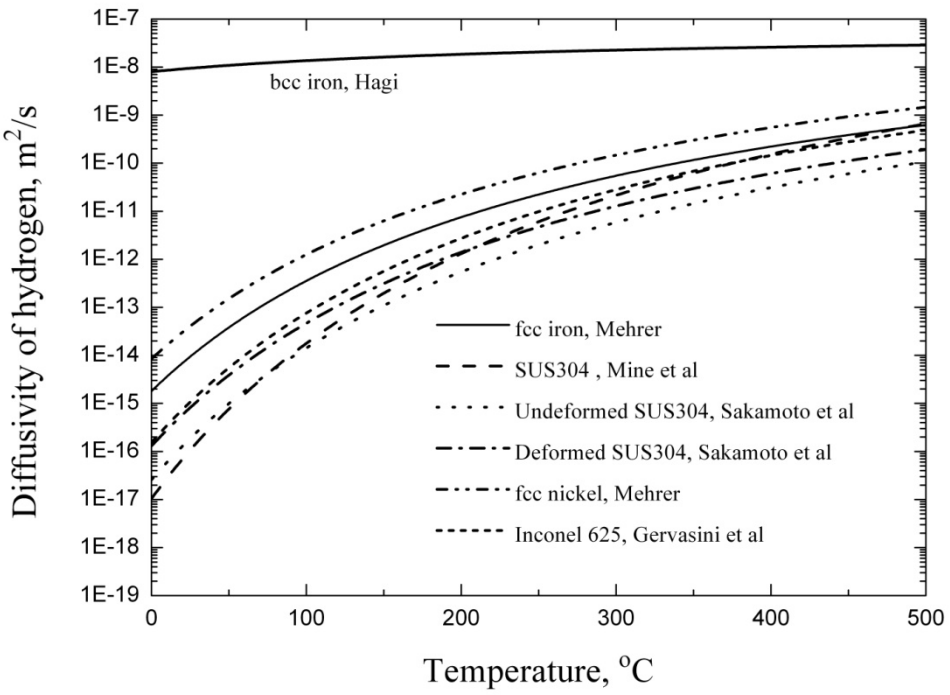

Fig.1 Diffusivities of hydrogen in fcc metal and bcc Fe in the literature.

6.3 Results and discussion

6.3.1 Variation of TDS with specimen size

There seem to be only a few reports on the size dependence of TDA curves of fcc metals. Lee and Lee [19] reported lucid thermal desorption spectra of Ni plates of varying thickness. Fig. 2 shows that if one uses the diffusivity of hydrogen in pure Ni [9], calculated and measured spectra are in good agreement except at the rising part. This lends support to the discussion by these authors [19].

Takai et al [5] reported thermal desorption spectra of Inconel 625. They carefully chose the charging time such that the amount of charged hydrogen was saturated with increasing charging time. Hence, one can assume that the concentration of charged hydrogen was constant initially. Also assuming that the trap site density was insignificantly small, simulations of these spectra were conducted using the diffusivities proposed by Takai et al and Gervasini et al [10]. While the former diffusivity yielded peak temperatures ~100°C greater than experimental curves, the latter gave peak temperatures only 15~30°C greater than experiment at all plate thicknesses. It is shown in Fig. 3 that the agreement with measured curves is improved further if one uses the diffusivity two times greater than that of Gervasini et al. These results indicate that lattice diffusion plays a prominent role in the desorption of hydrogen in this alloy as in pure Ni.

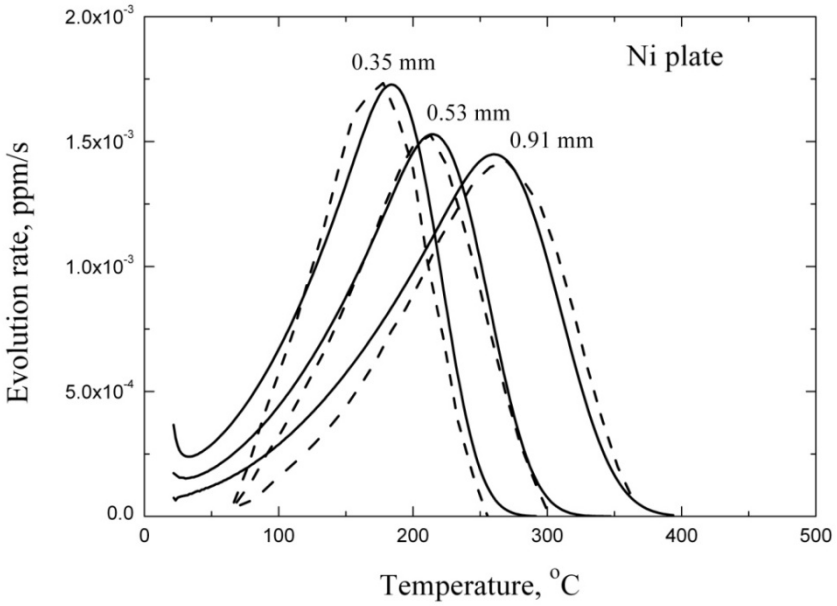

Fig.2 Comparison of simulated thermal desorption spectra of hydrogen of Ni plate specimens of 0.35, 0.53 and 0.91 mm thickness with experiment (dashed curve) [19].

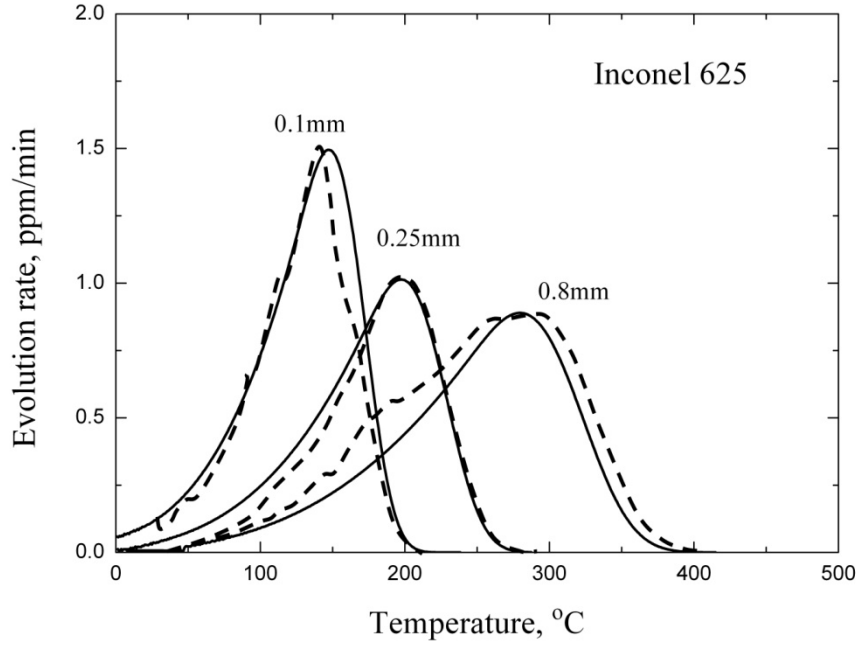

Fig.3 Comparison of simulated (solid curve) and experimental (dotted curve) [5] TDA curves of Inconel 625 plate specimen.

6.3.2 Simulation of TDS in non-deformed SUS304 charged under high-pressure hydrogen atmosphere

In the experiment by Mizuno et al [7] SUS304 steel specimen was charged with hydrogen at 85°C under the pressure of 140 MPa, at which the surface concentration of hydrogen is calculated to be c_s = 71 ppm from eq. (5). With this c_s value the diffusion profile of hydrogen in the specimen of 0.77 mm thickness was simulated using the diffusivity proposed by Sakamoto and Katayama [12]. However, this yielded a considerably lower peak, ca. one-half in peak height, than that reported experimentally [7]. This can be attributed to too small surface concentration and/or lattice diffusivity used in the simulation. In view of the fact that another diffusivity reported by Mine et al [11] gives a similar value at the charging temperature (=85°C, see Fig. 1) a higher surface concentration (=150 ppm) was employed, and results at 10, 100 and 1000 hr charge are shown in Fig. 4a. It is seen that hydrogen penetrated progressively deeper into the specimen with time, but not yet achieved a uniform concentration at 1000 hr. Fig. 4b shows TDA curves simulated at these charging times as well as assuming uniform distribution that would be obtained by pre-charge for infinitely long time together with an experimental curve of 1000 hr charge (dashed curve). Whereas the assumed diffusivity is somewhat too small, presumably two to three times, a notable feature of these spectra is that two broad peaks are present in the experimental and simulated curves pre-charged for 100 and 1000 hr. This is also the case with SUS316L reported by the same authors [7]. In order to understand this hydrogen diffusion profiles during ramping are calculated for the same charging time and results at several temperatures are shown in Fig. 5. It is seen that hydrogen near the rim of the specimen quickly diffused and escaped from the surface. At the same time a substantial fraction of hydrogen diffused inward at first and came back to the surface later to form the 2nd higher temperature peak. The shape and relative heights of the 1st and 2nd peaks may

vary with subtle combination of diffusion coefficient, charging time and the amount of hydrogen.

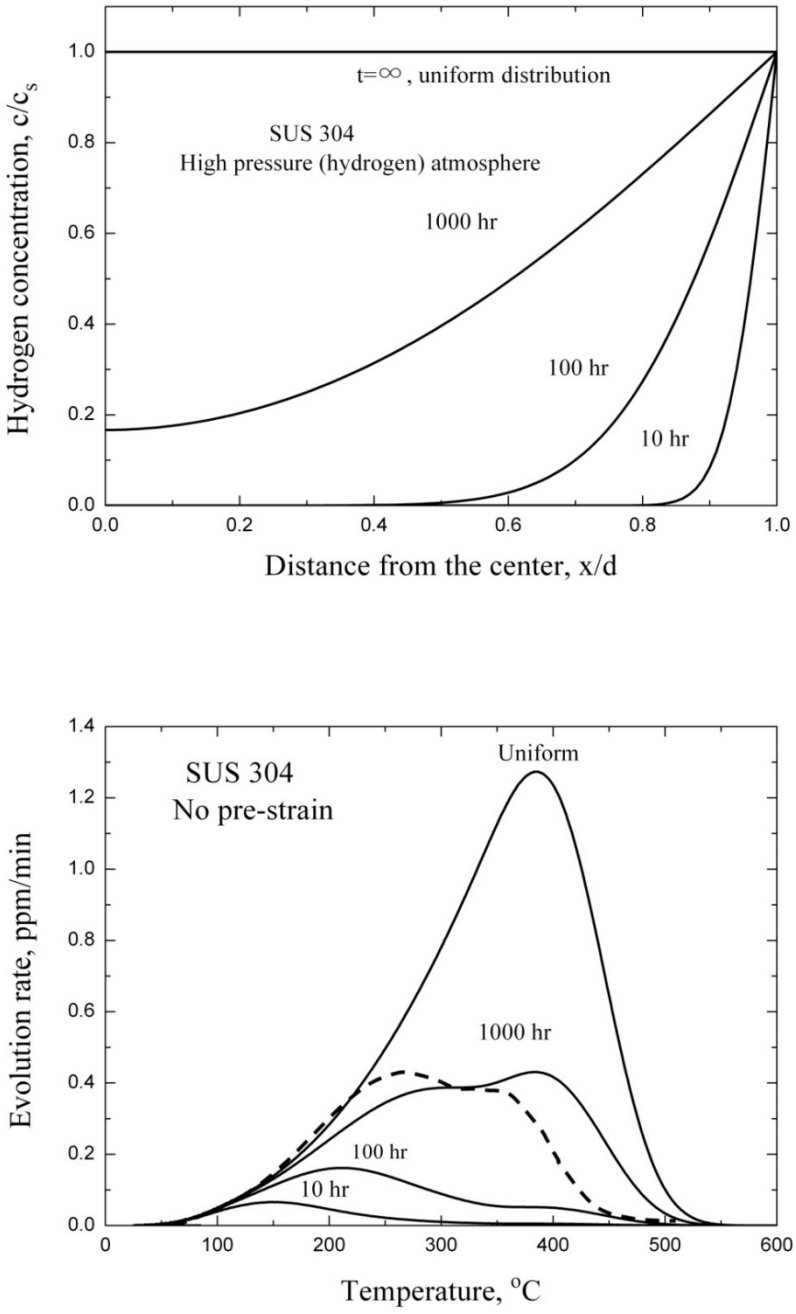

Fig.4 a) Hydrogen diffusion profiles and TDA curves of SUS304 steel charged for 10, 100 and 1000hr under high pressure atmosphere. Calculated with the surface concentration of 150ppm and the specimen thickness of 0.77 mm. Dashed curve in b) is taken from ref. [7].

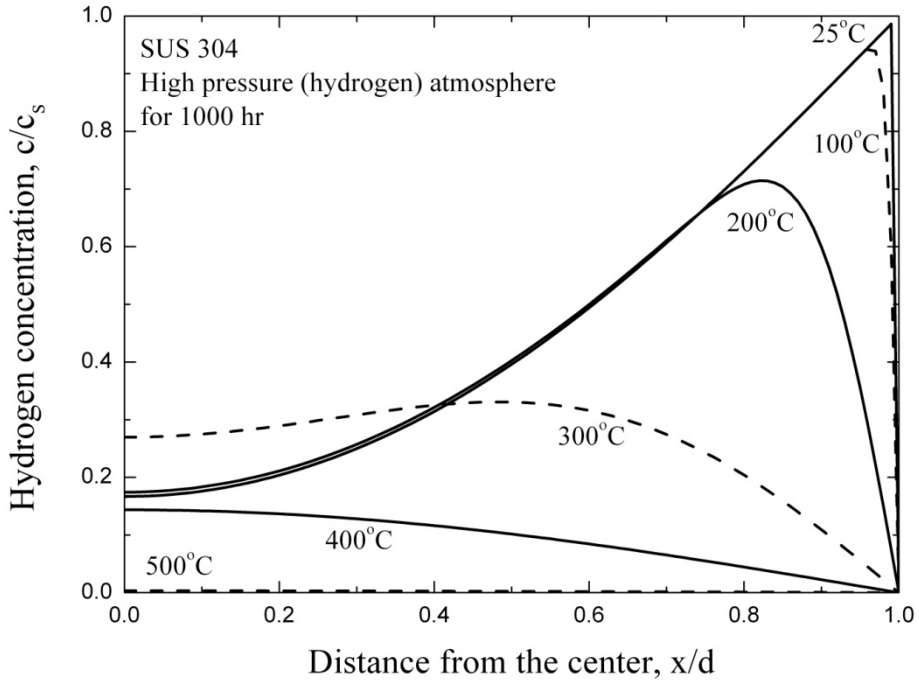

Fig.5 Calculated evolution of hydrogen profile in the specimen charged for 1000hr under high pressure hydrogen atmosphere. The time of each curve is shown by temperature during ramping at 100°C/hr.

6.3.3 Simulation for cathodically charged SUS304 steel

Mizuno et al [7] also reported TDA curves of cathodically charged SUS304 specimens, see Table 2. Fig. 6a and 6b show that the penetration of hydrogen is limited to the peripheral region and thereby, the surface concentration of ~400 ppm is required to accumulate hydrogen which accounts for the peak area of the observed thermal desorption spectrum (dashed curve). This surface concentration is equivalent to the hydrogen fugacity of 6.2GPa (=6.2×10^4 atmosphere). This appears to be considerably greater than that expected from the relationship proposed by Takai et al [5] for cathodic charge which indicates that the current density of 50 A/m^2 is equivalent to 1.2GPa. It is immediately seen in Fig. 6b that the peak temperature is a little above 100°C, much lower than that in Fig. 4b. This is clearly because hydrogen is confined initially in the region near the surface in the cathodically charged specimens. Thus, the distribution of hydrogen prior to temperature ramp has a profound influence on both peak temperature and shape of TDA curves in austenitic steel.

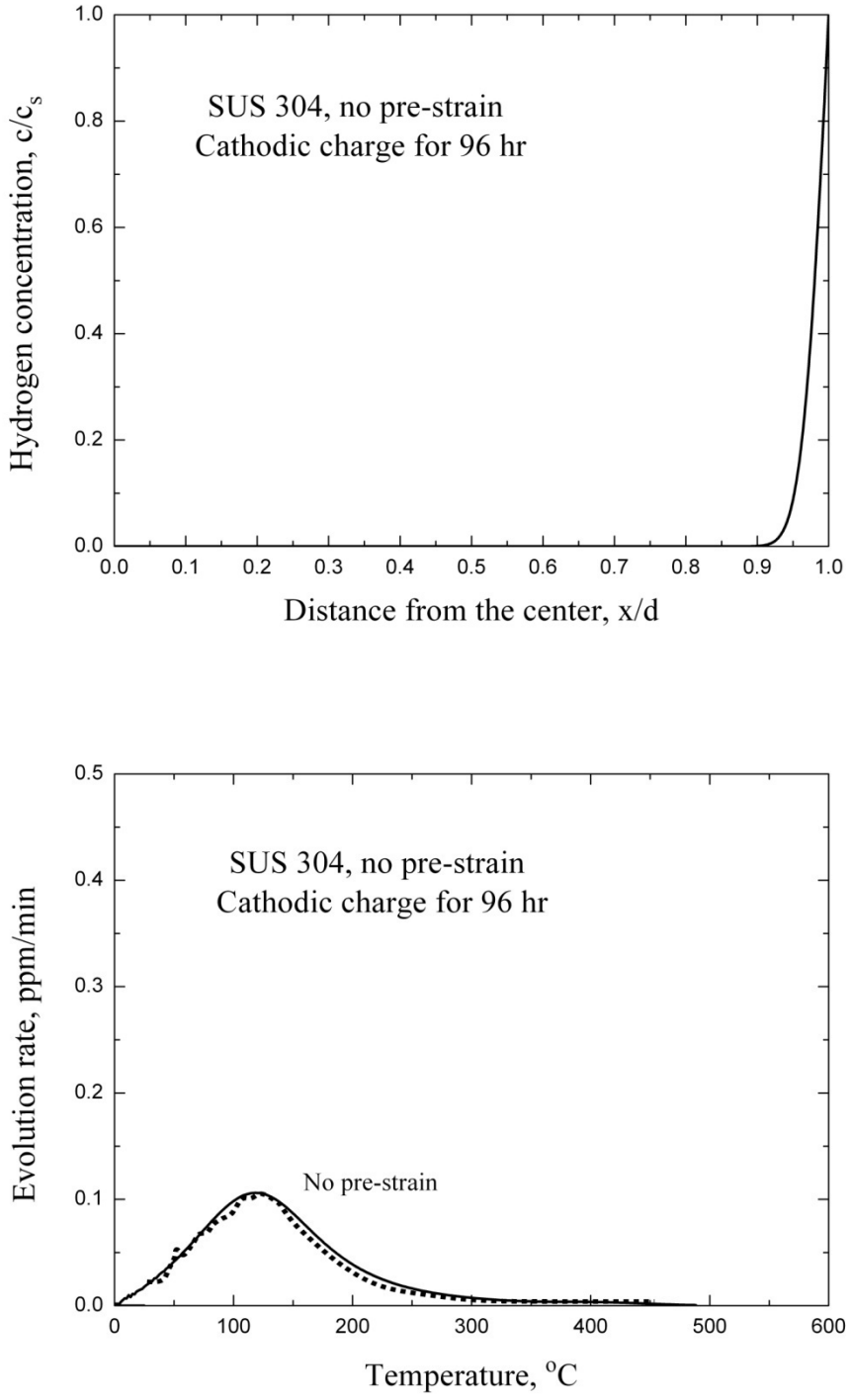

Fig.6 a) Penetration of hydrogen in the specimen cathodically charged for 96hr at room temperature and the current density of 10A/m^2. b) Comparison of simulated thermal desorption spectrum with experiment. Dotted line was reported by Mizuno et al [7].

6.3.4 Effects of deformation on TDS of stainless steel

It was reported that the deformation increased the peak height remarkably in SUS304 steel [7]. This was the case with both cathodic charge and high-pressure hydrogen environment. At first glance this could be due to the hydrogen trap at dislocations and/or vacancies introduced by deformation. However, a large increase in the amount of hydrogen in deformed SUS304 steel can not be accounted for even if all dislocations introduced by deformation captured hydrogen. The amount of hydrogen in the trap sites would be even less because all trap sites are unlikely to be occupied due to the relatively small binding energy of dislocations. The fact that the amount of hydrogen did not increase substantially in SUS316L steel [7] which is fully austenitic after deformation, lends support to this consideration. Indeed, as shown from Fig. 7, the spectra of SUS304 steel containing 100 ppm uniformly distributed hydrogen initially does make an appreciaple difference with and without dislocation (ρ_d=5x10^{14} m^{-2}) as trap site.

Accordingly, one can alternatively assume that the diffusivity of hydrogen increased by the formation of martensite during deformation in SUS304 steel. Sakamoto and Katayama [12] reported that the diffusivity increased ca. four times at room temperature by cold rolling of SUS304 (see Fig. 1) in which presumably a small amount of martensite was formed. Fig. 8 shows that the amount of hydrogen absorbed in the deformed specimen markedly increased assuming the enhanced diffusivity of hydrogen, which in turn increased the peak height of TDA curve 3-4 times in specimens hydrogen-charged under high-pressure atmosphere. A similar observation was made in cathodically charged SUS304 steel [7].

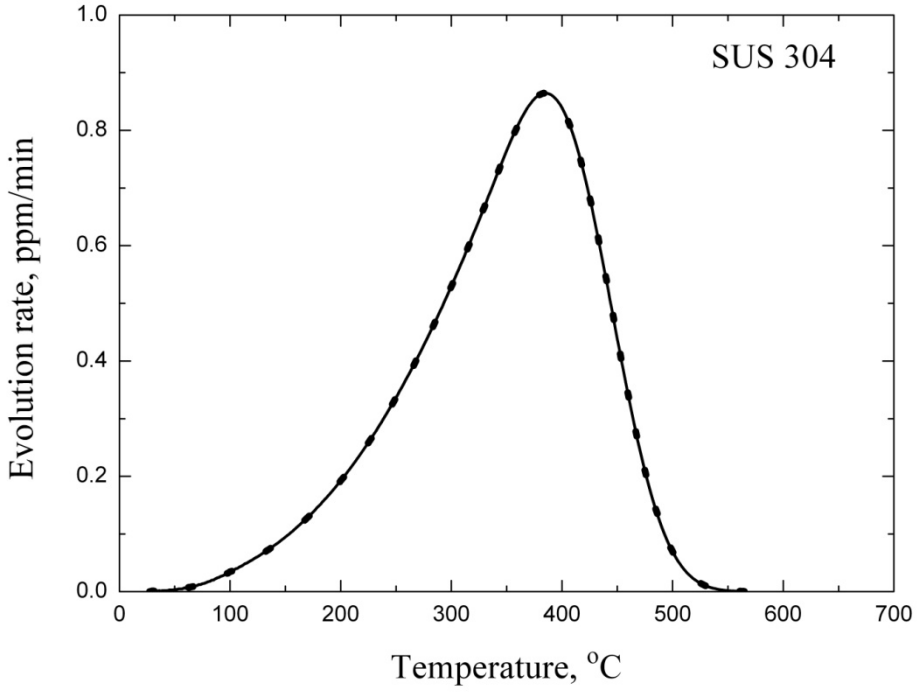

Fig.7 TDA curve of SUS 304 steel simulated with (dashed curve) and without dislocation (solid curve) as hydrogen trap sites. It was assumed that 100 pm hydrogen was distributed uniformly and, the lattice diffusivity of non-defromed case [12] was used.

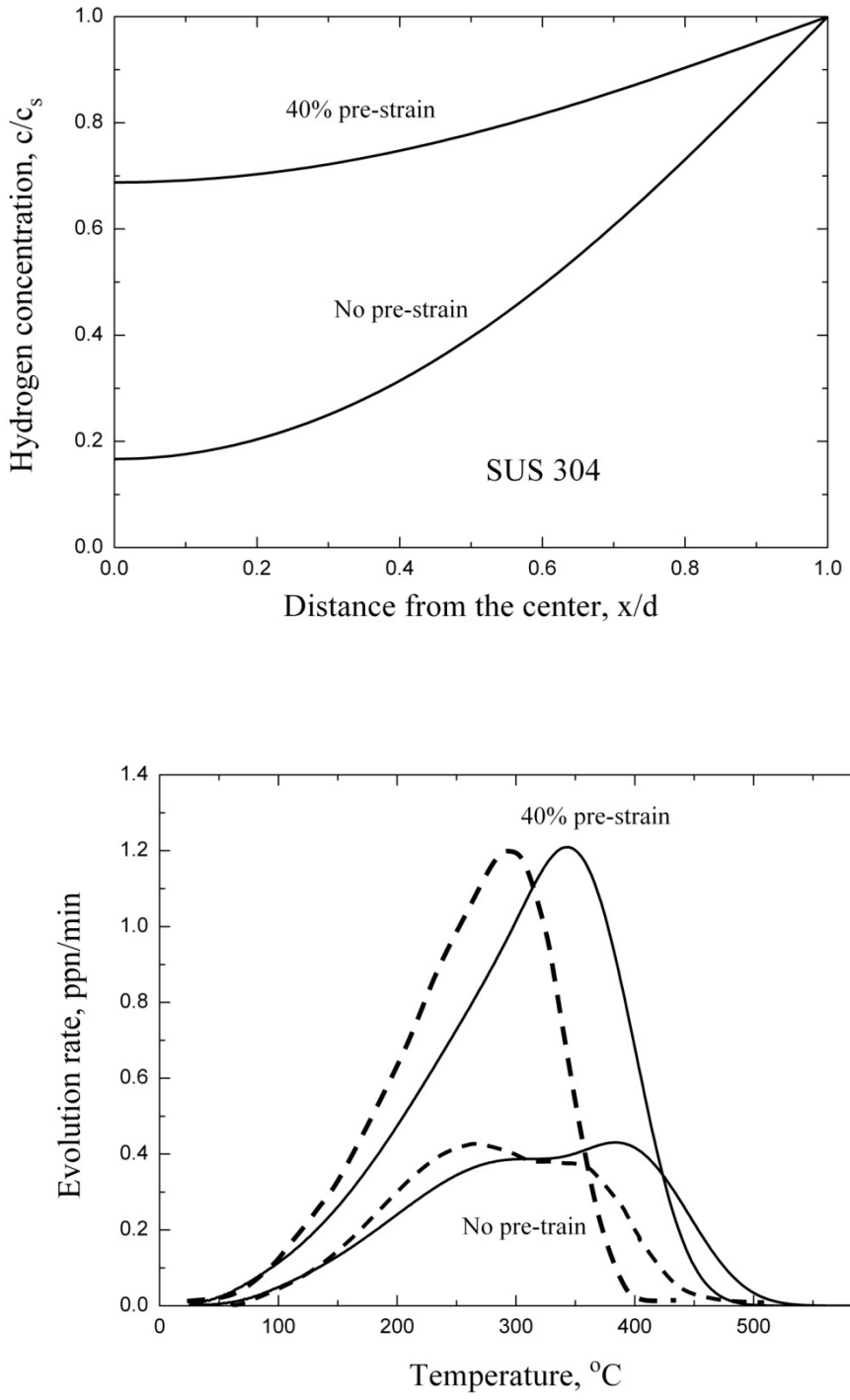

Fig.8 a) Hydrogen distributions, and b) TDA curves of SUS304 steel simulated with pre-strain (larger diffusivity) and without pre-strain. Charged with hydrogen under high pressure atmosphere for 1000hr. The specimen thickness is 0.77mm.

6.3.5 Applicability of Choo-Lee analysis in austenite stainless steel

As discussed in previous papers [20, 21], the Choo-Lee plot of peak temperature which is based upon the relationship,

$$\frac{\partial \ln\left(\phi / T_p{}^2\right)}{\partial\left(1/T_p\right)} = -\frac{E_d}{R} \tag{8}$$

is applicable to the evaluation of the detrapping energy in diffusion-controlled desorption as long as a certain period of pre-exposure is conducted prior to temperature ramp. In contrast, the plot proposed by Lee and Lee [22], i.e, □*ln(φ/T*$_p^2$*)*/□*̃ι*□$_p$□*̃*□$_d$*/R* does not yield a correct value of detrapping energy. In plate specimen the pre-exposure has to be long enough so that the hydrogen content decreases to 60% of the initial amount [21]. In this period the diffusion profile of hydrogen in the specimen evolves to the one which ensures the applicability of Kissinger-type formula for thermal desorption. In the present case, however, no appreciable difference in peak temperature is observed with and without pre-exposure probably because the required diffusion profile has been achieved when the peak temperature is reached. Fig. 9a compares simulated and experimental TDA curves of Inconel 625 [5] and in Fig. 9b, the corresponding Choo-Lee plot was made. In view of the fact that the detrapping energy obtained from the slope is equal to the activation energy of diffusion in this case, the detrap energy (=41.0±8.2 kJ/mol) derived from experimental peaks is somewhat smaller than that obtained from calculated peaks (E_D=52.6 kJ/mol).

Since the peak temperature depends greatly on the initial distribution of hydrogen it is interesting to see if the Choo-Lee plot correctly yields the detrapping energy E_d or diffusion activation energy E_D when the hydrogen concentration is non-uniform initially. Thus, TDA curves of SUS304 steel pre-charged for 10, 1000 hr and infinitely long time (uniform distribution) under high pressure atmosphere were simulated at varying ramp rates using the diffusivity by Sakamoto and Katayama [18]. Results are shown in Figs.

10a through 10c. While the peak temperatures of specimens pre-charged for 10 hr are considerably lower than those of 1000hr and infinitely long time, the peak temperatures of the latter two sets of specimens are almost identical as long as the higher peak temperatures are taken for specimens of 1000 hr. Moreover, the slopes of the Choo-Lee plot are all similar to the activation energy of diffusion (E_D=53.5 kJ/mol) as shown in Fig. 11. This indicates that as far as the detrapping energy is concerned, non-uniform distribution of hydrogen due to insufficient hydrogen pre-charge may not cause an erroneous value from the Choo-Lee plot. Thus, it is likely that the fairly large difference in the slope of Choo-Lee plot on Inconel 625 (Fig.9b) is caused by experimental scatter.

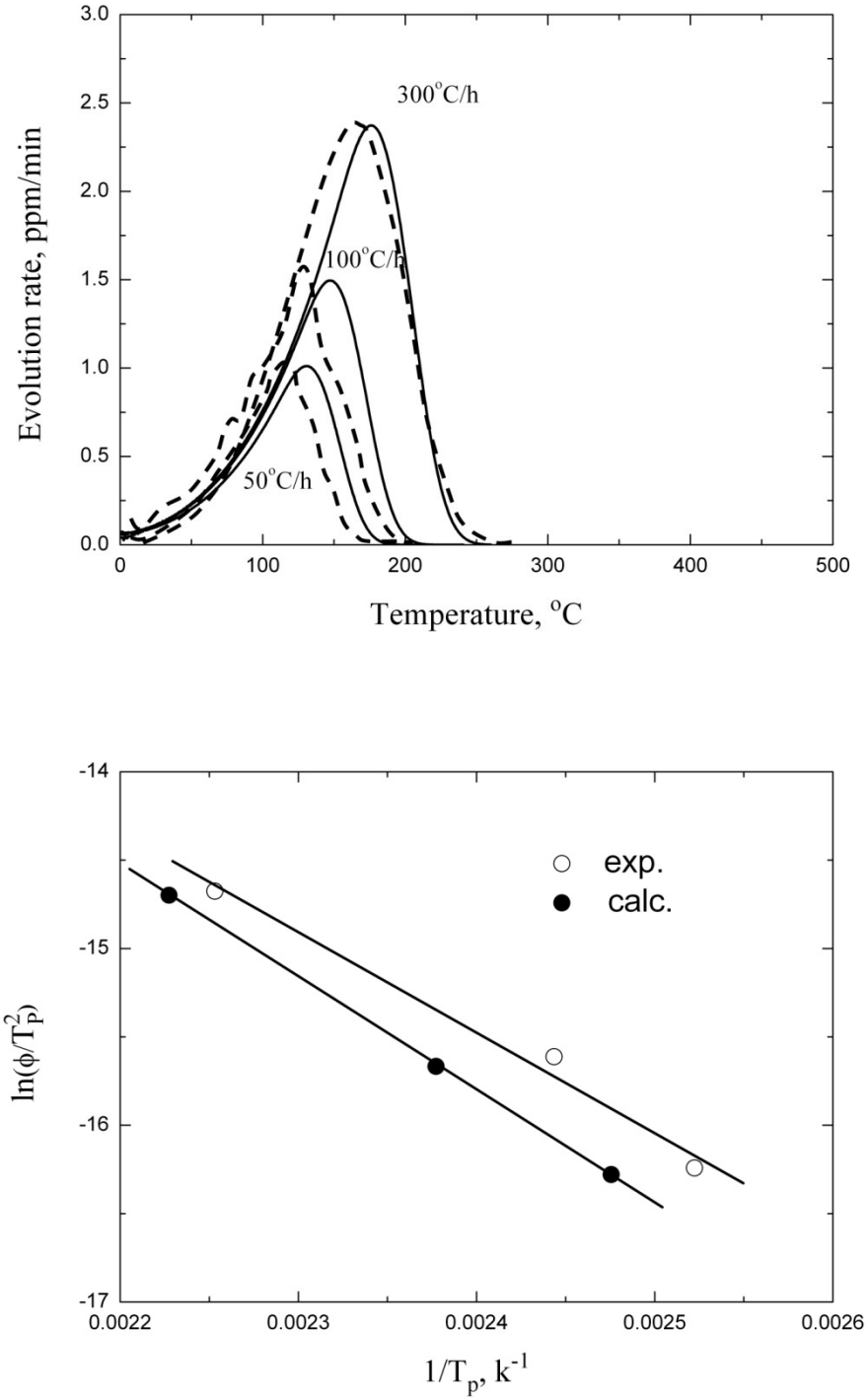

Fig.9 a) Thermal desorption spectra of Inconel 625 specimen at varying ramp rates, and b) the corresponding Choo-Lee plot of peak temperature.

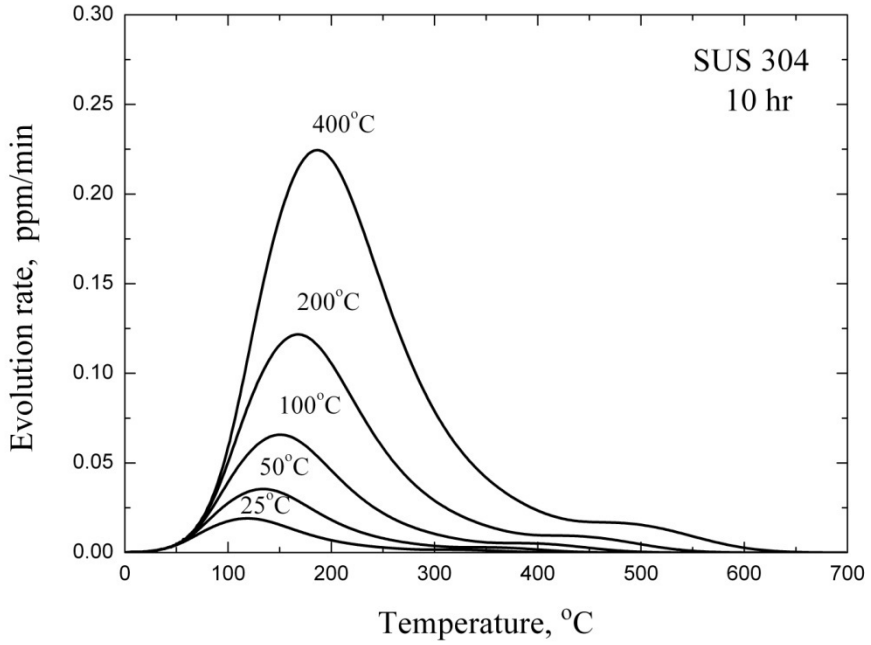
SUS 304
10 hr
400°C
200°C
100°C
50°C
25°C
Evolution rate, ppm/min
Temperature, °C
0.00
0.05
0.10
0.15
0.20
0.25
0.30
0
100
200
300
400
500
600
700

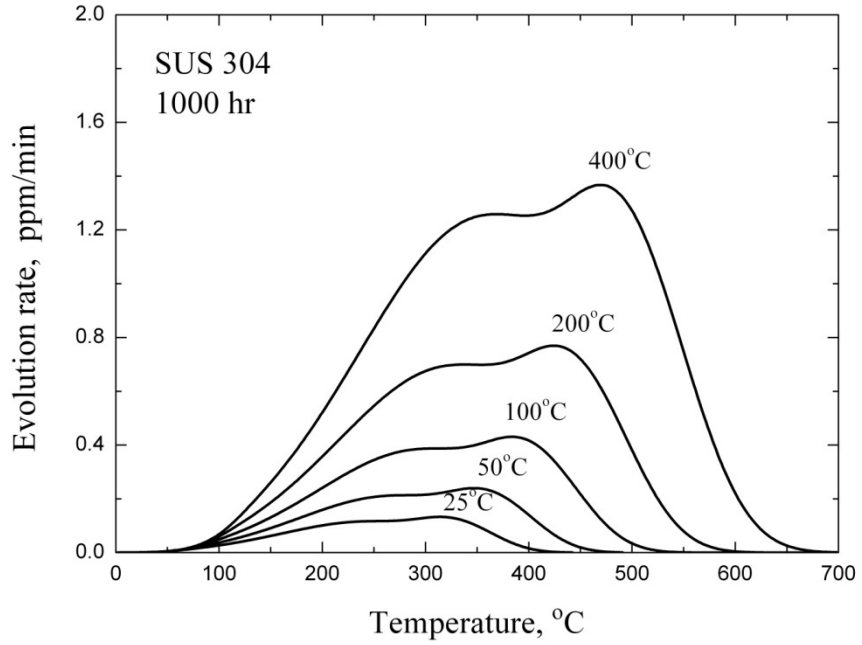
SUS 304
1000 hr
400°C
200°C
100°C
50°C
25°C
Evolution rate, ppm/min
Temperature, °C
0.0
0.4
0.8
1.2
1.6
2.0
0
100
200
300
400
500
600
700

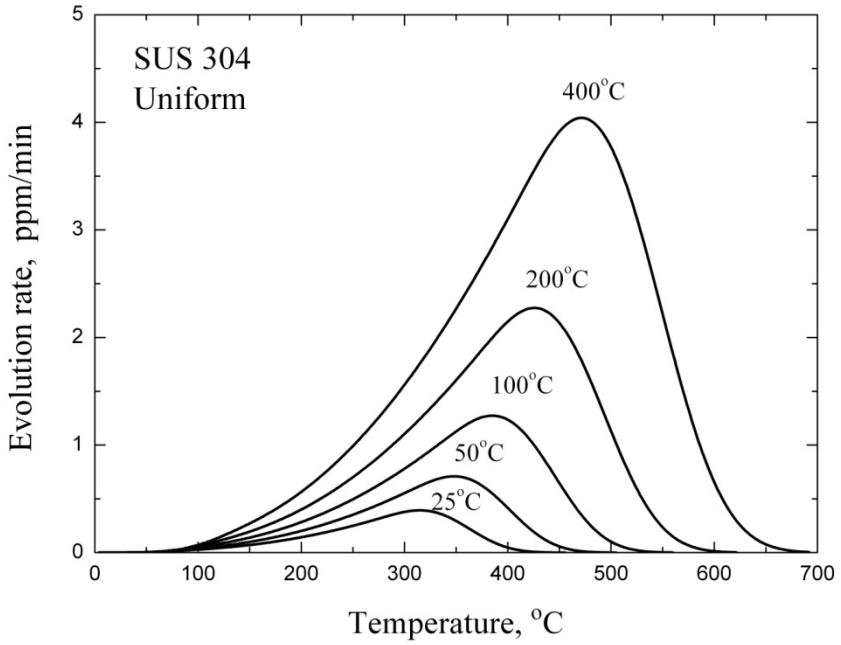

Fig.10 a) TDA curves of SUS304 steel specimens charged under high-pressure atmosphere a) for 10 hr, b) 1000 hr and c) for infinitely long time simulated at varying ramp rates.

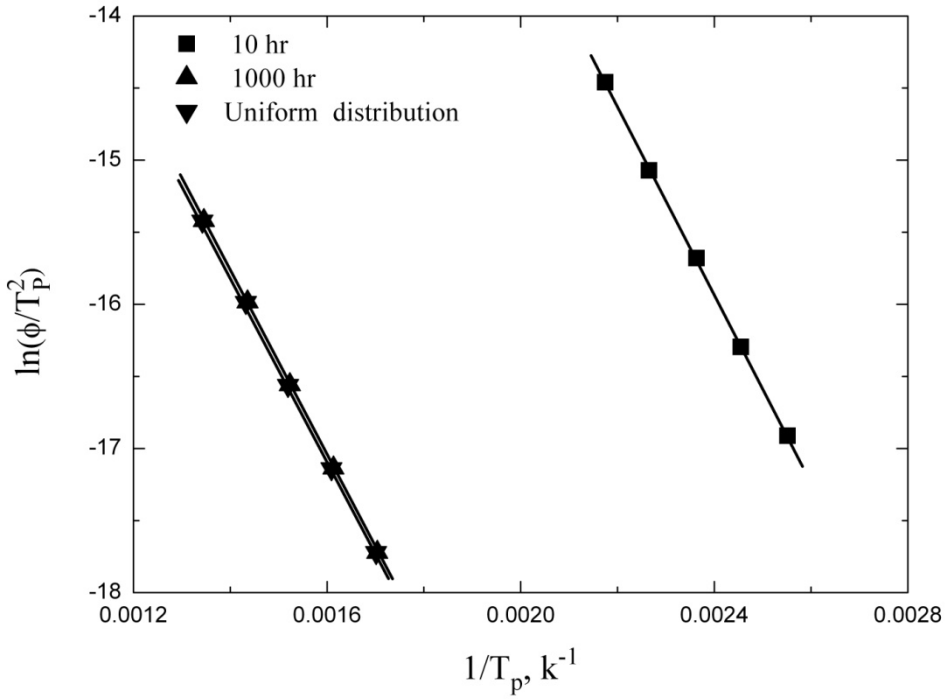

Fig.11 Choo-Lee analysis of peak temperatures of the curves shown in Figs. 10a through 10c.

6.4. Summary

TDA curves of Ni alloys and austenitic stainless steels were computer simulated in various hydrogen pre-charge and testing conditions by means of McNabb-Foster equations. Whereas the diffusivity and the surface concentration of hydrogen deduced from the equation or relationship in the literature did not yield TDA curves exactly fitting those of experiment, the following features of thermal desorption spectrum metals are noted in fcc metals.

1) TDA curves can be simulated using a single diffusivity and no appreciable difference in activation energy of detrapping is observed from that of lattice diffusion. This is presumably because local equilibrium between lattice and the trap sites is readily achieved due to the small binding energy of trap sites.

2) Because of the large activation energy of diffusion the peak temperature depends considerably on specimen size, ramp rate and hydrogen distribution prior to temperature ramp. As a result, insufficient pre-charge of hydrogen which leads to a non-uniform distribution casues a much lower peak temperature than that of specimen pre-charged for a sufficiently long time. Moreover, two peaks can arise out of highly non-uniform initial distribution solely from lattice diffusion.

3) A large increase of hydrogen uptake in deformed SUS304 stainless steel is unlikely to be due to hydrogen trapping at defects, but is attributed to the enhanced diffusion of hydrogen due to deformation-induced martensitc transformation.

4) The Choo-Lee plot can be used to evaluate the detrapping energy or diffusion activation energy of hydrogen unless the density of lattice defects is too large. The error which might be caused due to insufficient pre-charging or inhomogeneous initial distribution is likely to be small.

References

[1] M. Nagumo, Fundamentals of Hydrogen Embrittlement, Uchida-Rokakuho, Tokyo, 2008, pp. 244-289.

[2] K.H. Lo, C.H. Shek, and J.K.L. Lai, Mater. Sci. Eng. R 65(2009) 39-104.

[3] A. San-Martin and F.D. Manchester, Phase Diagrams of Binary Iron Alloys, ed. H. Okamoto, ASM, Metals Park, OH, 1993, pp. 161-170.

[4] N.R. Quick and H.H. Johnson, Metall.Trans.A, 10A(1979) 67-70.

[5] K. Takai, K. Murakami, N. Yabe, H. Suzuki, and Y. Hagiwara: J. Japan Institute of Metals, 72(2008) 448-456.

[6] Y. Yagodzinsky, O. Todoshchenko, S. Papula, and H. Hänninen, Steel Research International, 82(2011) 20-25.

[7] H. Mizuno, J. Sakai, K. Yokoyama, K. Suzuki, M. Imade, T. Omura, and R. Okuma, Proc. Symp. of Common Bases for Hydrogen Embrittlement Studies, The Iron and Steel Institute of Japan, Tokyo, September, 2012, pp.13-16.

[8] A. McNabb and P.K. Foster, Trans. TMS-AIME, 227(1963) 618-627.

[9] A.D. Le Claire, Numerical data and functional relationships in science and technology, Landolt-Börnstein, New Series, vol.26, ed.H. Mehrer, 1990, pp.511-548.

[10] G. Gervasini, J. Camposilvan, and F. Reiter, Fusion Technol., 6(1984) 428-433.

[11] Y. Mine and T. Kimoto, Corros. Sci., 53(2011) 2619-2629.

[12] Y. Sakamoto and H. Katayama, J. Japan Institute of Metals, 46(1982) 805-814.

[13] H. Hagi, Mater. Trans. JIM, 35(1994) 112-117.

[14] A. Atrens, N. F. Fiore, and K. Miura, J. Appl. Phys. 48(1977) 4247-4251.

[15] S. Taketomi, R. Matsumoto, and N. Miyazaki, Acta Mater., 56(2008) 3761-3769.

[16] T. Shintani and Y. Murata: Acta Mater., 59(2011) 4314-4322.

[17] D. Kalish and M. Cohen, Mater. Sci. Eng., 6(1970) 156-166.

[18] A. Turnbull, R.B. Hutchings, and D.H. Ferriss, Mater. Sci. Eng. A238(1997) 317-328.

[19] S.M. Lee and J.Y. Lee, Metall. Trans., 17A(1986) 181-187.

[20] F.G. Wei, M. Enomoto, and K. Tsuzaki, Comput. Mat. Sci., 51(2012) 322-330.

[21] L. Cheng, M. Enomoto, and F.G. Wei, ISIJ Int., 53(2013) 250-256.

[22] J.Y. Lee and J.L. Lee, Philos.Mag. A 56(1987), 293-309.

Chapter 7

Conclusions

In this study, numerical simulation of thermal desorption spectrum (TDS) of hydrogen in high strength martensitic and austenitic stainless steels was conducted. The following conclusions can be drawn:

1) In detrapping-controlled desorption, specimen shape and size, and initial occupancy have no effects on TDS. However, for one kind of trap sites the increase in specimen size and trap sites density will induce hydrogen desorption to deviate from detrapping-controlled desorption to diffusion-controlled desorption.

2) In diffusion-controlled desorption, the TDS peak temperature increases with specimen size and trap site density in the specimens with the same initial occupancy. At constant trap site density, peak temperature increases with decreasing initial occupancy. Meanwhile, with the same radius or half-thickness, the peak temperature increases in the order of sphere, cylinder and plate.

3) In both detrapping-controlled desorption and diffusion-controlled desorption, TDS peak temperature and corresponding evolution rate at the peak temperature increases with ramp rates. Meanwhile, Choo-Lee plot analysis can be utilized in both cases to deduce the hydrogen detrapping energy from the trap sites.

4) The Kissinger formula, including its derivative forms like the Choo-Lee plot, provides a simple and reliable technique for hydrogen thermal desorption analysis with an accuracy as high as that analyzed on the base of the McNabb-Foster model if the thermal desorption experiment is performed under proper conditions. In detrapping-controlled condition one can evaluate the activation energy of detrapping and the pre-exponential factor of detrapping coefficient from one TDS if the specimen size is sufficiently small and the ramp rate is not too fast. In diffusion-controlled

condition one can evaluate not only the activation energy of detrapping, but also the density of traps from coefficient A which depends on specimen size. Pre-exposure for a sufficiently long time is necessary prior to temperature ramping, the duration of which depends on specimen shape.

5) The temperature and shape of TDS peak and moreover, the 50~100°C difference in peak temperature between deformed iron and low and medium carbon martensite could be accounted for carbon segregation to the dislocation. Whether or not carbon segregates prior to thermal desorption analysis (TDA) may have a significant influence on the spectrum shape, but does not appear to have an appreciable influence on the peak temperature unless it is too low.

6) TDS of fcc metals can be simulated using a single diffusivity and no appreciable difference in activation energy of detrapping is observed from that of lattice diffusion. Because of the large activation energy of diffusion in fcc metals the TDS peak temperature depends considerably on specimen size, ramp rate and hydrogen distribution prior to temperature ramp.

7) Insufficient pre-charge of hydrogen in fcc metals which leads to a non-uniform distribution causes a much lower peak temperature than that of specimen pre-charged for a sufficiently long time. Moreover, two peaks can arise out of highly non-uniform initial distribution solely from lattice diffusion. In particular, a large increase of hydrogen uptake in deformed SUS304 stainless steel is unlikely to be due to hydrogen trapping at defects, but is attributed to the enhanced diffusion of hydrogen due to deformation-induced martensitc transformation.

8) The Choo-Lee plot can be used to evaluate the detrapping energy or diffusion activation energy of hydrogen in fcc metals with even insufficient pre-charge of hydrogen unless the density of lattice defects is too large.